University of Alberta

Evaluation of SI-HCCI-SI Mode-Switching Using Conventional Actuation on a
CNG Engine

by

Jason Bradley Boddez

A thesis submitted to the Faculty of Graduate Studies and Research in partial
fulfillment of the requirements for the degree of

Master of Science

Department of Mechanical Engineering

ABSTRACT

Homogeneous Charge Compression Ignition (HCCI) operation is desirable for its high thermal efficiency and low emissions of NOx and particulates. Difficulty with cold starting and maximum achievable speed/load highlight the desire for mode-switching to traditional spark ignition (SI) operation.

Mode-switching between SI and HCCI is investigated using only actuation of throttle, CNG injector pulse width, and CNG injection timing on a single cylinder CFR engine. Open-loop control achieves a one cycle mode-switch between two adjustable IMEP levels. Sequences are repeatable as demonstrated by 10 mode-switches with the same inputs.

Performance is evaluated using a developed mode-switch performance criterion (MSPC) by considering duration between steady-states of operation, smoothness of IMEP, and knock based on maximum rate of pressure rise. Comparing the results with subjective analysis (the current standard) reveals good correlation. Throughout development, mode-switching performance is shown to improve by a factor of 60.

Acknowledgements

I wish to thank my supervisors, Dr. David Checkel and Dr. Bob Koch, for their technical and financial support. They have made this endeavor a very fulfilling experience that I will benefit from for many years to come.

Also, I would like to thank the staff in the Mechanical Engineering Department for their assistance and expertise, namely Bernie Faulkner, Rick Conrad, and Roger Marchand. Your contributions and involvement were greatly appreciated.

To my co-researchers and friends, Ahmad, Ali, Dan, Dallin, Darren, Gillian, Mahdi, Masoud, Michael, Roberto, Rory, and many others, thank you for your assistance and providing an enjoyable learning environment.

And last but not least, I must acknowledge Colleen, my parents (Walter and Jeannine), family, and friends for their never ending support and encouragement.

TABLE OF CONTENTS

LIST OF FIGURES

LIST OF TABLES

Nomenclature

aTDC   After Top Dead Center on the compression stroke

bIVO   Before Intake Valve Opening

bTDC   Before Top Dead Center on the compression stroke

CA50   Crank Angle Degrees @ 50% mass fraction of fuel burned, relative to Top Dead Center

CI   Compression Ignition

CNG   Compressed Natural Gas

CO_2 Carbon Dioxide

CO   Carbon Monoxide

DAQ   Data Acquisition

EVC   Exhaust Valve Closing

EVO   Exhaust Valve Opening

HC   Unburned Hydrocarbons

HCCI   Homogeneous Charge Compression Ignition

IMEP   Indicated Mean Effective Pressure

IVC   Intake Valve Closing

IVO   Intake Valve Opening

MSPC   Mode-Switching Performance Criterion

NO_x Oxides of Nitrogen

O_2 Oxygen

PI   Proportional-Integral Controller

PPC   Pulse Per Cycle

PPM   Parts Per Million

PPR   Pulse Per Revolution

PW   Fuel Injector Pulse Width

ROPR   Maximum Rate of Pressure Rise in the cylinder

RSS   Root Sum of the Squares

SI   Spark Ignition

TDC   Top Dead Center on the compression stroke

TDLA   Thermodynamic Loss Angle

Symbols

β Volumetric thermal expansion coefficient, approximated as 1/T for ideal fluids [1/K]

δR Uncertainty in the result of a root sum of the squares

δX_i Uncertainty of one component being considered in a root sum of the squares

η_{vol} Volumetric efficiency [%]

$\mu_{\mathrm{IMEP\_trans}}$ Average IMEP during a mode-switch, equal to the mid-point between the two steady-state values [bar]

μ_{IMEP} Average of a set of IMEP values [bar]

μ_{MSPC} Average MSPC for a set tests [-]

ν Kinematic viscosity [m^2/s]

ρ_{mix} Mixture density [kg/m^3]

$\sigma_{\mathrm{IMEP\_trans}}$ Standard deviation of IMEP during a mode-switch transition [bar]

σ_{IMEP} Standard deviation of a set of IMEP values [bar]

$\sigma_{\mathrm{MSPC\_cyl}}$ Standard deviation of MSPC between cylinders on a multiple cylinder engine, averaged over a series of tests [-]

σ_{MSPC} Standard deviation of MSPC for a set of tests [-]

A_{conv} Area for convection heat transfer [m^2]

a Crank radius [m]

B Cylinder bore [m]

C Polytropic constant [kPa (m^3)^n]

C_{p_air} Constant pressure specific heat capacity of air [J/g °C]

C_{p_CNG} Constant pressure specific heat capacity of CNG [J/g °C]

$CNG\ PW$ Commanded pulse width of CNG injector for one cycle [ms]

$COV_{\text{IMEP\_trans}}$ Transient coefficient of variation of IMEP [%]

COV_{IMEP} Coefficient of variation of IMEP [%]

$Duration$ Number of cycles to complete a mode-switch based on MSPC definition [-]

g Gravitational acceleration [m/s^2]

Gr_D Grashof Number [-]

h Average convection coefficient [W/m^2 °C]

$IMEP_{\text{actual}}$ Experimental IMEP [bar]

$IMEP_{\text{final}}$ Steady-state IMEP in operating mode (SI/HCCI) following mode-switch [bar]

$IMEP_{\text{initial}}$ Steady-state IMEP in operating mode (SI/HCCI) before mode-switch [bar]

$IMEP_{\text{target}}$ Desired IMEP [bar]

J	Number of tests [-]
k	Thermal conductivity [W/m °C]
l	Connecting rod length [m]
L_c	Characteristic length [m]
M	Number of cylinders [-]
m_{Air}	Mass of air injected for one cycle [mg/cycle]
m_{CNG}	Mass of CNG injected for one cycle [mg/cycle]
$\dot{m}_{\text{Air}}$	Mass flow rate of air [g/s]
$\dot{m}_{\text{CNG}}$	Mass flow rate of CNG [g/s]
$\dot{m}_{\text{res}}$	Mass flow rate of residual gases [g/s]
$MSPC$	Mode-Switching Performance Criterion (MSPC) evaluated from a single test (or average among cylinders in a multiple cylinder engine) [-]
$MSPC_{\text{cyl}}$	MSPC for one cylinder in a multiple cylinder engine [-]
N	Engine rotational speed [rev/s]
n	Polytropic index [-]
n_{r}	Number of revolutions for a complete set of strokes ($n_r = 2$ for a 4-stroke engine) [rev/cycle]
Nu	Nusselt number [-]
Num	Number of uncertainty components [-]

P	Pressure [kPa]
P_{cyl}	Cylinder pressure [bar]
P_{IVC}	Pressure at IVC [kPa]
Pr	Prandtl Number [-]
Q_{conv}	Convection heat transfer [W]
R_{air}	Gas constant for air, 287.06 [J/g °C]
R_{CNG}	Gas constant for CNG (approximated as methane), 518.27 [J/g °C]
Ra_D	Rayleigh number [-]
$ROPR$	Maximum rate of pressure rise for one cycle [bar/CAD]
$Stabilize$	Number of cycles after initiating a mode-switch until propagating knock is reduced below the knock limit of 10 bar/CAD [-]
T	Temperature [K]
T_{∞}	Room temperature [K]
T_{mix}	Mixture temperature [K]
T_{res}	Residual gas temperature [K]
T_{s}	Surface temperature [K]
V	Volume [m^3]
V_{cyl}	Cylinder volume [m^3]
V_d	Displacement volume [m^3]

CHAPTER 1

INTRODUCTION

Internal combustion engines present a means of harnessing the chemical energy stored in various fuels to provide useful mechanical work [1]. This procedure has been employed for over a century with integration into numerous industries including automotive, stationary industrial, marine, and power generation. The wide variety of applications present a similarly wide array of operational requirements, design considerations, weight restrictions, and performance demands. However, combustion in these diverse instances remain mostly unchanged and conventionally takes the form of either a spark ignition (SI) or compression ignition (CI) design.

Concerns over diminishing fossil fuel resources, increasing greenhouse gas concentrations, and other harmful emissions demand further attention toward improving the effectiveness of these designs [2]. Homogeneous charge compression ignition (HCCI), a relatively new engine cycle, offers the combined benefits of improved thermal efficiency and lower exhaust emissions of NO_x and particulates. Tradeoffs exist including higher emissions of hydrocarbons (HC) and carbon monoxide CO, operational speed/load limitations, and greater difficulty in controlling ignition timing and cold starting. Significant research effort has been devoted to alleviating these challenges with HCCI since its discovery in the 1970's [3].

1.1 Research Objective

The focus of this study is to devise a mode-switching strategy to transition between SI and HCCI operation through control of only conventional actuators (throttle and fuel injection). This allows HCCI operation while maintaining existing SI capabilities for cold starting and speed/load extension. Mode-switching in this manner is particularly interesting for applications with nearly constant load and speed operation, such as stationary engines, where additional actuators are viewed as unnecessary complexity requiring additional maintenance. Port-injected compressed natural gas (CNG) is selected as the fuel to tailor the study toward this application.

Performance during a mode-switch is difficult to evaluate due to its transient nature. Typical evaluations are qualitatively based, describing the smoothness and quickness of a mode-switch along with a subjective level of knock or misfire cycles if any are experienced. A quantitative method of evaluating mode-switch performance would provide a useful means of tuning a mode-switch for optimization during development. Acceptable levels of mode-switch performance may then be determined for various applications to help define control actuators requirements. Development of quantitative evaluation criteria for combustion mode-switching is another focus of this study.

1.2 Thesis Outline

The contents of this thesis are organized into 6 chapters. Chapter 2 documents a literature survey of HCCI engines and existing mode-switching methods. The experimental setup and methodology pertaining to the evaluation of mode-switching performance is presented in Chapter 3. Test results are presented in Chapter 4 showing the progression of mode-switch performance throughout development to highlight the effectiveness of the evaluation method. Chapter 5 contains discus-

sion of the experimental results. A summary of conclusions and avenues for future work are given in Chapter 6. Several appendices are included to provide greater detail of procedures, calibrations, uncertainty analysis, and computer programs implemented.

1.3   Contributions

Several contributions have been made through the research in this study:

- Accurate control of intake pressure and repeatable transients are made possible with an electronic throttle and reduced intake manifold volume.

- Expanding the compression ratio test method to incorporate intake manifold pressure for consistent readings with variations in atmospheric pressure.

- Thermodynamic loss angle is measured experimentally using spark noise, to predict top dead center (TDC) relative to the location of peak pressure while motoring, for improved accuracy of combustion analysis.

- Development of a LabVIEW based engine control program with synchronized functions of data logging, on-line combustion analysis, and actuator control, enabling research toward transient operations.

- Providing a simple and quick means of transitioning between SI and HCCI following cold starting or as required otherwise. Only conventional actuation of throttle and CNG injection are utilized to allow implementation on engines without sophisticated controls such as variable valve systems.

- Defining a mode-switching performance criterion (MSPC) to allow for quantitative evaluation of mode-switch effectiveness, thus allowing for optimization and comparison of various control strategies.

Chapter 2

Background Information

Discussion is presented here regarding the general operation of HCCI and its associated benefits and challenges. Suitability of natural gas for HCCI combustion is also explored. Mode-switching is presented as a means of cold starting for an HCCI engine or to widen the limited operating region by reverting to a traditional form of combustion. The proposed mode-switching strategy implementing only conventional controls is introduced along with its intended purpose. Finally, a quantitative means of evaluating mode-switching performance is discussed in comparison to the current subjective standard.

2.1   HCCI Fundamentals

Homogeneous charge compression ignition (HCCI) operates by inducting a homogeneous mixture of air and fuel into the combustion chamber before compression until autoignition. Mixture properties such as fuel composition, equivalence ratio, charge mass, temperature, and residual fraction have a strong influence on autoignition due to the dependence on thermodynamic properties and chemical kinetics during combustion [4–6]. Combustion occurs at many points throughout the compressed mixture simultaneously, demonstrated in Figure 2.1, as opposed to SI where a spark initiates a flame that propagates across the combustion chamber.

Accordingly, HCCI is insensitive to turbulence and swirl whereas these effects have significant influence over SI combustion [7].
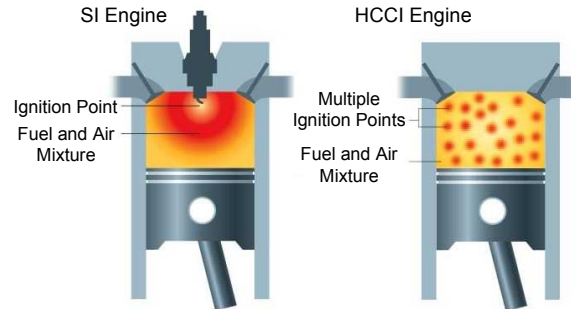
Figure 2.1: Combustion Mode Comparison. Adapted from [8].

2.1.1 Benefits

The primary benefits of HCCI focus on high thermal efficiency and low emissions of NO_x and particulates. High efficiency is related to the high compression ratios similar to CI engines [1, 2]. Lean mixtures limit the maximum rate of pressure rise while also leading to low combustion and exhaust temperatures, preventing the formation of any substantial NO_x emissions [9, 10]. A homogeneous mixture almost completely avoids the formation of particulates as commonly experienced by CI engines [9].

2.1.2 Challenges

While the benefits mentioned above are desirable, the nature of HCCI operation also introduces some challenges.

2.1.2.1 Combustion Timing Control

Combustion timing is not controlled directly as in SI or CI engines, but instead by adjusting the properties of the air/fuel mixture to influence its auto-ignition point during compression. Efficiency is closely related to combustion timing and

rate, suggesting that control of this sensitive event is necessary to realize the fuel efficiency benefit of HCCI operation [2]. Numerical modeling can be used to develop an understanding of HCCI combustion to predict engine outputs [4,11]. Controllers are then developed to utilize different actuators to modify ignition timing to an optimum value, including variable valve timing [12, 13], dual fuels [12–14], split fuel injection during exhaust negative valve overlap [15], reformer gas addition [16], intake air temperature [17,18], and pilot direct injection [19] to name a few.

Of interest among these different options is the range of control possible as well as the time required for adjustments to be made. Intake temperature, for example, is commonly referred to as a "slow" actuator as it requires numerous cycles to vary any significant amount. Fast thermal management installations implementing two intake air streams, one hot and one cool, can achieve faster response with some added complexity [17]. On the other hand, "fast" actuators such as fuel injection pulse width and variable valve systems are able to modify their output on individual cycles for a high degree of control. Use of these fast responding actuators is especially preferred when dealing with the added difficulty of disturbances or changes in operation such as engine speed [20].

2.1.2.2   Load/Speed Limitations

Operational boundaries limit the possible range of power and speed available during HCCI operation. Stable combustion is restricted between the misfire and knock limits as imposed by chemical kinetics and the rate of reaction, preventing the large power range associated with conventional SI engines. Similarly, rate of reaction imposes limitations on the maximum engine speeds at which combustion timing can be adjusted to extract useful work [6]. High boost pressures [21], pilot injection [22], and variable valve timing [23,24] offer some means of expanding the available HCCI operating region.

2.1.2.3 Cold Starting

Cold starting is challenging in the sense that typical HCCI operation depends on several aspects of an operating engine: combustion chamber surfaces are at a higher temperature in a warm engine to reduce heat loss during compression; intake air may be heated using coolant or exhaust gases, neither of which are available in a cold engine; and hot residual gases from previous combustion cycles promote ignition by heating the mixture and providing radicals to initiate chemical reactions. Without these conditions on a cold engine, it becomes difficult to achieve the required autoignition temperature to ignite the air/fuel mixture through HCCI. Preheating the intake manifold with a natural gas burner allows for starting directly into HCCI [17], although requires a lengthy period of time and the use of additional fuel. Using gasoline direct injection, it is possible to ignite one cycle in SI while motoring and use the hot residual to continue HCCI combustion on subsequent cycles [15]. Combustion is not ideal during early cycles, but further development may remedy this situation. This approach, however, does not assist port-injected engines. Fuels with higher autoignition temperatures, such as natural gas, may also experience increased difficulty in achieving HCCI combustion in a cold engine through this approach.

2.1.2.4 Low Temperature Exhaust Gases

Typical HCCI operation involves the use of highly dilute air/fuel mixtures and exhaust gas recirculation (EGR) to limit the maximum rate of pressure rise (ROPR). The resulting low combustion temperatures avoid NO_x generation, but low exhaust temperature becomes a concern when intake heating is implemented to condition the mixture. It is not feasible to run a large electric heater, as used in many studies for simplicity, due to a reduction in overall efficiency. Exhaust heat recovery must be considered with a practical limitation on intake air temperature imposed by the

operating exhaust and coolant temperatures.

2.1.2.5   HC and CO Emissions

Low temperature combustion and the dependence on chemical kinetics introduces potential for partial combustion in the peripheral regions. Compressed gas mixture trapped in crevice volumes or situated near combustion surfaces experience increased heat transfer to the surroundings, reducing mixture temperature below that achieved by the bulk mixture and leading to incomplete combustion [25]. This results in higher emissions of hydrocarbons (HC) and carbon monoxide (CO) in HCCI compared to SI since a larger region is affected. Oxidation catalysts have been shown to convert these chemical species to less harmful components, namely CO_2 and H_2O, with increasing efficiency even with the relatively low HCCI exhaust temperatures [25, 26].

2.1.3   Natural Gas HCCI

Compressed natural gas (CNG) is an interesting fuel for HCCI as it offers single stage combustion with quick burn rates [27]. A high autoignition temperature of approximately 1100 K requires the use of high compression ratio, intake air heating, hot residual exhaust, or a combination of these to achieve combustion.

Natural gas is a common fuel for stationary applications due to its high availability, low cost, and relatively low emissions of CO_2. Comparing the overall operating efficiency of SI and HCCI for power generation suggests that the two may not differ significantly [28]; however, ongoing development of HCCI is likely to improve efficiency further while increasingly strict emissions regulations require costly after treatment of NO_x for SI [29], making HCCI a more appealing alternative. Lean burn SI operation may be implemented to increase thermal efficiency and reduce NO_x emissions, but at the expense of reduced stability and higher emissions of

CO and HC [30]. All three of these emissions may be dealt with by implementing stoichiometric operation with EGR and a three-way catalyst [31], but strict control over equivalence ratio is necessary and fuel efficiency is still limited by a compression ratio necessary to avoid knock. HCCI offers a means of increasing fuel efficiency with CNG while reducing NO_x generation to the point where catalyst reduction of this emission is unnecessary, leaving only development of a suitable low temperature oxidation catalyst necessary to manage CO and HC as discussed above.

2.2 SI-HCCI-SI Mode-Switching

With HCCI prone to issues of cold starting and speed/load limitations, mode-switching is viewed as a method to realize its benefits in real world applications. For automotive, sufficient flexibility in control could allow HCCI operation during low to mid load operation, while relying on traditional SI combustion for cold starting, idling, high speed, and high load scenarios. Achieving this full integration of the two combustion modes requires additional actuation beyond conventional engines, adding to the complexity, cost, and maintenance. On the other hand, applications such as series hybrid vehicles and stationary industrial uses are exposed to more predictable operating speeds and loads over a smaller range [32]. Much of the additional complexity necessary for automotive use may be undesirable if the narrow operating region is designed specifically for HCCI operation and slower transitions are deemed acceptable. In these instances, a method of mode-switching using available actuators is desirable.

Achieving a mode-switch between SI and HCCI generally requires a significant shift in operating conditions. The mixture must be diluted significantly through leaner air/fuel mixtures or EGR addition to limit the rate of combustion in HCCI. Compression temperatures must reach the autoignition point for HCCI to ensue,

and this may be accomplished through a variety of means depending on the actuators implemented and the desired operating conditions. When transitioning back to SI, requirements are much simpler. An acceptable air/fuel mixture along with a suitable spark timing must allow for ignition similar to normal SI operation, and conditions must not be conducive to knock.

2.2.1   Existing Strategies

Variable valve technology has been the focus of significant mode-switching research. Cam-profile switching may be implemented to influence mixture quality by changing the lift and duration of valve events [15,33–35]. Further adjustment of the valve phasing can provide additional means of control: intake valve timing allows for quick variation of air induction, and exhaust valve timing can control the amount of trapped or re-breathed exhaust gases [24,36–40]. Fully variable valves provide flexibility of all valve parameters (timing, lift, and duration) for maximum control over combustion during mode-switching [38,41,42], but with significantly increased cost and complexity.

Other control schemes have also been tested for their ability to assist or initiate mode-switching. External EGR has been shown to reduce knock and combustion noise during the SI-HCCI transition similar to its effect during steady-state HCCI operation [33]. Early testing with fast thermal management and variable compression ratio show potential for mode-switching between SI and HCCI by modifying charge and compression temperatures [43,44]. Dual fuels also offer the capability to switch between these combustion modes by modifying the mixture's autoignition properties [14]. As always, the concern with a dual fuel system is the additional operator effort and infrastructure required to distribute two different fuels. Reformer gas produced on-vehicle from a primary fuel offers potential for controlling HCCI autoignition properties during HCCI operation [4,16], and could likely aid

control during a mode-switch as well. However, production of sufficient quantity to provide the primary fuel during either SI or HCCI operation is likely impractical or inefficient.

2.2.2   Proposed Strategy With Conventional Actuation

For this study, a method of mode-switching is desired using only conventional actuators. Fast controls include CNG mass injected per cycle, CNG injection timing, and throttle angle. Intake temperature and supercharger pressure upstream of the throttle are maintained throughout the mode-switch. Overlapping steady-state operating points for both SI and HCCI are necessary, with late spark timing and throttled operation necessary in SI to avoid knock. The ideology of this approach is that combustion in both modes may not be ideal at the mode-switch conditions, but will be stable. In a real world application, slow actuators would transition to the necessary conditions before initiating the mode-switch, then continue to the desired operating point in the new combustion mode, all while maintaining stable operation.

2.2.3   Mode-Switching Effectiveness

Successful mode-switching with each method described above can generally be tuned to provide a smooth transition over a few cycles under the conditions chosen. Each study contains a different set of operating conditions making comparisons difficult, and further, the extent of potential mode-switching points throughout the operating range of both combustion modes is generally not defined. Profiling the entire SI and HCCI operating region for this purpose is impractical in most research instances, but discussing the limiting conditions and potential for controller development provides some indication of flexibility comparison between methods. It can be reasonably assumed that methods implementing actuators with greater

control (for example, fully variable valves compared to just variable valve timing) or a greater number of useful actuators (for example, variable valve timing and cam profile switching as opposed to variable valve timing alone) will ultimately have a larger range of suitable mode-switching conditions.

Deciding on representative mode-switching conditions to evaluate different control strategies is application specific, but evaluating performance of any particular mode-switch should be relatively the same, where a change in combustion mode (and possibly steady-state power level) is initiated by some change in actuator values. The actuator control strategy remains a developmental issue specific to each engine, but engine response is of concern to the end user and may be viewed similarly for all scenarios.

Fluctuation in IMEP has been suggested to describe the stability of a mode-switch [40], but this does not factor in other important conditions of duration, severity, or repeatability. As there is no well established criterion to quantify mode-switching performance, evaluation is done by means of qualitative descriptions of "smoothness" and "quickness". Individual opinions assess the performance of each set of data differently, leading to inconsistent conclusions. On the other hand, knock and misfire are defined by more concrete definitions as these events are commonly discussed with regards to normal operation. The obvious goal is to avoid undesirable combustion altogether, but if it does occur these are also typically discussed with subjective descriptions of severity and frequency. Although the relative impact of these different aspects on engine operation is difficult to quantify, they may be combined in a consistent way to provide an overall indication of mode-switching effectiveness. This study develops a mode-switching performance criterion (MSPC) for qualitative evaluation of mode-switch effectiveness.

Chapter 3

Experimental Setup and Methodology

In this chapter, the experimental engine is described along with any modifications from previous studies by Hosseini [16] and Handford [19]. Two methods of evaluating intake pressure, cycle averaged and pressure at IVC (P_{IVC}), are introduced. A new control program for the engine is developed to offer synchronized data logging, control, and on-line analysis. Combustion parameters for this system are also defined and discussed. Finally, the developed mode-switching effectiveness criteria is presented.

3.1 CFR Engine Testbed

Testing is carried out on a modified Waukesha Co-operative Fuels Research (CFR) engine. The modifications are detailed in previous studies [16, 19]. This testbed provides a robust system capable of handling heavy knock that may be encountered during experimental work. The system is shown in Figures 3.1 and 3.2 with component descriptions in Table 3.1. Sensor calibration details are given in Appendix D.
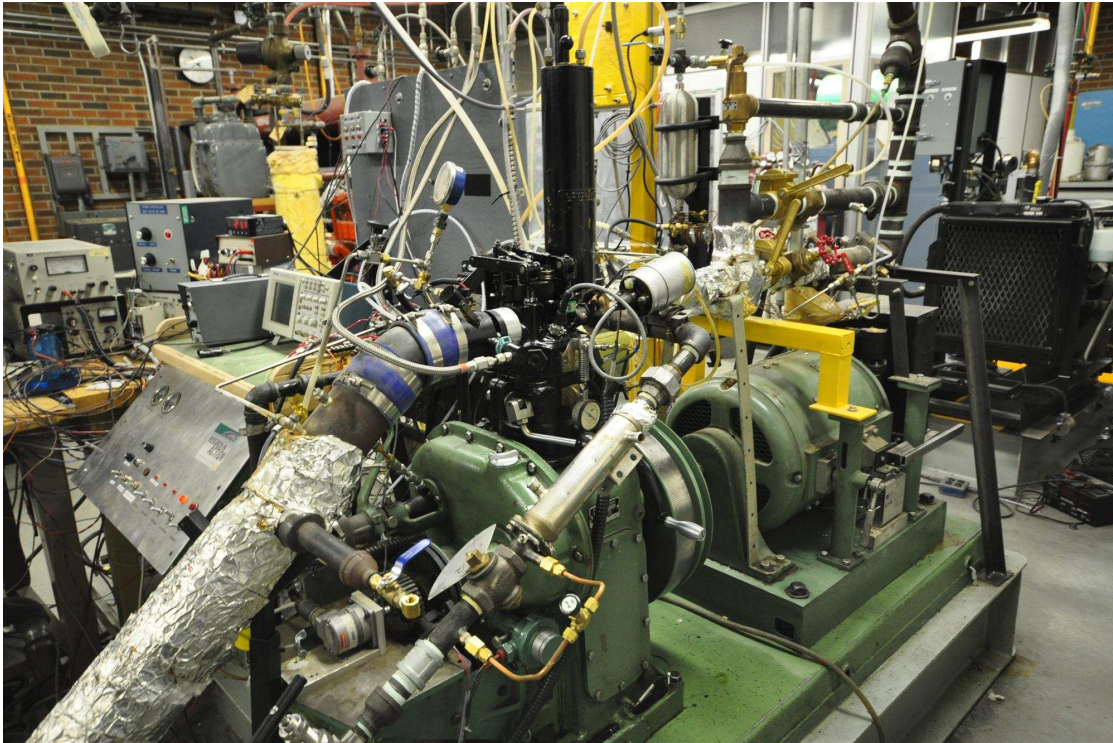
Figure 3.1: Experimental Waukesha CFR engine.

Table 3.1: Description of components used in experimental setup.

Item	Description	Manufacturer	Model
1	Air Pressure Regulator	Lincoln	600008
2	Air Mass Flow Meter	TSI	42350101
3	Pressure Relief Valve	Conbraco Ind.	13-202 (10 psi)
4	Bypass Valve	-	1" NPT
5	210 L Buffer Tank	-	-
6	Electronic Throttle	Woodward	8404-2019 (1" L-Series)
7	3 kW Electric Heater	-	-
8	CNG Fuel Injector	Ford	F5TE-B5A
9	Needle Valve	Swagelok	1/4"
10	Condensing Coils	-	1/4" Swagelok Tubing
11	CFR Engine	Waukesha	Optical Research Head
12	Spark Plug	NGK	BR8HS-10
13	EGR Loop	-	1" pipe
14	EGR Control Valve	Swagelok	SS-12NRF8-G
15	Gate Valve	WOG	2" 200
16	Needle Valve	Swagelok	1/4"
17	Condensing Coils	-	1/4" Swagelok Tubing
18	CNG Mass Flow Meter	Omega	FMA-A2117
19	3.5 L Buffer Tank	-	-
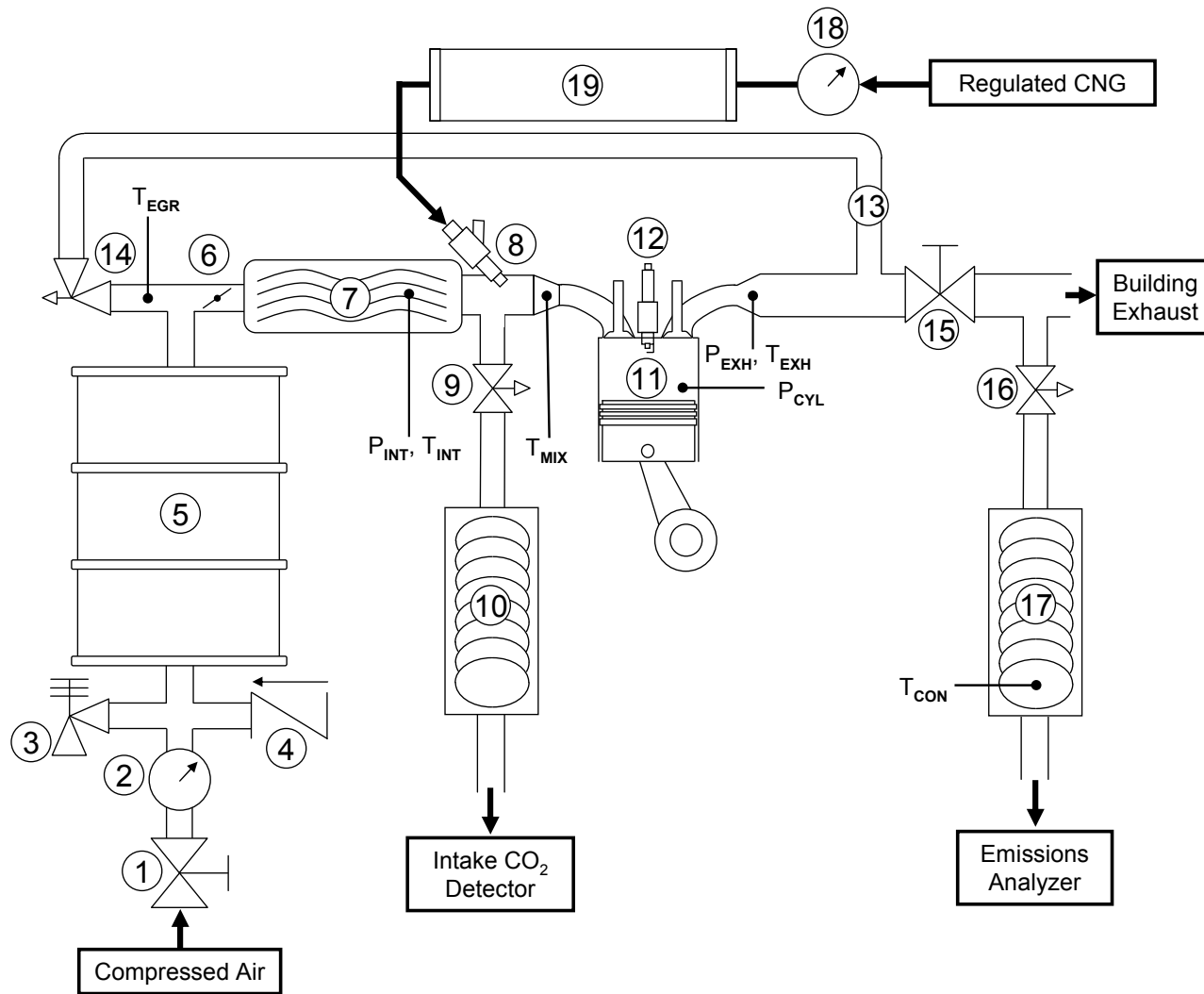
Figure 3.2: Experimental setup schematic diagram. Adapted from [19].

3.1.1 Engine Components

Specifications for the experimental engine are provided in Table 3.2. A Waukesha optical research head is installed to allow several side access ports to the combustion chamber. Cylinder pressure is sampled for detailed combustion analysis using a water cooled Kistler 6043A piezoelectric pressure transducer with the output conditioned by a Kistler 507 charge amplifier. Dynamic calibration of this sensor is detailed in Appendix D. Valve timing remains at the standard values for a CFR engine, shown in Table 3.3. Spark for SI operation is provided through the top port using a NGK BR8HS-10 spark plug and a Bendix Corporation ignition coil, model number 10-57460-100A. Spark timing is controlled with the manually adjustable pickup on the CFR engine and checked with a timing light against the crank position scale on the flywheel, which has been indexed to TDC as discussed in Appendix B.

Table 3.2: Engine specifications [45].

Symbol	Parameter	Value
-	Engine Type	Single-cylinder Waukesha CFR
-	Head Type	Optical Research
-	Combustion Chamber	Disk cylinder head, flat top piston
B	Bore	8.255 cm (3.250")
$2*a$	Stroke	11.43 cm (4.500")
V_d	Displacement	0.612 L (37.33 cu. in.)
l	Connecting Rod Length	25.4 cm

Table 3.3: CFR valve timing in reference to TDC on the compression stroke [45].

Valve Event	Timing
EVO	140° aTDC
IVO	350° bTDC
EVC	345° bTDC
IVC	146° bTDC

3.1.2 Intake System

Intake air is supplied from the room through a bypass valve or from compressed building air if supercharging if desired. Mass flow rate is measured upstream of a 210 L buffer tank in order to reduce flow pulsations and provide accurate readings. An electronic throttle is installed upstream of a large intake manifold, approximately 10 L in capacity, containing an electric heater, fuel injection ports, and various temperature and pressure sensors as indicated. Only room temperature compressed natural gas (CNG) port fuel injection is utilized in this study. EGR is not operated in this study.

Due to the large intake manifold volume, the standard 1" (2.54 cm) throttle body and plate are unable to reduce the intake pressure sufficiently low for SI operation. So, a sleeve with 5/8" (1.59 cm) inner diameter and custom throttle plate are fabricated.

Intake pressure is sampled at 1000 Hz using a Valedyne DP15 pressure transducer. With the large intake manifold, the average reading of all pressure measurements throughout one engine cycle is taken. This provides a relatively linear response with throttle positions of 0-33% as shown in Figure 3.5a. Larger throttle openings show little effect on air mass flow rate and average intake pressure. Mode-switching tests with the large 10 L intake manifold maintain throttle positions within 0-33% with linear demand, as shown in Figure 3.6a, to control air flow into the engine.

3.1.2.1 Modified Intake System and P_{IVC}

For the results in Section 4.7 and subsequent sections, the intake system is modified to reduce the throttled intake manifold volume to 0.5 L, or approximately one displacement volume. Referring to Figure 3.2, this involves moving the throttle (Item 6) and intake pressure sample point (P_{INT}) to the opposite side of the Item

7, a long 8.9cm (3.5") diameter pipe visible in the lower left of Figure 3.1 containing the electric air heater. Copper tubing flowing cool tap water is wrapped around the throttle actuator to prevent overheating in this arrangement, as shown in Figure 3.3. Heat loss through these cooling lines is determined in Appendix C.
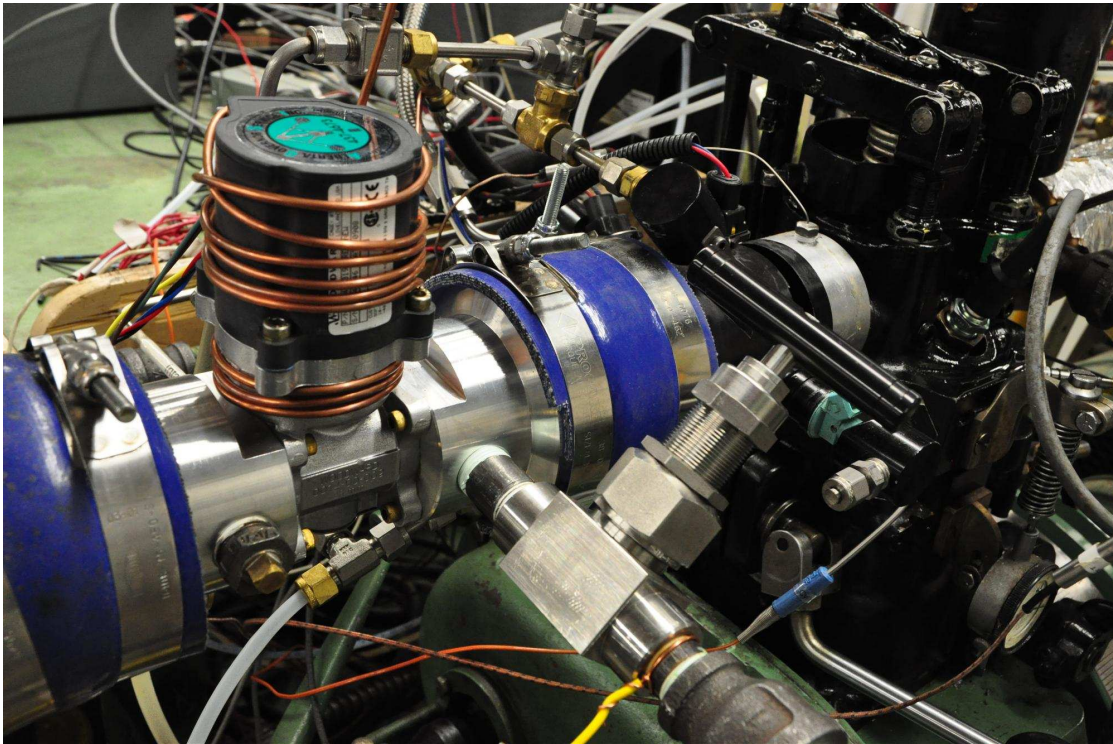
Figure 3.3: Electronic throttle positioned downstream of the intake heater for reduced manifold volume. Copper cooling lines prevent actuator overheating.

The smaller manifold volume is required to provide faster control over air delivery during the transition between the low SI and high HCCI intake pressures. Average intake pressure does not accurately represent the inducted air mass during each cycle due to a large pressure change occurring while the intake valve is closed, thus skewing the average value away from what is experienced while the intake valve is open. Instead, intake pressure is evaluated by taking 5% of the intake pressure readings before IVC and averaging to reduce noise. For example, at 700 RPM there will be 171 pressure readings taken at 1000 Hz in one engine cycle, so 8 of these readings immediately prior to IVC are averaged and recorded as P_{IVC}.

Since these measurements are time-based, fluctuation in engine speed throughout the engine cycle leads to an uncertainty of 1.1 CAD with respect to IVC, as calculated in Appendix E. Figure 3.4 shows the samples averaged for P_{IVC} at different throttle openings.
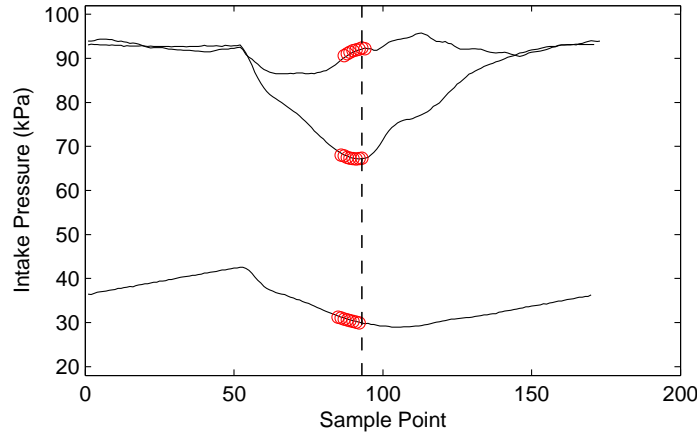
Figure 3.4: Intake pressure while motoring at 700 RPM with various throttle openings. Highlighted samples are averaged to determine P_{IVC}. Vertical dashed line indicates IVC.

Controlling throttle position with a PI to maintain a desired intake pressure becomes more challenging in this modified setup. Throttle performance is evaluated by comparing average intake pressure and P_{IVC} with air mass flow rate while motoring at different throttle positions. Strong non-linearities exist as shown in Figure 3.5b, making PI control through either pressure measurement unstable. By implementing a non-linear demand to throttle position calibration in the Woodward throttle controller, as given in Figure 3.6b, improved linear response is achievable as visible in Figure 3.7 throughout the entire throttle range, thus removing the 33% throttle limition with the large manifold. PI control is now suitable to maintain a desired P_{IVC}, with minor disturbances in supercharger pressure or engine speed resulting in deviations less than 2 kPa.

(a) Large
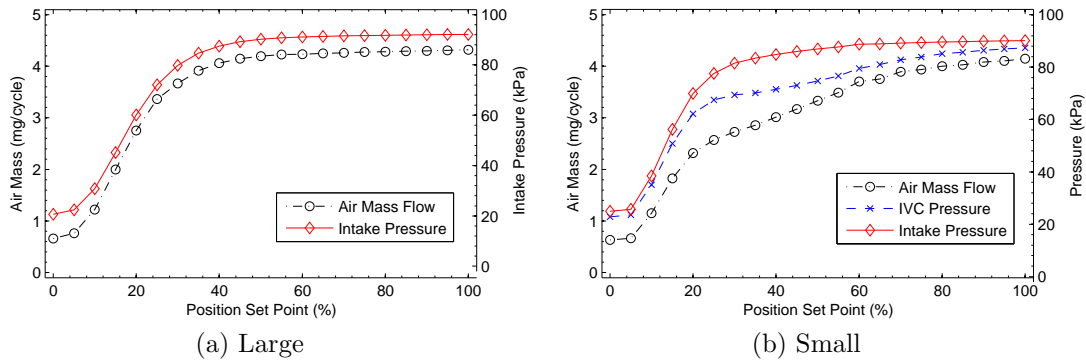
(b) Small

Figure 3.5: Intake response with direct control of Woodward throttle position for both intake manifolds.

(a) Large
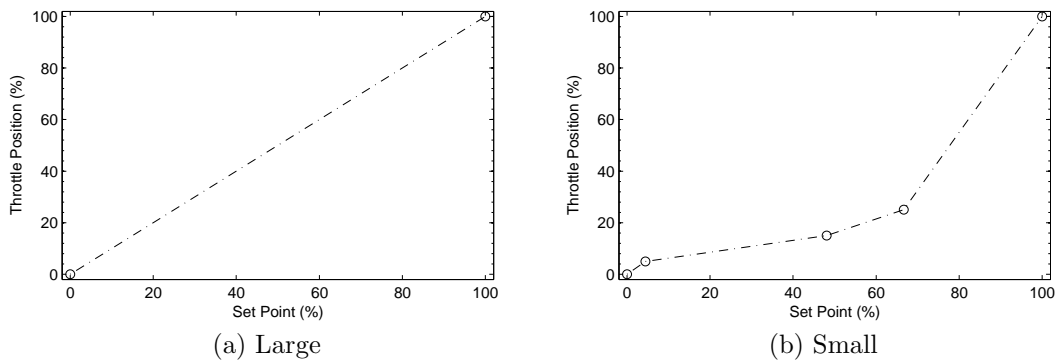
(b) Small

Figure 3.6: Throttle trend implemented in Woodward throttle while testing with both intake manifolds.
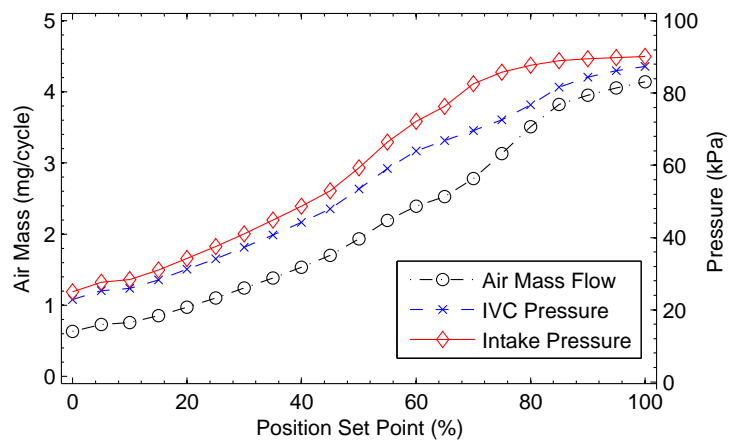
Figure 3.7: Small intake response with non-linear trend programmed in Woodward Throttle.

3.1.3 Exhaust System

Exhaust gases can exit through the building exhaust system or be routed back to the intake through the exhaust gas recirculation (EGR) circuit. A gate valve allows for adjustable back pressure to increase internal EGR fraction and allow EGR while supercharging. For this study, EGR is not utilized and the gate valve remains fully open for all tests. Exhaust gas temperature and pressure are measured 10 cm downstream of the exhaust valve.

3.1.4 Calculated Equivalence Ratio

During testing in Section 4.11, a measure of cycle by cycle mixture quality is needed to show variation between tests. As no lambda sensor is used and the mass flow meters do not respond quickly enough, the mixture quality is approximated by characterizing the fuel delivery with respect to injection pulse width and the engine's volumetric efficiency with respect to the measured P_{IVC}. Equivalence ratio is then calculated using

$$\phi = \frac{m_{\text{CNG}}/m_{\text{Air}}}{(m_{\text{CNG}}/m_{\text{Air}})_{\text{stoichiometric}}} \tag{3.1}$$

where m_{CNG} and m_{Air} are the mass of CNG and air per cycle, respectively. The associated error is discussed in Appendix E. Alternate options exist to measure this quantity directly for improved accuracy if desired in future studies [39].

3.1.4.1 CNG Pulse Width Characterization

Fuel delivery is defined by testing the interdependence of fuel injection pulse width and intake pressure on fuel mass flow rate. Holding the pulse width constant, intake pressure is varied during SI operation to detect any change in CNG flow rate. As shown in Figure 3.8, variation from a constant value is minimal and less

than the calibrated accuracy of the CNG mass flow meter. With this information, CNG mass flow rate is assumed to be primarily dependent on pulse width in the operating region of interest. Again during SI operation but at a constant intake pressure, the injection pulse width ($CNG\,PW$, specified in [ms]) is varied between the lean and rich limits covering the expected range for this study. Figure 3.9 shows a linear trend defined by the best fit line of

$$m_{\mathrm{CNG}} = 1.414\,CNG\,PW - 2.375 \pm 1\,[mg]\,(20:1) \tag{3.2}$$
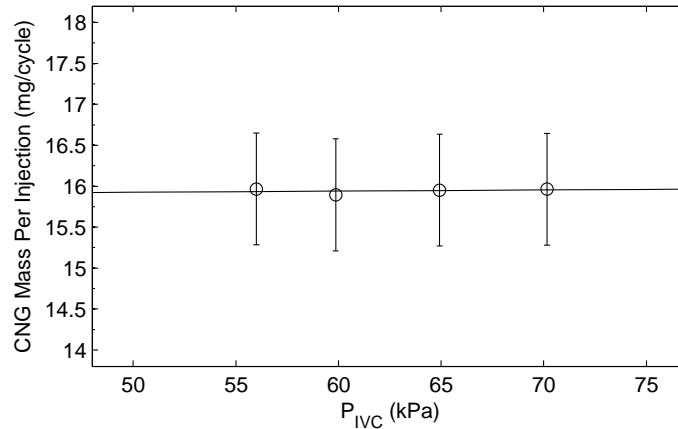
Figure 3.8: Injected CNG mass during SI operation showing very little dependence on intake pressure with a constant injector pulse width. Slope of the best fit line is 0.0013 [mg/cycle kPa].

3.1.4.2 Volumetric Efficiency Characterization

Pressure in the intake manifold is correlated with air mass flow rate using volumetric efficiency [1]. P_{IVC} is used instead of the average intake pressure as it provides a faster response time for approximating the quick and significant changes in air flow experienced during mode-switching. Since the engine can not be run stably in the region between SI and HCCI operation, the volumetric efficiency in this range must be predicted using measurements while motoring. Figure 3.7 presented previously
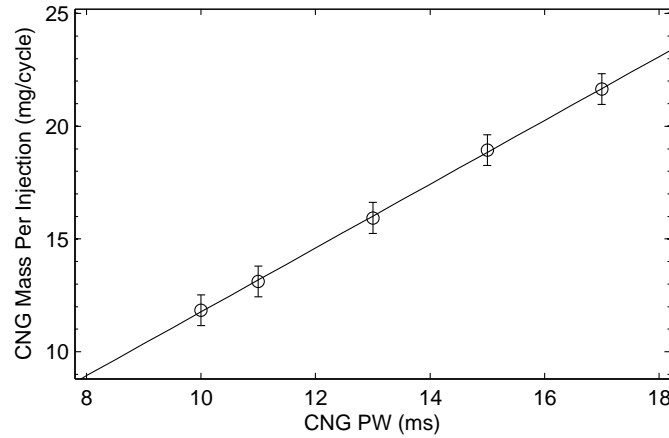
Figure 3.9: CNG mass flow rate during SI operation showing a linear response with injection pulse width at a constant intake pressure.

shows the relation between P_{IVC} and air mass flow rate with respect to throttle position set point; however, to represent the actual test conditions, the procedure is repeated in Figure 3.10 while motoring with the intake air supercharged and heated. The density of the mixture (ρ_{mix}) is calculated at each of these test points using

$$\rho_{\text{mix}} = \frac{m_{\text{air}}}{m_{\text{mix}}} \left(\frac{P_{\text{IVC}}}{R_{\text{air}} \, T_{\text{mix}}} \right) + \frac{m_{\text{CNG}}}{m_{\text{mix}}} \left(\frac{P_{\text{IVC}}}{R_{\text{CNG}} \, T_{\text{mix}}} \right) \tag{3.3}$$

where m is the mass of the indicated constituent, R is the gas constant for air (287.06 J/g °C) or CNG (approximated as methane, 518.27 J/g °C), and T_{mix} is the mixture temperature. Volumetric efficiencies over the range of throttle positions can then be determined using

$$\eta_{\text{vol}} = \frac{\dot{m}_{\text{mix}} \, n_r}{N \, \rho_{\text{mix}} \, V_d} \tag{3.4}$$

with $\dot{m}_{\text{mix}}$ and ρ_{mix} being the mass flow rate and density of the fuel/air mixture, respectively, n_r being 2 rev/cycle for a 4-stroke engine, N being engine speed, and V_d being displacement volume [1]. The results of this procedure are shown in Figure 3.11 with respect to throttle position.
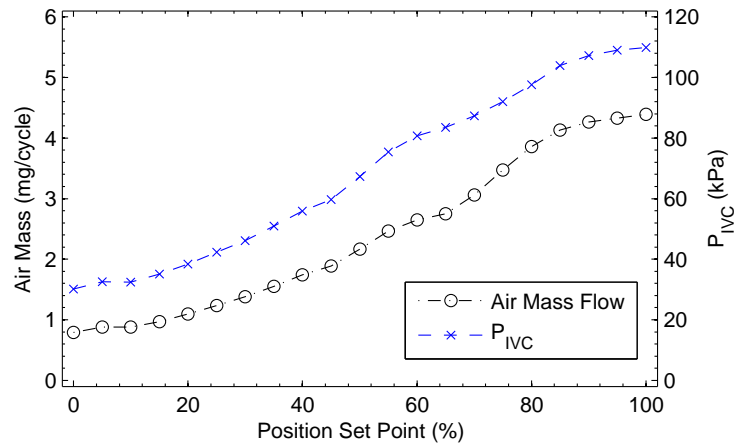
Figure 3.10: Intake pressure response with manifold air supercharged and heated to 140 °C.
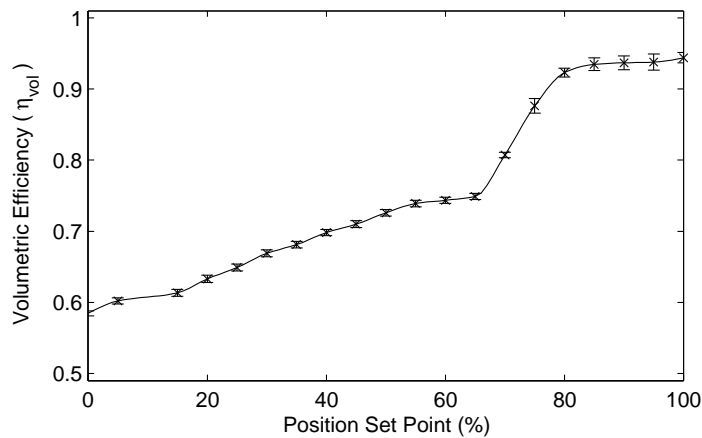
Figure 3.11: Volumetric efficiency while motoring with manifold air supercharged and heated to 140 °C. Error shown is only due to measurement variability. Absolute uncertainty is 0.07 for volumetric efficiency.

Due to limitations with the dynomometer, the engine must be motored at 900 RPM as opposed to 500 RPM used during testing. Adjustments are made to account for this discrepancy. First, the volumetric efficiency is linearly scaled to those measured in test points SI-HCCI 2 and HCCI-SI 4 given in Table 4.10. The throttle position of these test points are then used to scale the P_{IVC} values to the appropriate location in the trend given in 3.10. Figure 3.12 gives the resulting correlation between P_{IVC} and volumetric efficiency. Volumetric efficiencies of other test points from Table 4.10 as calculated from mass flow rates are plotted alongside the predicted results to show the close relationship. Only one point deviates from the trend, HCCI-SI 5 as visible at the upper right corner of the plot, but still falls within the total uncertainty of 0.07 determined for volumetric efficiency in Appendix E.
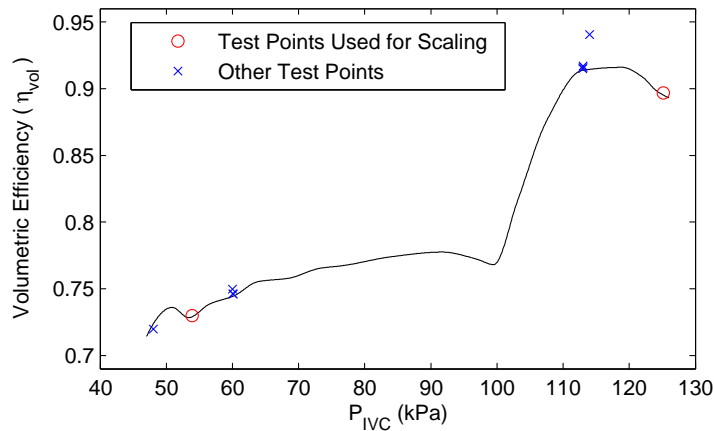
Figure 3.12: Volumetric efficiency at test conditions for Section 4.11. Test points refer to Table 4.10.

During testing, the air mass for each cycle is predicted using these values of η_{vol} based on the measured P_{IVC}. First, the density of the CNG and air mixture is approximated as 1.0 kg/m^3 in order to calculate the total mixture mass by rearranging Equation 3.4 and using T_{mix} as measured with a thermocouple. Air mass is found by subtracting the CNG mass from the total, which is then used to

recalculate the density. The process is repeated until the error in the calculated density is less than 0.1%. To confirm the accuracy of this approach, the air mass flow rate of the other steady-state conditions in Table 4.10 are predicted, with the results all falling within 1.5% of the measured values.

3.2 Engine Data-Logging/Analysis/Control Program

To carry out transient tests for mode-switching, a suitable control program is necessary. Using previous software from Handford and Hosseini as a basis [16, 19], an enhanced control program is developed to meet the following requirements: cycle-based synchronization; data collection from all sensors with on-line analysis to evaluate combustion; feedback capability using calculated parameters; open-loop control of actuators; and data logging of all measurements and calculations. Program operation is summarized in Figure 3.13.

The program is run on a single desktop PC operating with a Pentium IV 2.4 GHz dual-core processor and 2 GB of RAM. The Windows XP operating system is used along with LabVIEW version 7.1.1. All data-acquisition and control is carried out directly from the host PC. Details regarding channel configuration and program functionality can be found in Appendix F.
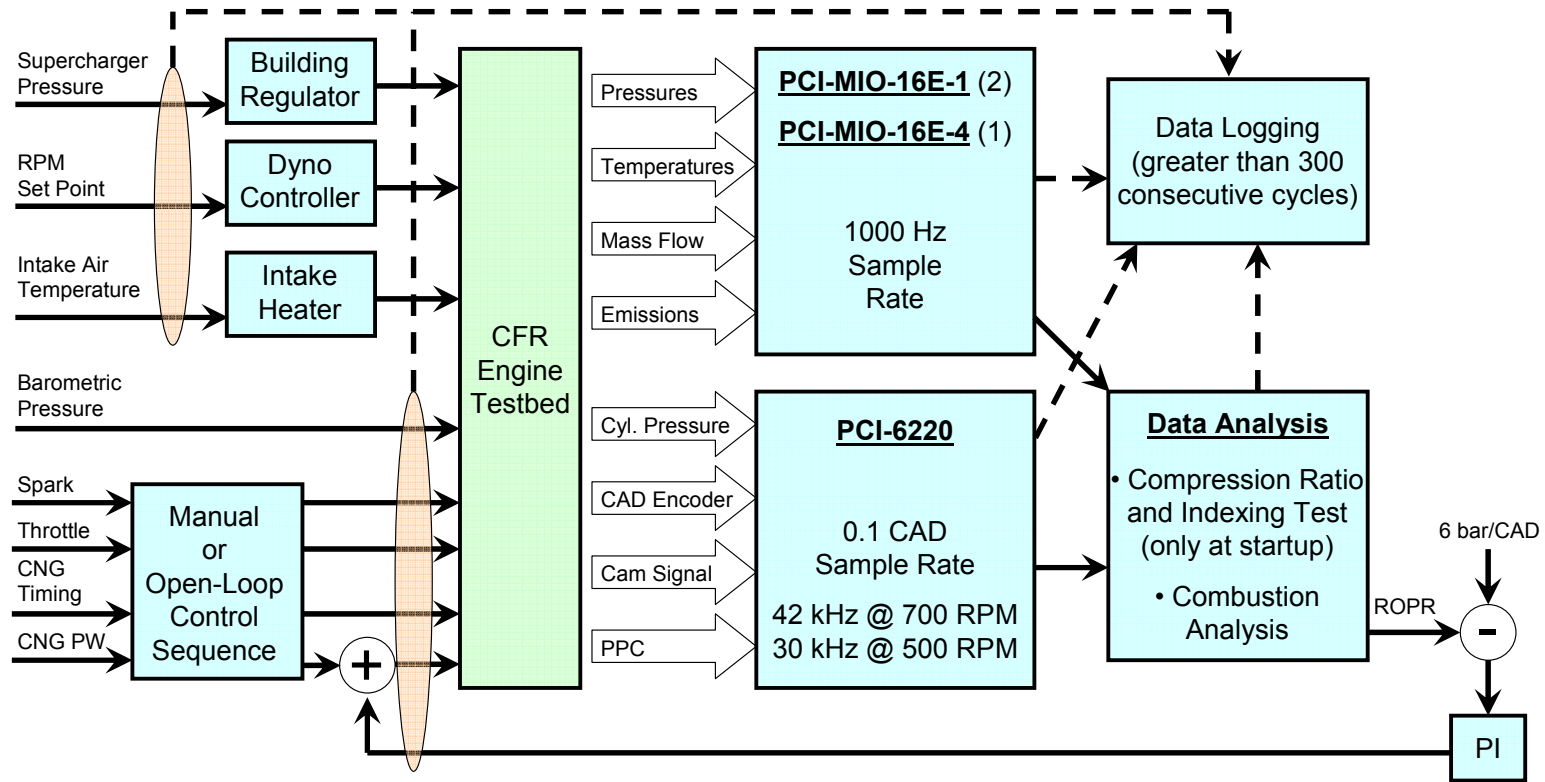
Figure 3.13: Engine Control Schematic.

3.2.1 Injection Timing Limitation

Calculations for evaluating combustion parameters initiate at a common point during the exhaust stroke on every cycle. As the system is busy and an external processor is not used, injection is not possible during this time. The affected region extends from 190° bIVO to approximately 40° bIVO at 700 RPM. As engine speed increases, the calculation time of approximately 14 ms remains unchanged, but the crank angle at which it finishes approaches IVO. To ensure sufficient calculation time and allow for variability, injection timing is restricted to IVO as the earliest point after the calculation period. Injection during the intake stroke is avoided so all CNG is inducted on a single engine cycle and not partially trapped in the intake manifold. Delaying the injection until after IVC incurs a one-cycle delay in fuel delivery. Figure 3.14 summarizes the possible injection timings considering these limitations. The labeled events indicate the limiting cases, while the timing is variable between IVO and the start of processing. Further details pertaining to fuel injection can be found in Appendix F.

3.2.2 Effective Compression Ratio

Compression ratio has a strong effect on combustion and is necessary to evaluate certain combustion parameters. Due to the optical head installed on the CFR engine and the high compression ratios necessary for natural gas HCCI, clearance volume can not be directly measured to determine compression ratio. A means of evaluating the effective compression ratio by comparing peak motored pressure to values obtained from a single zone chemical kinetic model using air as the working fluid was implemented previously [16,19]. Using a similar approach but augmenting intake pressure improves the repeatability despite atmospheric pressure changes. Details are provided in Appendix A.

Compression ratio is not varied throughout this study, but is checked and ad-
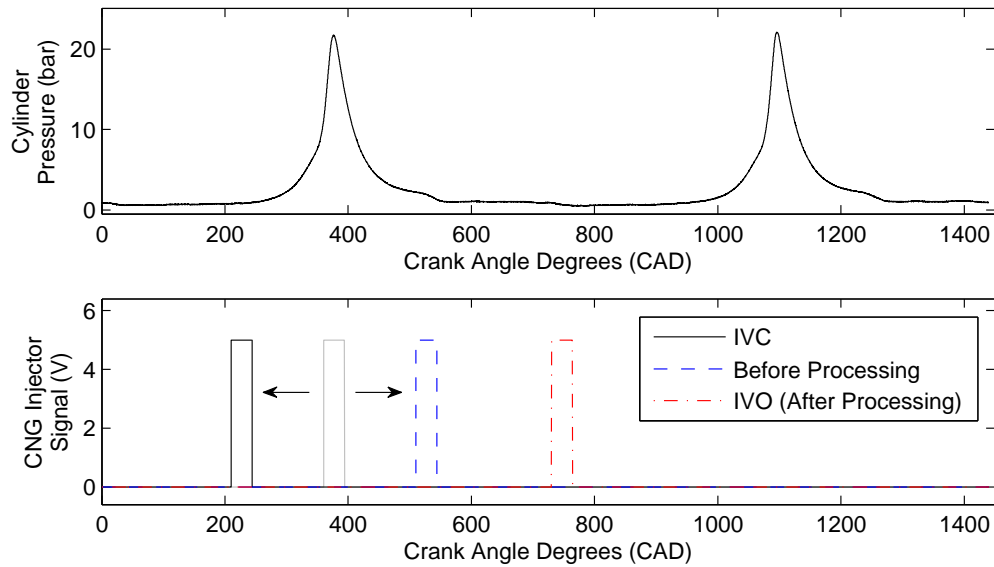
Figure 3.14: Possible CNG injection timings. Fully variable CNG timing between IVC and before processing, but injection not possible during processing before IVO. All injection events here fuel the second cylinder compression/expansion stroke shown.

justed as necessary on a daily basis to ensure it remains at 17.0 ± 0.1.

3.2.3 TDC Indexing

The engine flywheel is indexed to TDC using a dial gauge. Determining TDC in the control program is achieved by comparing the motoring cylinder pressure with an indexing pulse-per-revolution (PPR) signal that has been gated with the cam signal to occur as a pulse-per-cycle (PPC). Curve fitting to determine the peak motoring pressure provides a reference in the engine cycle that is near TDC, but offset by the thermodynamic loss angle (TDLA) [46]. These values have been experimentally determined using noise in the cylinder pressure measurement induced by activating the spark and setting it to occur at TDC. Details of this procedure are presented in Appendix B with discussion of the indexing signals available in Appendix F.

3.3 Combustion Analysis

Combustion timing (CA50), severity (maximum rate of pressure rise, ROPR), and power level (IMEP) are evaluated using the in-cylinder pressure trace, which is sampled at 0.1 CAD. Operating stability is characterized by variation in IMEP (COV_{IMEP}). These parameters are computed using the same methodology as Handford [19] with the exception of a different heat transfer correlation during SI operation for CA50. Detailed error analysis is carried out in Appendix E with a summary provided in Section 3.5 below.

3.3.1 CA50

Combustion timing is represented by the point at which 50% of the fuel has been burned (CA50). Values are presented as crank angle degrees after TDC on the compression stroke (°aTDC). Gross heat release is calculated by adding the calculated net heat release [47] to the heat loss. Since mode-switching between SI and HCCI is the focus of this study, different heat loss correlations are implemented for each mode. SI heat loss is evaluated using the traditional Woschni correlation [48], while a modified Woschni correlation [7] is used for HCCI operation similar to Handford [19]. The appropriate set of parameters is selected based on whether the spark is activated (SI) or not (HCCI).

The effect of CA50 being determined for HCCI combustion but using the SI heat loss relation results in the timing being retarded past the expected value by approximately 5° as shown in Table E.1. During mode-switching, the spark may remain activated for a few cycles where HCCI combustion is clearly evident in the cylinder pressure traces.

During misfire or partial combustion cycles, sufficient heat release may not be available to compute CA50 properly. These cycles are assigned a value of -60° aTDC for CA50. In data figures, these points fall below the displayed axis range

to improve readability of actual CA50 data.

3.3.2 IMEP

Engine power output is evaluated using indicated mean effective pressure (IMEP), which is calculated by integrating the cylinder pressure with respect to volume throughout an engine cycle, then dividing by the displacement volume [1]. This method of representing engine power neglects friction losses that are typically much higher in the CFR engine compared to a modern engine.

Discrete cylinder pressure measurements at 0.1 CAD resolution are made in this study, so IMEP is evaluated using

$$IMEP = \frac{\sum_{i=1}^{7200} P_i \, dV_i}{V_d} \tag{3.5}$$

where P_i is the cylinder pressure at each measurement and V_d is the displacement volume. The change in volume over each 0.1 CAD increment (dV_i) is calculated with the slider-crank relation

$$V = V_c + \frac{\pi B^2}{4}(l + a - a\cos\theta - \sqrt{l^2 - a^2 \sin^2\theta}) \tag{3.6}$$

where V is the cylinder volume for a given angular crank position past TDC (θ), B is the cylinder bore, l is the connecting rod length, and a is the crank swing (half of the stroke). The clearance volume (V_c) is calculated using

$$V_c = \frac{V_d}{r_c - 1} \tag{3.7}$$

where r_c is the compression ratio.

3.3.3 COV_{IMEP}

Stability of the engine is determined by observing the coefficient of variation among calculated IMEP values (COV_{IMEP}). This is done by dividing the standard deviation of a certain number of IMEP (σ_{IMEP}) cycles by the mean IMEP (μ_{IMEP}) as shown

$$COV_{\text{IMEP}} = \frac{\sigma_{\text{IMEP}}}{\mu_{\text{IMEP}}} \tag{3.8}$$

A total of 450 cycles are used to determine COV_{IMEP} for each steady-state operating point. Stable combustion is commonly limited at a COV_{IMEP} of 5% for modern engines [20, 21, 32]; however, a value of 10% is adoped in this study as is typical for research using CFR engines [19, 49].

3.3.4   Maximum Rate of Pressure Rise (ROPR)

Combustion severity or harshness is evaluated using the maximum rate of pressure rise (ROPR) of cylinder pressure. The cylinder pressure trace is first filtered using a low-pass butterworth filter (bidirectional 3rd order with normalized cutoff frequency of 0.10) to remove noise that may otherwise overestimate the degree of harshness, then the point of maximum slope is determined as

$$ROPR = \left(\frac{dP_{\text{cyl}}}{d\theta} \right)_{\text{max}} \tag{3.9}$$

Cycles with ROPR greater than 10 bar/CAD are considered knock as in previous studies [19, 49] and avoided where possible during mode-switching.

3.4   Test Procedure

Prior to starting the engine, the atmospheric pressure in the lab is measured using a mercury barometer and entered as an input to the control program. The engine

is motored at an intake pressure of 65 kPa, spark is activated at 5° aTDC, and fuel is injected at IVC to achieve stoichiometric combustion before switching the dynomometer to "absorb" mode. After running at 700 RPM until coolant temperature reaches steady-state of approximately 98 °C, fuel is turned off and the motor coasts to a stop. The engine is motored again at 1000 RPM with wide open throttle for 5 minutes to allow stabilization of coolant and cylinder wall temperatures. A compression ratio test is completed to measure compression ratio, rising cam edge location, and peak pressure location. Thermodynamic loss angle (see Appendix B) is automatically added to the peak pressure location based on the measured compression ratio to index the location of geometric TDC relative to the pulse per cycle (PPC) signal.

The engine is now ready to begin testing. First, the desired operating point must be achieved. Throttle and fuel are adjusted to initiate SI combustion and the dynomometer is again switched to "absorb" mode. RPM is set at the desired level, the intake heater activated, and building air regulator opened to supercharge the intake system. The engine is allowed to stabilize until mixture temperature (T_{mix}) remains within a $\pm$ 2 °C tolerance before open-loop mode-switching tests are initiated.

When running a mode-switch test, the intake air temperature controller is allowed to stabilize within 1 °C of set point before initiating data collection. After approximately 50 cycles in the initial combustion mode, the open-loop sequence is activated and the engine transitions to the other combustion mode. Data collection continues for a total of 300 cycles to capture the response from the emissions bench.

3.5 Mode-Switching Data Plots - Description and Uncertainties

To represent the repeatability of mode-switching strategies during development, a set of 10 tests are carried out for each open-loop control strategy. Plotting data individually for each test makes comparisons difficult. A method is developed to display all representative data in three figures per set of tests to simplify analysis.

The first figure contains all control inputs during the mode-switch and the IMEP response. Controls include intake pressure as adjusted by throttle position, CNG injector pulse width, and CNG injection timing for some tests. The second figure provides cylinder pressure traces immediately surrounding the mode-switch cycle to show combustion characteristics. The third figure presents the calculated combustion parameters CA50 and ROPR.

One test for each set of 10 is selected and displayed as an example with characteristics that best describe engine behavior. In order to display all 10 tests, shaded regions are used. A lighter colored region displays extremum of the 10 data sets at each cycle. The inner darker colored region displays the range of the 6 values of the data set at each cycle. The standard deviation is not used since the data are not always normally distributed. Using these two regions, visual inspection can be used to determine whether certain deviations are common or occur less than 2 times out of 10 tests. Error bars presented in these figures are not easily visible, so Table 3.4 lists the error for individual parameters as determined in Appendices D and E.

3.6 Mode-Switching Evaluation

Mode-switching is typically evaluated using a qualitative analysis labeling a transition by varying degrees of "smooth" and "quick". The definition of these descriptors varies among researchers, making it difficult to compare various methods of induc-

Table 3.4: Measurement uncertainty at 95% confidence for values presented in mode-switching data plots.

Parameter	Symbol	Uncertainty
Average Intake Pressure	$\epsilon_{IntakePressure}$	2.7 kPa
P_{IVC}	ϵ_{PIVC}	2.8 kPa
CNG PW	-	-
CNG Timing	$\epsilon_{CNGTiming}$	1.1 CAD
IMEP	ϵ_{IMEP}	0.06 bar
CA50 (SI/HCCI)	ϵ_{CA50}	3.1/0.89 CAD
ROPR	ϵ_{ROPR}	0.03 bar/CAD
Equivalence Ratio	$\epsilon_{EquivalenceRatio}$	12%

ing a mode-switch in an engine. A quantitative evaluation of these conditions is needed to provide comparisons between methods as well as a means of optimizing a mode-switch through a tuning process.

Conditions requiring consideration include duration of the transition, IMEP during the transition, and undesirable combustion including knock and misfire cycles. A quantitative evaluation should include a means of monitoring these events and reflect their influence on the overall performance of the mode-switch. Combining these parameters with suitable weighting factors allows for a single mode-switching performance criterion (MSPC) to quantify the performance of the mode-switch, with lower values indicating better mode-switch performance. The MATLAB code developed for this analysis is included in Appendix G.

3.6.1   Duration

The number of cycles required to complete a mode-switch must be defined. The combustion occurring during the period between stable operation in SI and HCCI may consist of hybrid cycles showing characteristic of both forms of combustion. This is interesting from a research standpoint, but the desirable parameter to monitor is the power developed during these transitional cycles. IMEP should, in the ideal case, step from the steady-state level in the initial mode of operation to

the desired steady-state level in the target combustion mode and remain constant thereafter until controlled otherwise. This definition covers all possible mode-switch scenarios, including a step up in power, a step down in power, or maintaining a given power level.

The start of the mode-switch is easily defined as the first cycle after the switch has been commanded by the control system. This is indicated by a change in any actuator from its initial state of stable operation.

Difficulty arises in deciding when the engine shall be considered stable at the new IMEP under the different form of combustion. Because COV_{IMEP} is a common measure for combustion stability, this value should suitably define this condition. By calculating a running value of COV_{IMEP}, the point at which this value drops below some threshold is considered the last cycle of the mode-switch. A COV_{IMEP} of 5% is commonly associtated with the maximum variablilty in IMEP suitable for stable performance, and is adopted as the threshold for this criterion. An exception exists when the state being transitioned into carries a higher steady-state COV_{IMEP} than 5%, suggesting that the mode-switch will never be considered complete based on this criteria. For this study, only Section 4.5 falls into this category, where operation in SI carries a COV_{IMEP} of 11%, dictating the minimum threshold to define the end of the mode-switch.

The number of cycles used to evaluate COV_{IMEP} is determined from early testing. Figures 4.2, 4.6, and 4.10 show a typical transition period of 15 cycles between steady-state IMEP in SI and HCCI combustion modes. This is selected as a suitable period over which to calculate COV_{IMEP} to determine whether the engine has achieved steady-state operation. Smaller numbers of cycles increase the sensitivity of COV_{IMEP} toward variability that may include normal operation in the final state, while larger numbers may predict the mode-switch to be complete sooner than is reasonable. The procedure used to determine duration of the mode-switch

is outlined Figure 3.15.

Initialize:
Duration = 1

IMEP from cycles after mode-switch:
(Duration) to (Duration + 14)

Calculate: $COV_{IMEP} = \sigma_{IMEP} / \mu_{IMEP}$

Compare
$COV_{IMEP} < 5\%$

Duration + 1   No

Yes

Mode-Switch
Duration
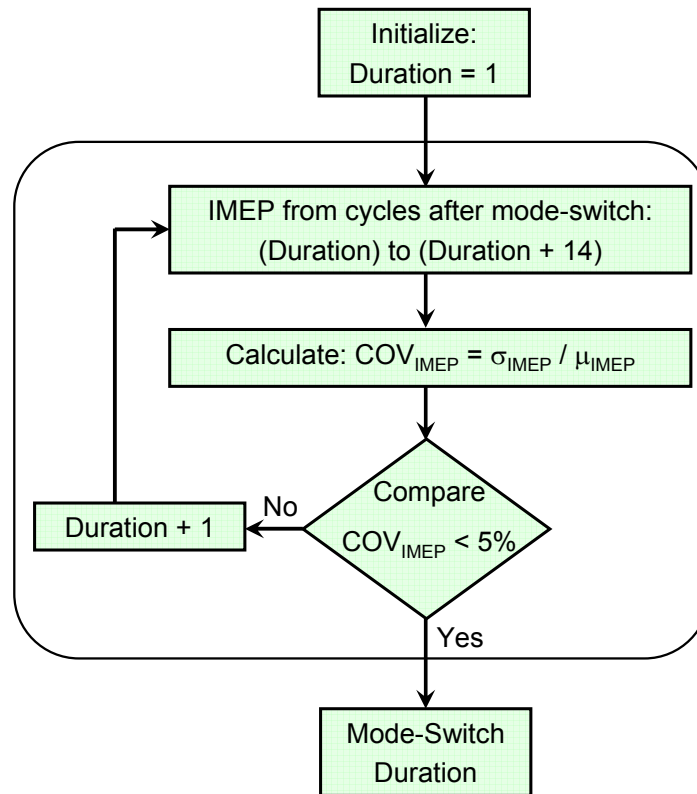
Figure 3.15: Procedure to determine mode-switch duration.

This method of defining mode-switch duration neglects the fact that actuator control may still be occurring to maintain stable operation in the new combustion mode, but this is not of concern in end-use applications. The purpose of an engine is to develop the required power; any actuation to achieve this goal is considered necessary as in all control applications. As the engine stabilizes in the new combustion mode, modifying control parameters should still allow some degree of control. Engine response may be restricted during these early cycles compared to control at a more stable operating point.

3.6.2 Smoothness

Similar to steady-state operation, it is desirable to minimize variability of IMEP from the desired trend throughout a mode-switch. These target values must be defined for a variable number of cycles as determined by the duration above. Steady-state values for IMEP in both the initial and final combustion modes can be evaluated as the average of the same 15 engine cycles for which COV_{IMEP} is calculated. For the intermediate cycles during the mode-switch, a linear progression is chosen to represent the smoothest transition.

Comparing experimental IMEP to this target trend, a transient form of COV_{IMEP} is calculated. Instead of computing standard deviation with an average IMEP, the residuals are considered for each cycle throughout the duration using

$$\sigma_{\text{IMEP\_trans}} = \sqrt{\frac{1}{Duration} \sum_{i=1}^{Duration} (IMEP_{\text{actual}} - IMEP_{\text{target}})^2} \qquad (3.10)$$

Mean IMEP for the mode-switch ($\mu_{\text{IMEP\_trans}}$) is the average between the initial and final states

$$\mu_{\text{IMEP\_trans}} = \frac{IMEP_{\text{initial}} + IMEP_{\text{final}}}{2} \qquad (3.11)$$

Finally, $COV_{\text{IMEP\_trans}}$ is evaluated as

$$COV_{\text{IMEP\_trans}} = \frac{\sigma_{\text{IMEP\_trans}}}{\mu_{\text{IMEP\_trans}}} \qquad (3.12)$$

3.6.3 Knock

High rates of pressure rise lead to harsh combustion having several drawbacks. Advanced combustion timing is typically associated with knock in HCCI and may lead to less efficient operation, significantly increased NO_x emissions, higher peak pressures, audible noise, and potential engine damage.

Similar to steady-state operation, ROPR is used to detect knock. Any cycles producing ROPR greater than 10 bar/CAD are considered knock cycles. A penalty is applied for each of these cycles during the mode-switch thereafter until knock propagation has ceased. The end of this stabilization period is determined, similar to the duration parameter, through a 15 cycle running check for knock.

3.6.4   Misfire

Misfire cycles occur when the air/fuel mixture does not ignite. This results in a negative IMEP value and a significant disturbance in power output and emissions. Partial burn cycles are also of concern in HCCI where only a portion of the fuel energy is released, leaving a large portion unburned with the associated reduction in power delivery. Both of these conditions will influence the smoothness parameter as described above, but a further penalty may also be deemed necessary.

3.6.5   Weighting Factors

Combining the above factors into a single value to describe mode-switch performance introduces the possibility of weighting the components differently. Duration is chosen as the basis with each cycle during the transition carrying a weight of 1.

Smoothness is calculated similar to steady-state operation where a commonly accepted COV_{IMEP} of 5% dictates the stability limit. As such, $COV_{\text{IMEP\_trans}}$ can be normalized around 5% with any value greater than 1 incurring a penalty. A weighting of half the duration is found to correlate with qualitative evaluation and provide a duration-sensative component for proportional penalties.

Knock is considered when ROPR exceeds the threshold value of 10 bar/CAD, with any offending cycles incurring a penalty. Since knock is associated with potential engine damage, a more severe penalty is necessary. The degree of knock is taken into account by applying a linear penalty of 1 for every 2 bar/CAD over

the threshold at each knock cycle. This weighting is not dependent on duration as knock is event specific and not a relative measure such as smoothness.

Misfire cycles already carry a heavy penalty based on the smoothness criteria, with partial burn cycles incurring a proportionally smaller impact. A further penalty for misfire cycles is deemed unnecessary at this point.

All conditions are combined to determine the MSPC using

$$
MSPC = \begin{cases} Duration \\ + \dfrac{Duration}{2} \left(\dfrac{COV_{\text{IMEP\_trans}}}{0.05} - 1 \right)_{COV_{\text{IMEP\_trans}} > 0.05} \\ + \dfrac{1}{2} \left(\displaystyle\sum_{i=1}^{Stabilize} ROPR_i - 10 \right)_{ROPR_i > 10} \end{cases} \tag{3.13}
$$

The weight factors being applied here may be considered to be application specific; however, this may not be the case. For example, large industrial engines with high flywheel mass are less sensitive to IMEP variability than small automotive engines. These two applications also require different levels of response time, with smaller automotive-type engines being required to reach the new operating mode and desired power output much more quickly than heavy industrial engines. Knock follows the same trend with industrial engines being less prone to damage than smaller engines. With all conditions having more stringent requirements for automotive in comparison to industrial engines, this suggests that the needs of different applications may be met by specifying a different minimal level of MSPC to design toward as opposed to shifting the weighting factors.

Chapter 4

SI-HCCI-SI Mode-Switch Results

The primary objective of mode-switching is to transition between combustion modes. This chapter focuses on developing an open-loop strategy to transition between SI and HCCI at 700 RPM in a smooth and quick manner using only conventional actuators: throttle, CNG injection pulse width, and CNG injection timing. The mode-switching performance criterion (MSPC) described in Chapter 3 is used to highlight areas where attention is necessary for improvement. After optimizing the control strategy based on MSPC to a one-cycle step in IMEP between combustion modes, stability is evaluated by quickly repeating mode-switches. Flexibility is explored by profiling various levels of IMEP before/after the mode-switch at a slower engine speed of 500 RPM.

4.1 Steady-State Operating Conditions - Large Manifold

To examine mode-switching, compatible SI and HCCI steady-state operating points are found. The requirement for compatibility is that parameters such as intake temperature that can not be changed quickly must be similar for both modes. It can be difficult to find compatible points since a high intake temperature leads to knock in SI while a low intake temperature may result in HCCI ignition not occurring. Two operating points, shown in Table 4.1, are one example of compatible points

that will be used for testing with the large intake manifold.

Intake pressures are chosen based on a throttling limitation in SI for the super-charger pressure required for HCCI operation. Throttle openings greater than 33% have little influence on intake pressure due to the large intake manifold volume and are avoided to simplify control.

Late spark timing of 5° aTDC is required in SI mode since the intake tempera-ture is high (115 °C). This leads to late combustion timing of CA50 = 48° aTDC. Stability in SI mode is poor as indicated by the COV_{IMEP} of 11% slightly above the misfire limit of 10%. To allow HCCI operation at the same intake air temperature, the combustion instability of 11 % is accepted as a compromise.

Operating in HCCI at this point is also not highly stable due to the low in-take temperature. With CNG pulse width (CNG PW) set to the value shown, the engine may eventually misfire or knock after a period of time. A manually tuned PI controller applies adjustments to the nominal CNG PW to maintain ROPR at 6 bar/CAD. Slow response is attained through gains of 0.120 for proportional and 0.050 for integral, while variability in HCCI combustion is handled by aver-aging ROPR over 5 previous cycles for the reference value. These settings remain unchanged throughout testing.

4.2   SI-HCCI: Intake Pressure - Step Increase

Achieving the new steady-state conditions as quickly as possible using open-loop tuning of CNG amount and throttle position is the first mode-switch strategy. The throttle is opened over 3 cycles for a compromise between intake pressure response time and overshoot, while CNG delivery is adjusted to maintain suitable combustion throughout the transition. The sequence of fuel values is developed by iteration through repeated switching and manual tuning. Fuel delivery is initially set low on each cycle to induce misfire rather than knock, with successive tests

Table 4.1: Steady-state operating conditions for mode-switching tests - large (10 L) intake manifold.

Set Points	SI	HCCI
CNG System Pressure	5.5 bar	5.5 bar
Effective Compression Ratio	17.0	17.0
Engine Speed	700 RPM	700 RPM
Intake Air Temperature	115 °C	115 °C
Intake Pressure	53 kPa	120 kPa
Spark Timing	5° aTDC	-
Actuators		
CNG Injection Timing	520° bIVO	520° bIVO
CNG Pulse Width	10.4 ms	~12.0 ms
Throttle Position	6%	33%
Measurements		
Air Mass Flow	1.3 g/s	3.4 g/s
CNG Mass Flow	76 mg/s	90 mg/s
Equivalence Ratio	1.0	0.46
Exhaust Pressure	91 kPa	92 kPa
Exhaust Temperature	460 °C	250 °C
Mixture Temperature	97 °C	101 °C
Calculated		
CA50	48° aTDC	9° aTDC
COV_{IMEP}	11%	4%
IMEP	2.6 bar	4.5 bar
ROPR	0.9 bar/CAD	6.0 bar/CAD
Thermal Efficiency	25%	36%
Exhaust Emissions		
Carbon Monoxide (CO)	0.09%	0.07%
Carbon Dioxide (CO_2)	11%	4.5%
Hydrocarbons (HC)	1500 ppm	3600 ppm
Oxides of Nitrogen (NO_x)	670 ppm	40 ppm
Oxygen (O_2)	2.3%	13%

increasing CNG PW until suitable combustion quality is achieved. Combustion quality is evaluated through IMEP, CA50, and ROPR to detect when combustion is deteriorating to either misfire or knock, with the desired response being to approach the steady-state values as quickly as possible while maintaining ROPR at less than the 10 bar/CAD knock limit. Adjustments to the fuel sequence are made according to the following methodology:

- IMEP too low - more fuel on given cycle and possibly previous cycles

- CA50 advances/retards - decrease/increase fuel on given cycle and future cycles

- ROPR too high - reduce fuel on given cycles (typically correlates with advancing CA50)

- ROPR too low (approaching misfire) - increase fuel of surrounding cycles (typically correlates with retarding CA50)

The above conditions are interrelated to one another, so a compromise is necessary to maintain combustion and minimize knock and/or misfire.

A set of 10 mode-switch tests are performed with a sample set of results shown in Figure 4.1. IMEP has a narrow range for the first 5 HCCI cycles showing repeatable performance; however, IMEP is not stable during subsequent HCCI operation with several tests experiencing partial burn cycles. To alleviate this problem, the PI control for CNG PW introduced in Section 4.1 is activated on the fifth HCCI cycle, after the highly transient portion of the mode-switch. The drawback of this PI implementation is the necessity for sampling cylinder pressure to calculate ROPR as the reference value. This requires the use of an in-cylinder pressure transducer that does not exist in typical engines, but is a common requirement for HCCI control schemes. Substituting this condition with other knock detection

techniques, such as a vibration sensor or ion current sensing with the available spark plug [50–52], could provide similar results.
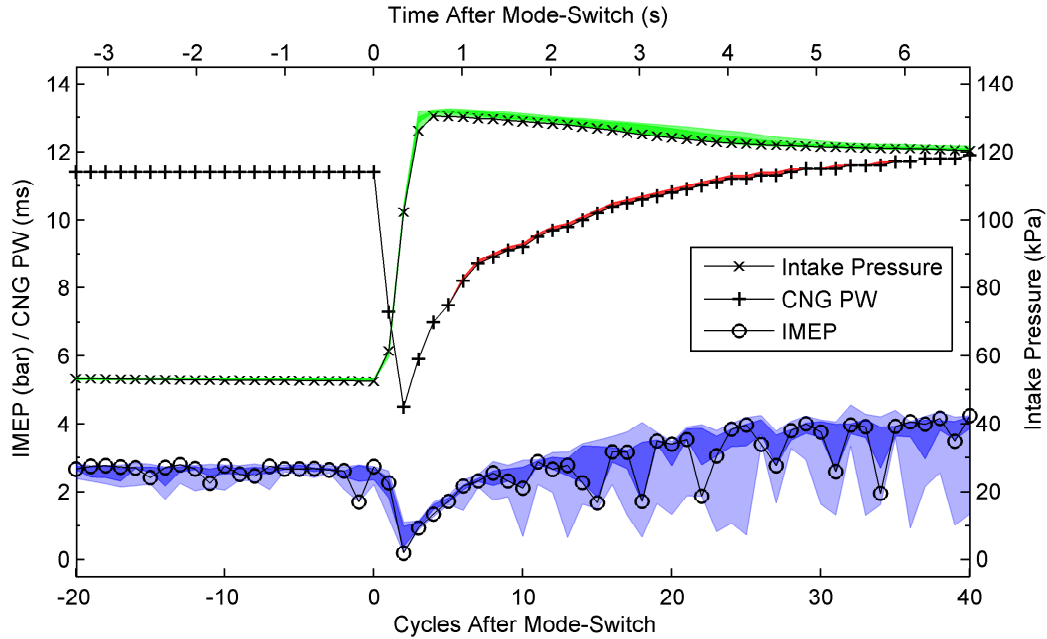
Figure 4.1: SI-HCCI mode-switch using step increase in intake pressure without feedback control. $\epsilon_{IMEP} = 0.06$ bar, $\epsilon_{IntakePressure} = 2.7$ kPa

Repeating the test but with the PI active after cycle 5 is shown in Figure 4.2 indicating much less variation in HCCI IMEP. Similar to Figure 4.1, there is a drop in IMEP during the first 7 cycles of the HCCI mode. Lower CNG delivery during this period correlates with the reduced power, but further investigation is necessary to understand why the low fuel delivery is necessary. To do this, the cylinder pressure traces immediately surrounding the mode-switch (cycles -1 to 7) are plotted in Figure 4.3 and a shift in combustion timing is apparent during the shift from SI to HCCI. Figure 4.4 indicates that CA50 advances before TDC initially after the mode-switch, then gradually retards back to the steady-state value of 9° aTDC in HCCI mode. The first cycle demonstrating HCCI combustion (HCCI 2), having a steep pressure rise near TDC, contains hot SI residual gases from the previous cycle (HCCI 1) resulting in early combustion at a reduced intake

pressure compared to steady-state [41]. Subsequent HCCI cycles have an intake pressure slightly above the desired intake pressure of 120 kPa and have HCCI residuals present, yet continue to produce early combustion timing with very lean mixtures. ROPR is maintained below the knock limit of 10 bar/CAD (except for a few occurrences near cycle 25 and 35) with the low CNG PW shown in Figure 4.2, but at the expense of reduced IMEP. This behavior is attributed to the hot combustion chamber surfaces and a hot exhaust valve (from SI mode) promoting early ignition [24, 40]. This advanced combustion following a mode-switch from SI to HCCI needs to be counteracted in future tests to achieve a smoother transition and will be considered in the next section.
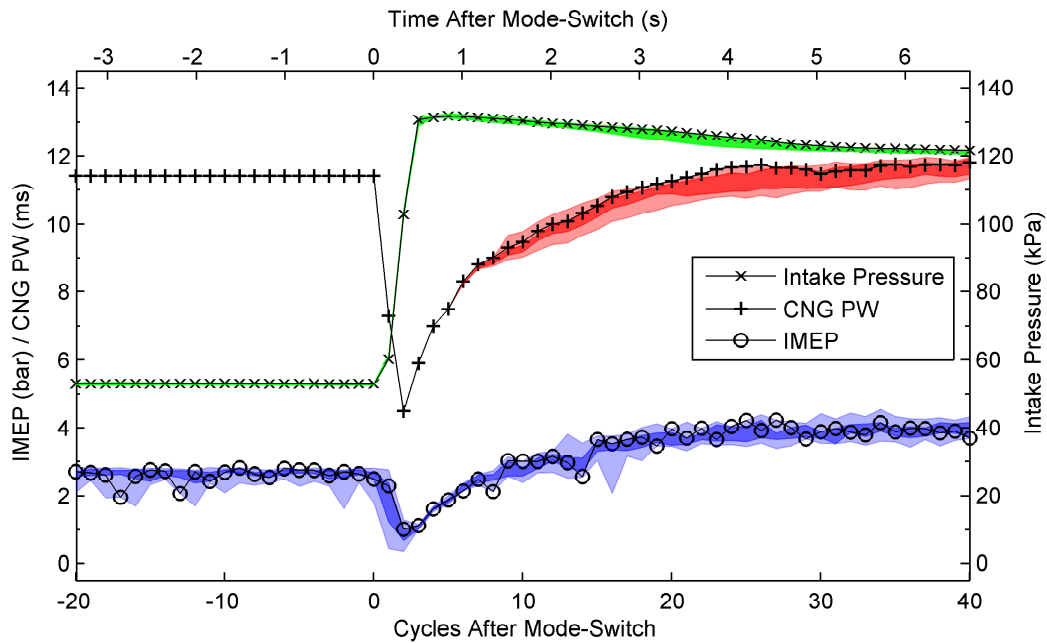
Figure 4.2: SI-HCCI mode-switch using step increase in intake pressure with PI control of fuel activated after 5 HCCI cycles[1]. $\epsilon_{IMEP} = 0.06$ bar, $\epsilon_{IntakePressure} = 2.7$ kPa

---

[1]CNG PW during steady-state SI operation is 11.4 ms instead of 10.4 ms as in other tests with the large manifold. Rich operation is confirmed by increased levels of HC and CO in the exhaust measurements. This setting was chosen to achieve a stoichiometric mixture based on the mass flow rates of CNG and air. Calibration error and/or variation in CNG composition [53] are potential causes for this discrepancy.

Figure 4.3: In-cylinder pressure traces during SI-HCCI mode-switch using step increase in intake pressure with PI. The arrow indicates cycle progression. Stars indicate CA50.

Figure 4.4: CA50 and ROPR during SI-HCCI mode-switch using step increase in intake pressure with PI using ROPR of 6 bar/CAD as the target parameter. ϵ_{CA50} = 3.1/0.89 CAD (SI/HCCI), ϵ_{ROPR} = 0.03 bar/CAD

Mode-switching effectiveness is evaluated using the MSPC outlined in Chapter 3. Individual IMEP data for each of the 10 tests is provided in Figure 4.5 along with the calculated MSPC components in Table 4.2. These results support the observable performance discussed above, with the drop in IMEP during early HCCI operation causing a significant penalty in the smoothness value (higher values indicate less desirable mode-switch performance).

Figure 4.5: IMEP data from Section 4.2 to evaluate smoothness for MSPC. Experimental data sets are shown with the desired trend.

Table 4.2: MSPC data for Section 4.2.

Test Date	Test Number										Average	Standard
2010_03_17	17	18	19	20	21	22	23	24	25	27	Average	Deviation
Duration	16	19	16	15	18	16	22	34	23	20	19.90	5.65
Smoothness	40.80	40.17	33.40	35.89	49.08	38.45	38.48	45.62	43.38	37.75	40.30	4.66
Stabilize	16	19	16	15	18	26	22	34	23	20	20.90	5.76
Knock	0.00	0.00	0.00	0.00	0.00	1.01	0.00	0.00	0.00	0.00	0.10	0.32
MSPC	56.80	59.17	49.40	50.89	67.08	55.46	60.48	79.62	66.38	57.75	60.30	8.86

4.3 SI-HCCI: Intake Pressure - First-Order Increase

A method to avoid HCCI cycles having combustion timing that are too advanced (CA50 bTDC) immediately following an SI/HCCI mode-switch is investigated. One approach to retard HCCI combustion timing is to reduce compression temperatures, thus delaying the point where auto-ignition conditions are achieved. Lower intake pressure reduces the total mass of gases inducted into the engine equating to lower compression temperatures. To implement this on the engine, intake pressure is increased at a slower rate than the previous test and the fuel sequence is determined using the same criteria. To constrain the number of variables for manual tuning, the intake pressure is increased at a rate dictated by a step increase in throttle position. The large intake manifold produces a first-order increase in intake pressure with a time constant that varies with the magnitude of step in throttle position.

The timing of the throttle step with respect to the mode-switch is now an added parameter that must be determined. In the previous test, the large increase of intake pressure between two cycles provided a trigger to switch to HCCI. In this case with a slower pressure rise, however, no such trigger exists. If the switch is made too early, then subsequent HCCI cycles are highly sensitive to intake pressure and CNG PW, and not easily maintained between misfire and knock with open loop control. If the mode-switch is delayed too long after the throttle step, then knock may occur. Through testing, it is found that inducing HCCI combustion on the fourth cycle after initiating the mode-switch provides the smoothest transition with open-loop control.

Deciding on the fuel delivery during the initial 5 cycles after the throttle step is more difficult than in the previous test since these cycles fall outside normal SI and HCCI operating regions and neither mode of combustion is stable. An approach of supplying progressively leaner mixtures is implemented to gradually promote HCCI combustion by reducing the cooling effect of room temperature CNG injected into

the hot intake air. The natural tendency toward advanced combustion found in Section 4.2 should be beneficial in this scenario by promoting HCCI ignition during these unstable cycles. The spark remains on during the initial 5 cycles after the throttle step to further promote ignition.

Figure 4.6 shows that this strategy with a slower intake pressure rise presents an improvement over the previous tests in Section 4.2 as the drop in IMEP is removed. Higher combustion variability in CA50 is apparent during the first few cycles, particularly cycle 3 after mode-switch. Figure 4.7 confirms this with combustion occurring late in SI mode for the first 2 cycles and little apparent combustion in the third cycle. Starting with the fourth cycle, HCCI combustion occurs with late CA50 timing. CA50 and ROPR shown in Figure 4.8 support this observation with CA50 quickly advancing on the third cycle and ROPR increasing thereafter - note that the step in CA50 between cycles 5 and 6 after mode-switch is attributed to a change in Woschni coefficients as the spark is turned off.

High sensitivity to the amount of fuel delivered each cycle is experienced using this method, making it difficult to develop an open-loop sequence. Combustion during the unstable cycles early in the mode-switch sometimes produce misfires while other cycles ignite normally or even knock slightly. As is visible in the CNG PW values at cycles 2-3, adaptive adjustment is necessary during the 10 tests since in consecutive tests combustion deteriorated on the third cycle.

HCCI combustion is influenced by previous cycles through the exhaust residual and this coupling of cycles can lead to unstable combustion dynamics. For example, some tests progress to knock while others transition to late combustion timing and misfire.

With the reduction in IMEP removed from the initial 7 HCCI cycles, the smoothness criteria for MSPC shown in Table 4.3 is reduced by 26.8 compared to the previous tests in Table 4.2. The average MSPC is reduced by half primar-
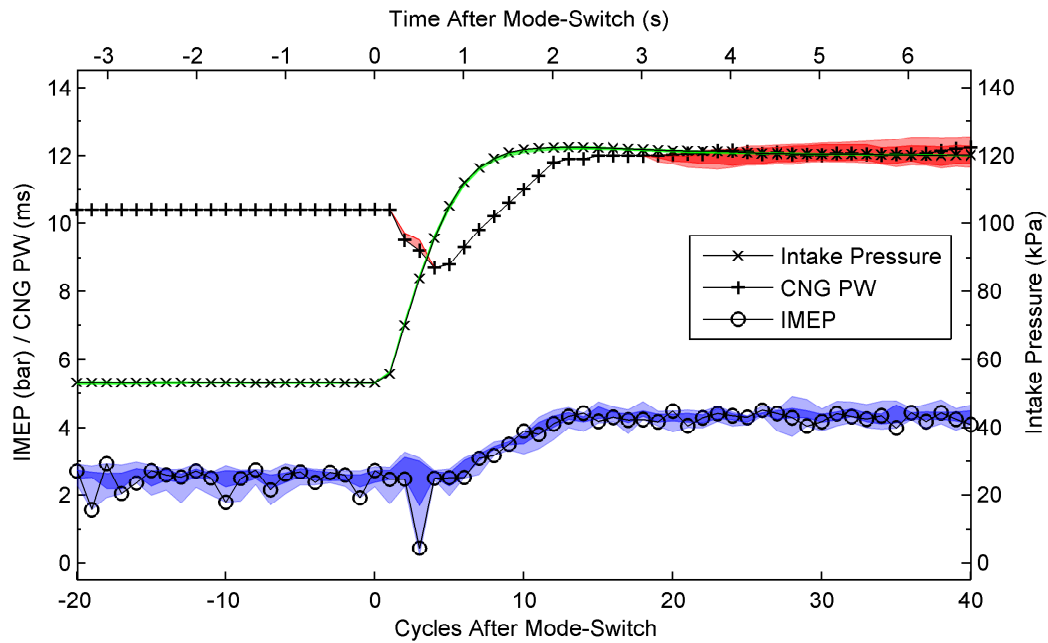
Figure 4.6: SI-HCCI mode-switch using a step increase in throttle position. ϵ_{IMEP} = 0.06 bar, $\epsilon_{IntakePressure}$ = 2.7 kPa
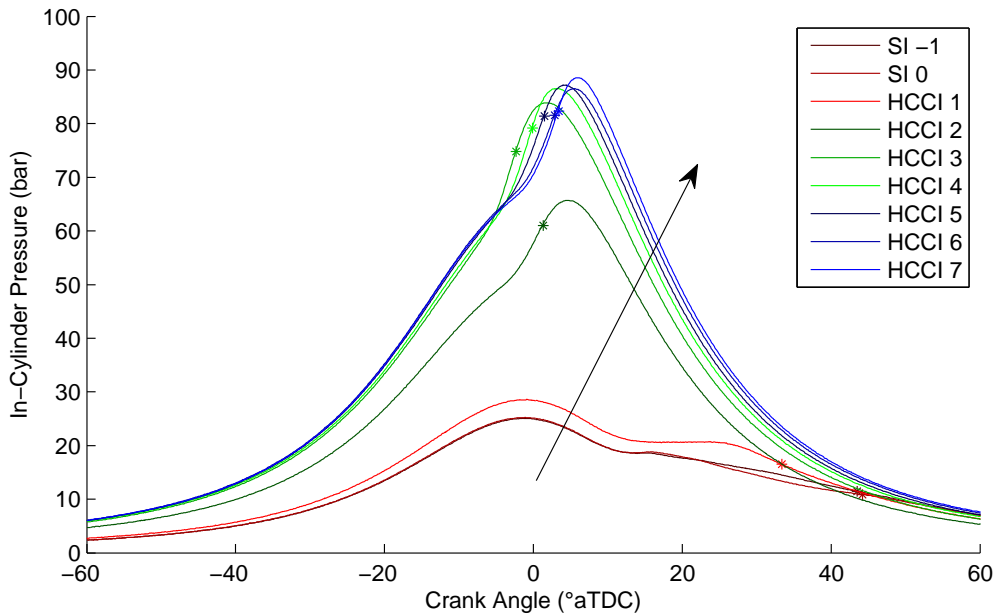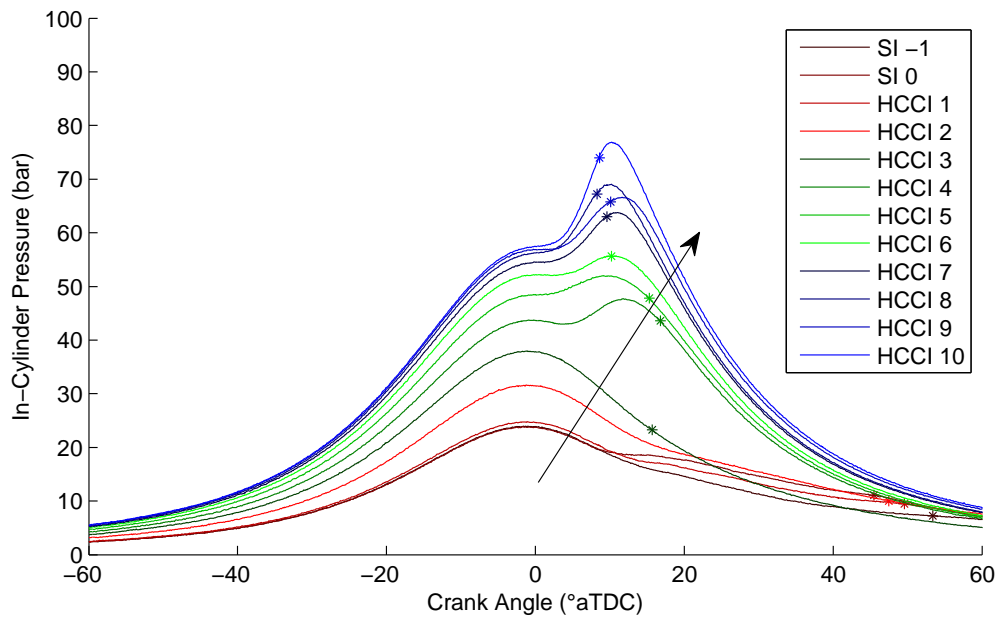

Figure 4.7: In-cylinder pressure traces during SI-HCCI mode-switch using a step increase in throttle position. The arrow indicates cycle progression. Stars indicate CA50.
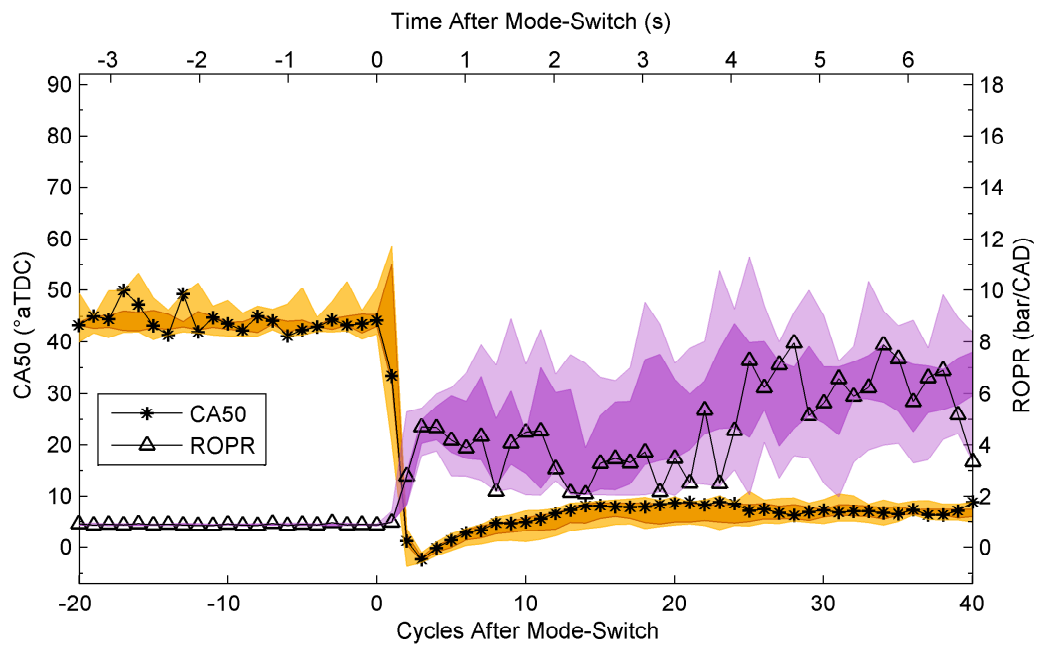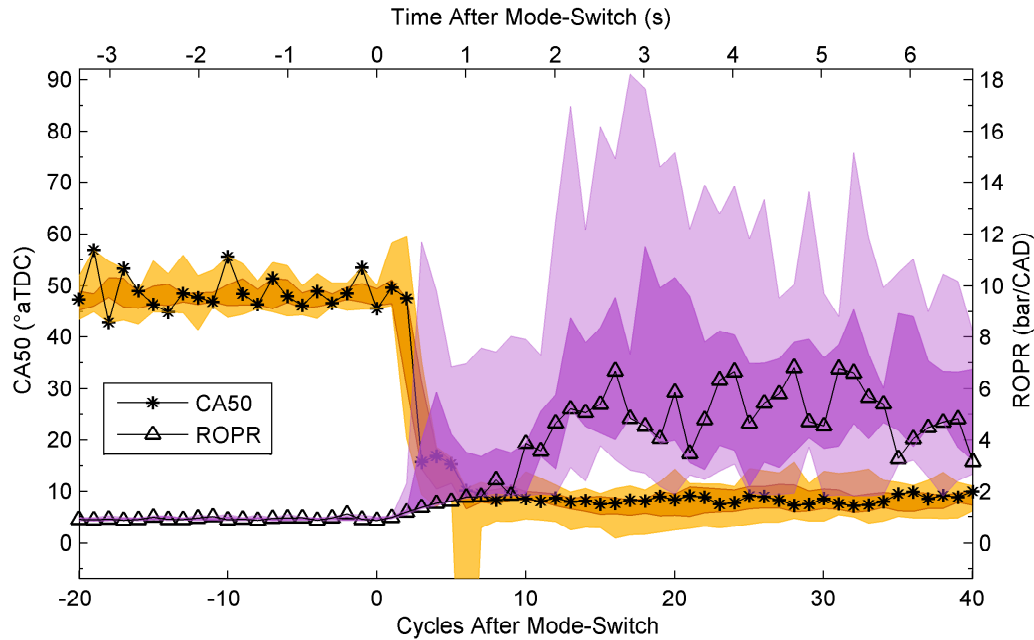
Figure 4.8: CA50 and ROPR during SI-HCCI mode-switch using step increase in throttle position. $\epsilon_{CA50} = 3.1/0.89$ CAD (SI/HCCI), $\epsilon_{ROPR} = 0.03$ bar/CAD

ily due to this effect. However, partial burn with reduced IMEP on cycle 3 after mode-switch is visible in two of the tests in Figure 4.9 with an associated penalty in smoothness. Also, a significant knock penalty is applied to the last test (2010_08_09 - 39), where although the IMEP follows the desired trend more closely, knock experienced during this test (indicated by the upper ROPR values in Figure 4.8) reduces the overall mode-switch effectiveness. Minor knock penalties are applied to three of the other tests as well, indicating that they exceeded an ROPR of 10 bar/CAD by a small margin on a low number of cycles. The stabilize values, being larger than the duration for these tests, indicate that these knock cycles occur after the IMEP had achieved the steady-state HCCI level, as confirmed by Figure 4.8. This suggests reduced combustion stability as the engine proceeds toward true steady-state operation. In summary, these occurrences of partial burn and knock raise the standard deviation of MSPC to represent the greater variability between tests using this control strategy with a step increase in throttle position.

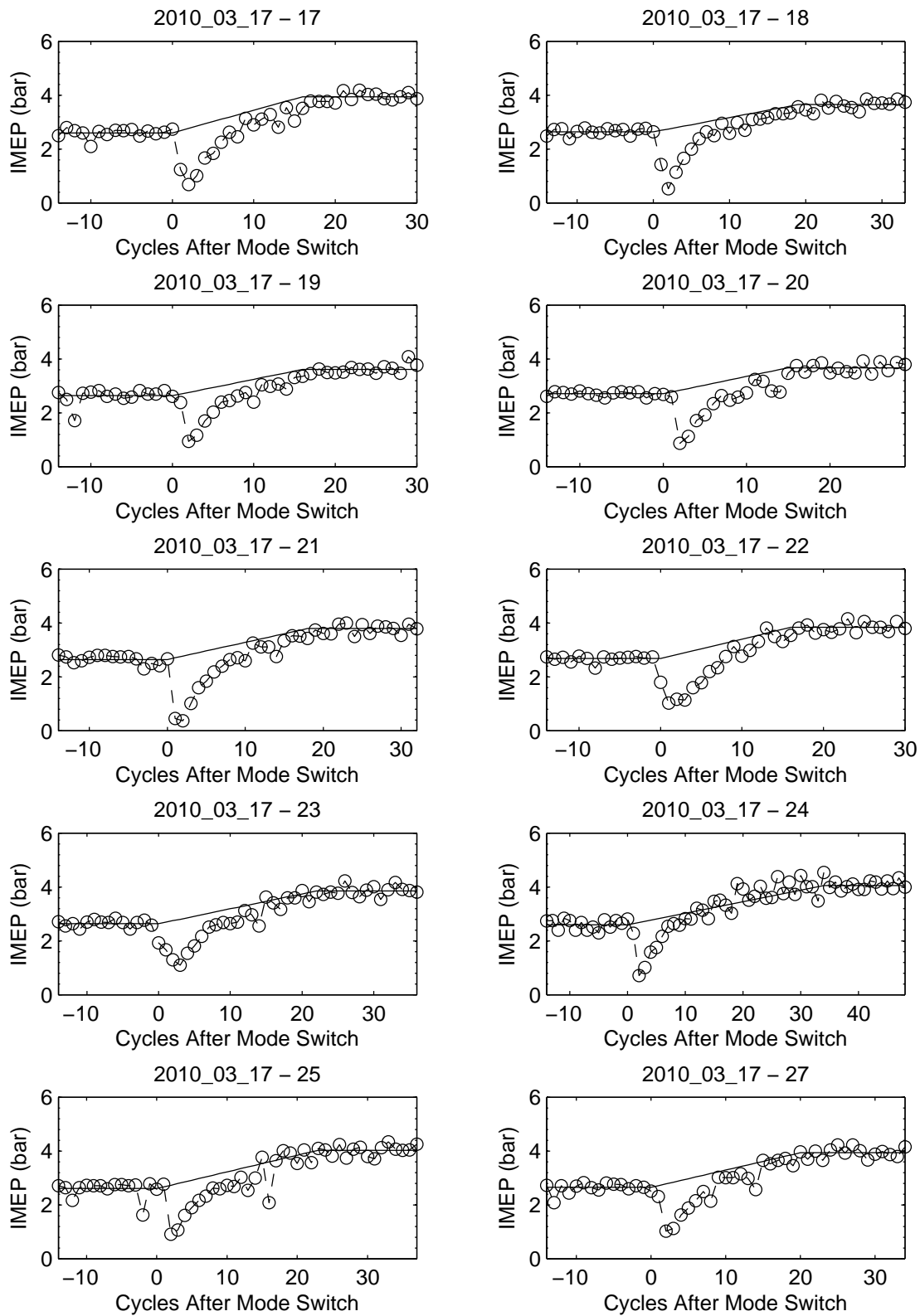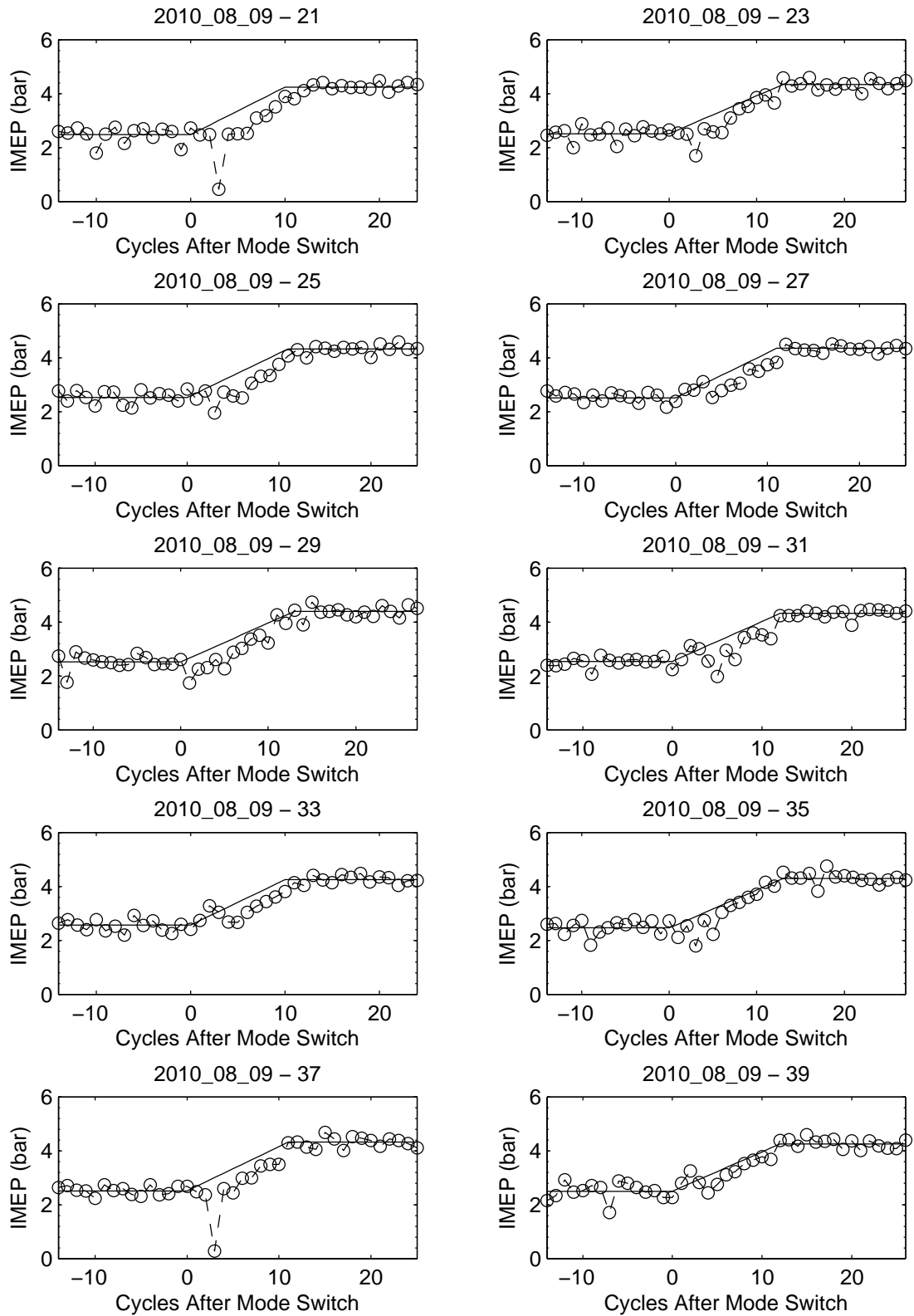Figure 4.9: IMEP from Section 4.3 to evaluate smoothness for MSPC. Experimental data sets are shown with the desired trend.

Table 4.3: MSPC data for Section 4.3.

Test Date	Test Number										Average	Standard
2010_08_09	21	23	25	27	29	31	33	35	37	39	Average	Deviation
Duration	10	13	11	11	13	12	10	13	11	12	11.60	1.17
Smoothness	23.66	12.46	13.67	8.50	14.01	14.15	8.02	10.47	24.47	5.35	13.47	6.29
Stabilize	10	13	11	11	13	12	21	50	21	40	20.20	13.85
Knock	0.00	0.00	0.00	0.00	0.00	0.00	1.24	2.55	0.31	39.97	4.41	12.52
MSPC	33.66	25.46	24.67	19.50	27.01	26.15	19.26	26.02	35.78	57.32	29.48	11.08

4.4   SI-HCCI: CNG Injection Timing

One main goal of this thesis is to control SI-HCCI mode-switching using only actuators available on standard engines. To mitigate the variability of combustion for early HCCI mode cycles in Figures 4.6-4.8, a cycle by cycle fast actuator is needed. CNG injection timing influences charge stratification during SI operation [54] and is found to influence HCCI ignition as well. Early injection at IVC of the previous cycle provides more stable operation in SI at the high intake temperatures used for mode-switching, while advancing the injection toward IVO (moving the injection timing to the right in Figure 3.14) has the effect of promoting auto-ignition in HCCI.

Starting with the fuel sequence from the previous test in Figures 4.6-4.8, fuel injection timing is added to assist ignition during the unstable cycles. Minor adjustments are then made to the fuel values to compensate for improved combustion. Figure 4.10 shows the resulting mode-switch which has reduced uncertainty during the early cycles compared to Figure 4.6. The cylinder pressures in Figure 4.11 show that although not ideal, combustion is occurring on all cycles.

A smooth transition for CA50 between the two steady state values, along with ROPR showing some cases of knock in the early cycles but rarely thereafter, is shown in Figure 4.12. The drop in ROPR visible at the end of the sample test is due to the PI fuel controller overcompensating and not a sign of ensuing misfire.

The SI-HCCI mode-switch transition time using this control strategy can not be easily reduced without inducing knock. The slow increase in fuel delivery is designed to counter-act the natural advancing tendency of the engine as determined previously in Figure 4.4, thus limiting IMEP throughout the process.

Advancing injection timing through the mode-switch carries an associated effect of improved stability in HCCI, demonstrated by lower variability in all parameters toward the end of the provided data. With all other conditions the same as previous

tests, including the PI controller tuning, much smoother operation is possible in HCCI. Again, this is likely due to improved mixing promoting more consistent ignition for the low intake air temperature of 115 °C.
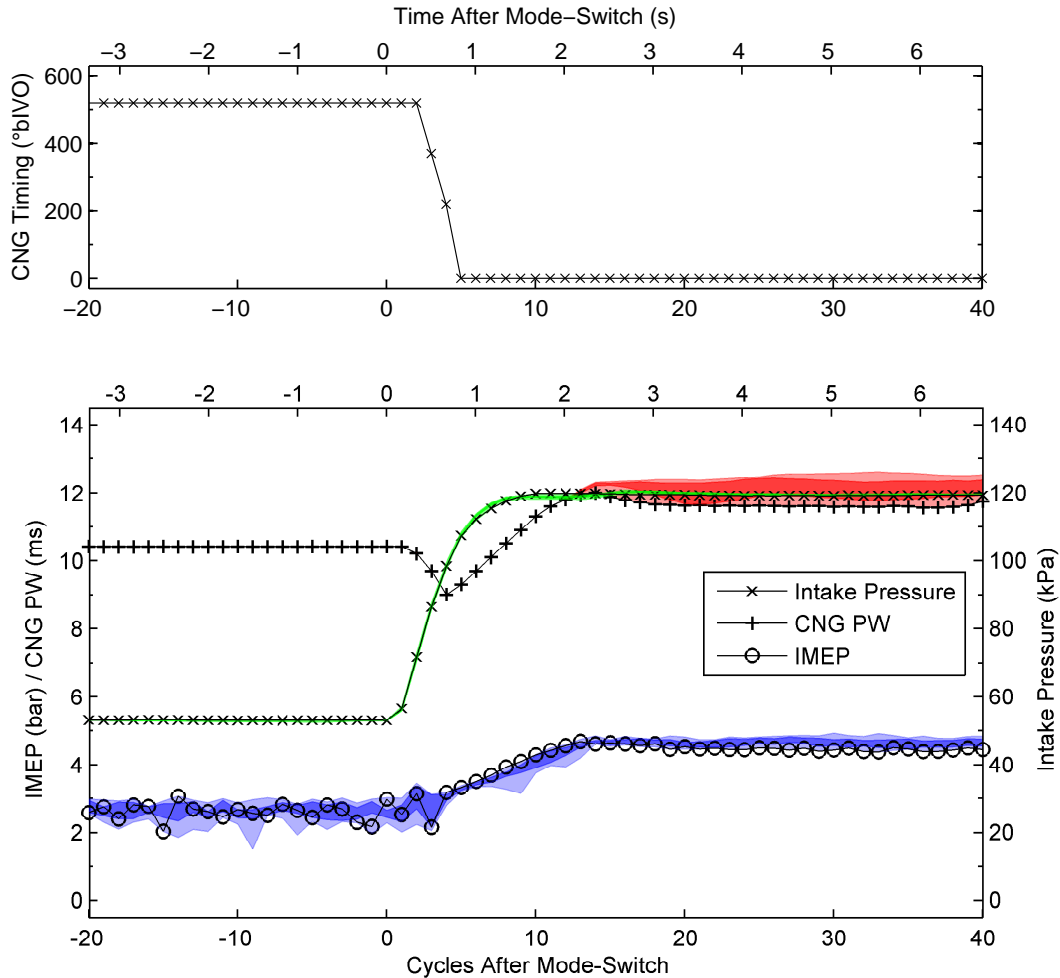
Figure 4.10: SI-HCCI mode-switch using fuel timing adjustment. $\epsilon_{IMEP} = 0.06$ bar, $\epsilon_{IntakePressure} = 2.7$ kPa, $\epsilon_{InjectionTiming} = 1.1$ CAD

Using CNG injection timing, the partial burn cycles are removed as shown in Figure 4.13 when compared to the previous tests in Figure 4.9. This signifies less variability between tests as reflected by the lower standard deviation of MSPC in Table 4.4. More stable combustion in HCCI with CNG injection at IVO is apparent with less variation in IMEP near the end of the transition. The duration of the switch is reduced by 1.3 cycles on average compared to Table 4.3 along with a
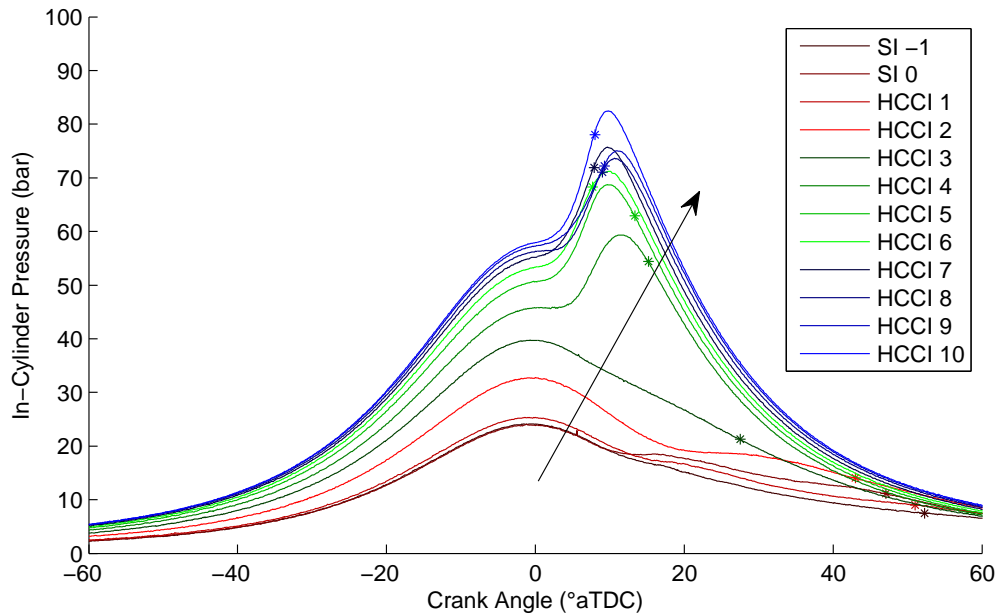
Figure 4.11: In-cylinder pressure traces during SI-HCCI mode-switch using fuel timing adjustment. The arrow indicates cycle progression. Stars indicate CA50.
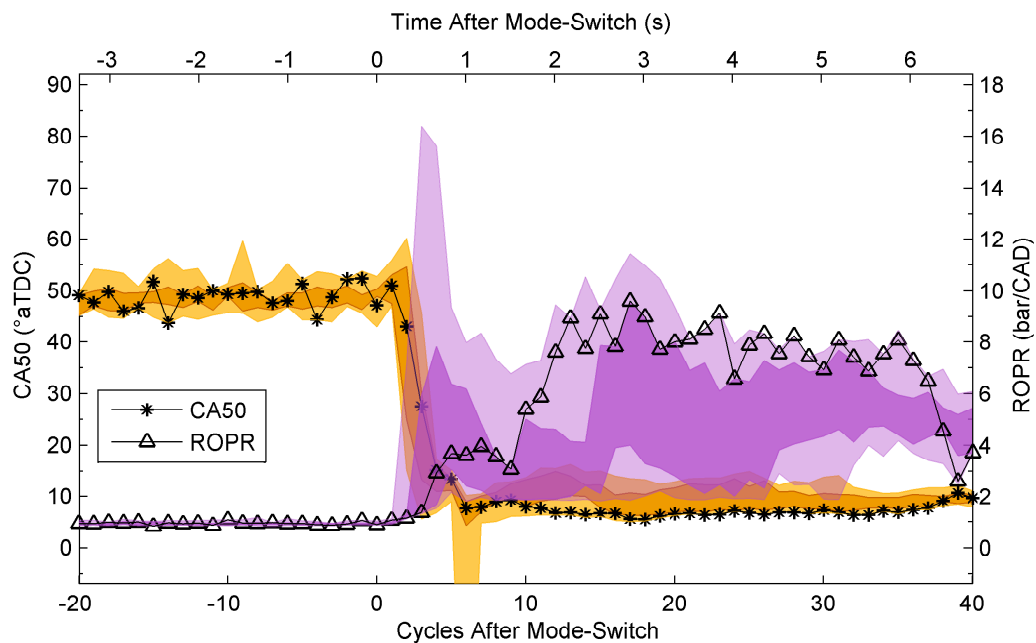
Figure 4.12: CA50 and ROPR during SI-HCCI mode-switch using fuel timing adjustment. $\epsilon_{CA50} = 3.1/0.89$ CAD (SI/HCCI), $\epsilon_{ROPR} = 0.03$ bar/CAD

reduction in smoothness of 5.8 on average. Knock is only present in two of the tests and much less significant than before. All these effects combine to reduce the average MSPC by 10.5, or approximately one third, compared to Table 4.3 without CNG timing adjustment.
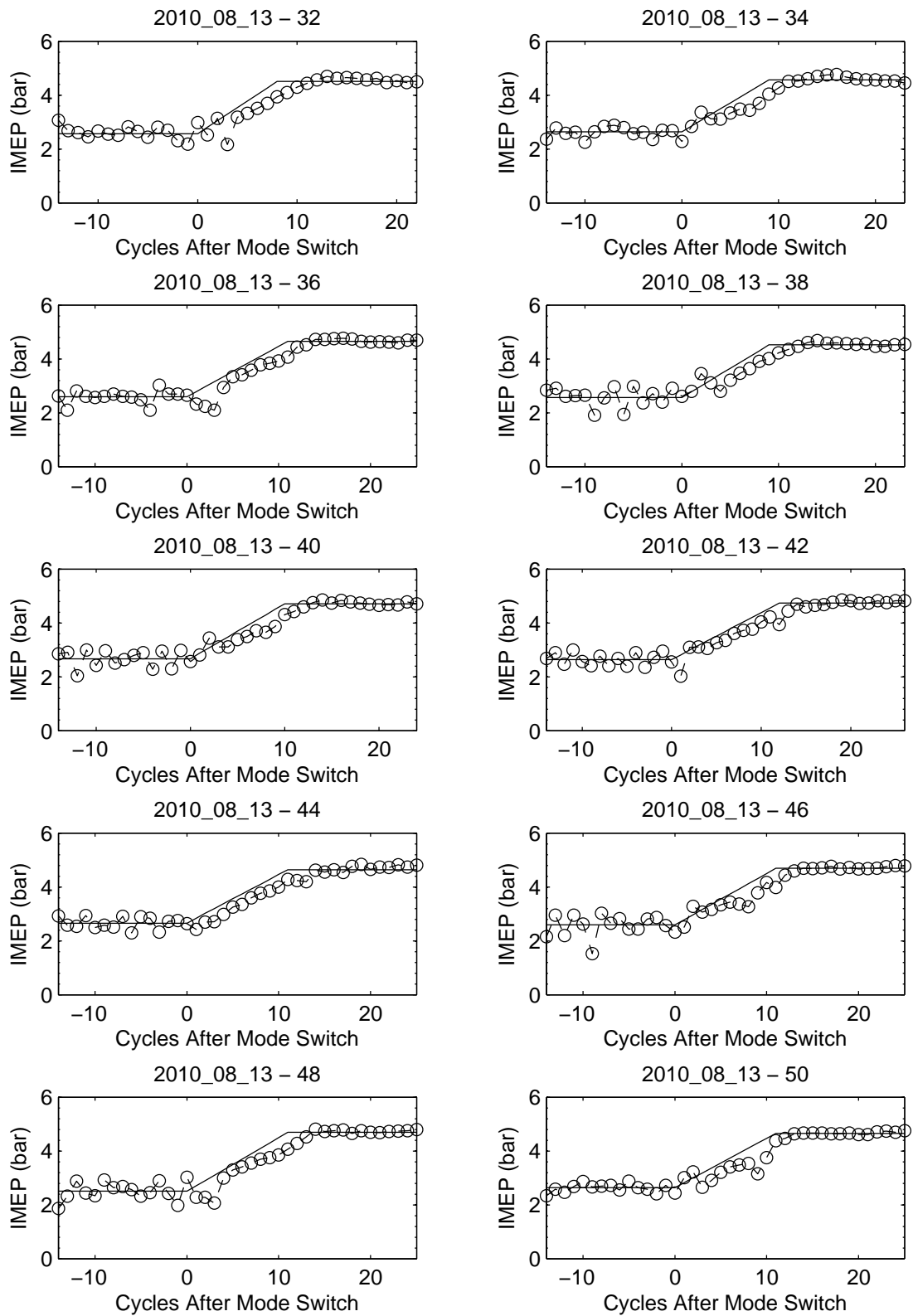
Figure 4.13: IMEP from Section 4.4 to evaluate smoothness for MSPC. Experimental data sets are shown with the desired trend.

Table 4.4: MSPC data for Section 4.4.

Test Date	Test Number										Average	Standard
2010_08_13	32	34	36	38	40	42	44	46	48	50	Average	Deviation
Duration	8	9	11	9	10	12	11	11	11	11	10.30	1.25
Smoothness	8.21	6.20	10.20	5.73	5.69	7.13	5.77	7.65	10.40	10.05	7.70	1.93
Stabilize	8	18	11	20	10	12	11	11	11	11	12.30	3.71
Knock	0.00	0.01	0.00	3.45	0.00	0.00	0.00	0.00	0.00	5.99	0.94	2.08
MSPC	16.21	15.21	21.20	18.18	15.69	19.13	16.77	18.65	21.40	27.04	18.95	3.56

4.5 HCCI-SI: Slow Intake Pressure Drop

The HCCI-SI mode-switch is generally simpler than SI-HCCI since the spark provides a direct method of setting ignition timing in SI. Only the air/fuel ratio and spark timing have a large influence on combustion timing (CA50). The main concern is that the mixture does not auto ignite and produce unexpected knock. Due to limitations with the injection system as discussed in Section 3.2.1 and Appendix F.2, injection must remain between IVC of the previous cycle and 220° bIVO.

With the large intake manifold, the engine requires approximately 30 cycles to reduce the pressure in the intake manifold down to the steady-state SI level of 53 kPa. Attempting to mode-switch into SI on the first cycle after closing the throttle leads to heavy knock. Instead, three cycles are controlled to remain as HCCI combustion using knowledge from previous testing:

- CNG injection timing begins at IVC so that advancing this parameter can promote HCCI ignition as the intake pressure drops for the first 3 cycles.

- CNG PW is slowly increased for the first 3 cycles to supply a richer mixture then steady-state HCCI, again to promote HCCI combustion.

- At cycle 4, CNG PW is increased further to provide a richer mixture for SI combustion, followed by a reduction similar to intake pressure. CNG injection timing begins retarding at this point to reduce the tendency of knock.

The results presented in Figure 4.14 show that this strategy can produce repeatable HCCI-SI mode-switches. Figure 4.15 shows that the first few cycles following the mode-switch appear similar to spark-assisted HCCI with relatively late combustion timing [55]. CA50 and ROPR follow a smooth transition between the two steady-state points as shown in Figure 4.16. Note that the CA50 values retard past the steady-state value of 48° aTDC and require many cycles to slowly return to

this value. Lean mixtures are used to deter knock until the intake pressure reaches the steady-state level for stable SI combustion with a stoichiometric mixture.

Although these results show that a slow transition (20-30 cycles) is possible from HCCI to SI, evacuating the large intake manifold is a physical constraint preventing a faster transition. To increase the rate that the intake pressure can be reduced, a smaller manifold is needed - the subject of the next section.

Figure 4.14: HCCI-SI mode-switch with large intake manifold volume. $\epsilon_{IMEP} = 0.06$ bar, $\epsilon_{IntakePressure} = 2.7$ kPa, $\epsilon_{InjectionTiming} = 1.1$ CAD

Mode-switching effectiveness of this HCCI-SI mode-switch is given in Table 4.5. Duration and smoothness values for the HCCI-SI mode-switch show high variability between tests compared to Table 4.2 (the first SI-HCCI mode-switch in this study)

Figure 4.15: In-cylinder pressure traces during HCCI-SI mode-switch with large intake manifold volume. The arrow indicates cycle progression. Stars indicate CA50.

Figure 4.16: CA50 and ROPR during HCCI-SI mode-switch with large intake manifold volume. $\epsilon_{CA50} = 3.1/0.89$ CAD (SI/HCCI), $\epsilon_{ROPR} = 0.03$ bar/CAD

associated with fluctuations in IMEP visible in Figure 4.5. COV_{IMEP} in SI at this operating point is 11% requiring MSPC to be adjusted to determine the end of the mode-switch as discussed in Chapter 3. This low stability in the final combustion mode increases difficulty achieving a smooth and quick mode-switch, leading to the high average and standard deviation in MSPC for this control strategy.

Figure 4.17: IMEP from Section 4.5 to evaluate smoothness for MSPC. Experimental data sets are shown with the desired trend.

Table 4.5: MSPC data for Section 4.5.

Test Date	Test Number										Average	Standard Deviation
2010_08_17	12	14	20	24	26	30	32	34	36	38	**Average**	**Deviation**
Duration	35	19	15	26	30	40	28	17	37	18	26.50	9.01
Smoothness	55.78	18.25	21.64	38.44	47.12	81.94	42.30	17.50	66.78	19.74	40.95	22.36
Stabilize	35	19	15	26	30	40	28	17	37	18	26.50	9.01
Knock	0.00	0.00	0.00	0.00	0.00	0.00	0.00	0.00	0.00	0.00	0.00	0.00
MSPC	90.78	37.25	36.64	64.44	77.12	121.94	70.30	34.50	103.78	37.74	67.45	31.22

4.6   Steady-State Operating Conditions - Small Manifold

The intake manifold is modified to 0.5 L so the volume downstream of the electronic throttle is approximately one engine displacement. This is typical for production engines and allows for quicker changes in intake pressure. Based on the change in intake response, a slightly modified set of compatible steady-state operating conditions to mode-switch between are summarized in Table 4.6.

Air mass flow rate is maintained at the same level for both SI and HCCI as with the large manifold in Table 4.6. The measurement of P_{IVC} at these flow rates is recorded and used as the set point. Intake air temperature is increased to achieve the same mixture temperature in HCCI, leading to a cooler mixture in SI due to several factors explored in Appendix C. The lower mixture temperatures in SI leads to more stable combustion and reduced tendency toward knock, but otherwise SI operation is similar to previous testing.

CNG injection timing is advanced to IVO during the SI-HCCI mode-switch; however, timing must be retarded to allow for HCCI-SI mode-switching without a misfire resulting from the controller limitation described in Section 3.2.1 and Appendix F.2. CNG PW is not set directly in HCCI, but as before is controlled toward a ROPR value of 6 bar/CAD for stable HCCI operation. With the other conditions adjusted as described above, the resulting leaner mixtures lead to a lower IMEP in HCCI. With the focus of this mode-switching development being to achieve stable HCCI combustion, the reduction in IMEP, compared with previous testing using the large intake manifold, is accepted as the most stable HCCI operating point using the small intake manifold. Variation of IMEP in both SI and HCCI steady-state combustion modes surrounding a mode-switch is the topic of Section 4.11.

Table 4.6: Steady-state operating conditions for mode-switching tests - small (0.5 L) intake manifold.

Set Points	SI	HCCI
CNG System Pressure	5.5 bar	5.5 bar
Effective Compression Ratio	17.0	17.0
Engine Speed	700 RPM	700 RPM
Intake Air Temperature	140 °C	140 °C
P_{IVC}	58 kPa	113 kPa
Spark Timing	5° aTDC	-
Actuators		
CNG Injection Timing	520° bIVO	200° bIVO
CNG Pulse Width	10.6 ms	~10.4 ms
Throttle Position	28%	86%
Measurements		
Air Mass Flow	1.3 g/s	3.4 g/s
CNG Mass Flow	74 mg/s	72 mg/s
Equivalence Ratio	1.0	0.37
Exhaust Pressure	91 kPa	92 kPa
Exhaust Temperature	460 °C	250 °C
Mixture Temperature	85 °C	102 °C
Calculated		
CA50	49° aTDC	5° aTDC
COV_{IMEP}	3%	3%
IMEP	2.8 bar	3.5 bar
ROPR	0.8 bar/CAD	6.0 bar/CAD
Thermal Efficiency	27%	35%
Exhaust Emissions		
Carbon Monoxide (CO)	0.08%	0.10%
Carbon Dioxide (CO_2)	10%	3.7%
Hydrocarbons (HC)	1600 ppm	3500 ppm
Oxides of Nitrogen (NO_x)	690 ppm	9 ppm
Oxygen (O_2)	1.8%	14%

4.7 HCCI-SI: Quick Intake Pressure Drop

The tests in Section 4.5 are repeated but with the smaller intake manifold. Comparing the results of Figure 4.14 and 4.18 show that in Figure 4.18 a faster change in P_{IVC} and IMEP occurs as expected. In addition, tuning of this mode-switch is much easier since fewer transition cycles exist in the unstable region between the two steady-state points; thus, there is a reduction in parameters that need to be tuned. The pressure traces in Figure 4.19 show only one cycle with late SI combustion as opposed to several in the previous test. This is supported by comparing Figures 4.20 and 4.16, indicating that the combustion timing advances to the steady-state SI value of 49° aTDC much more quickly corresponding to the faster drop in intake pressure and an earlier recovery to stoichiometric mixtures. Engine stability is significantly improved during the mode-switch and in both steady-state combustion modes resulting from the reduced intake manifold volume and modified operating conditions.

The small intake manifold and quicker intake pressure drop provide a significant improvement in mode-switch effectiveness as shown in Table 4.7 - average MSPC is reduced by 94% compared with mode-switching with the large manifold in Table 4.5. IMEP data in Figure 4.21 indicate only minor variations between tests. The first and last test in this set show a smoothness value of 0, indicating that COV_{IMEP} is maintained below 5% throughout the mode-switch and during subsequent operation in SI.
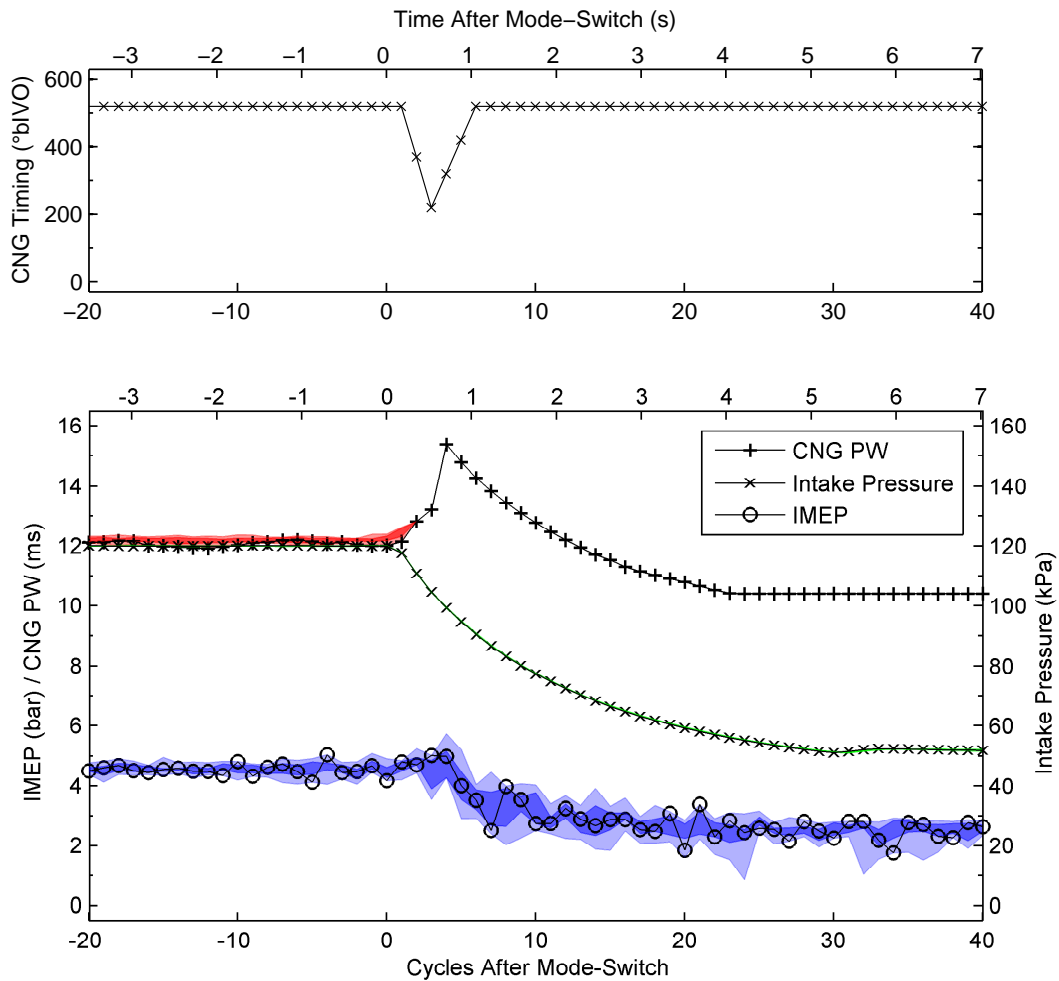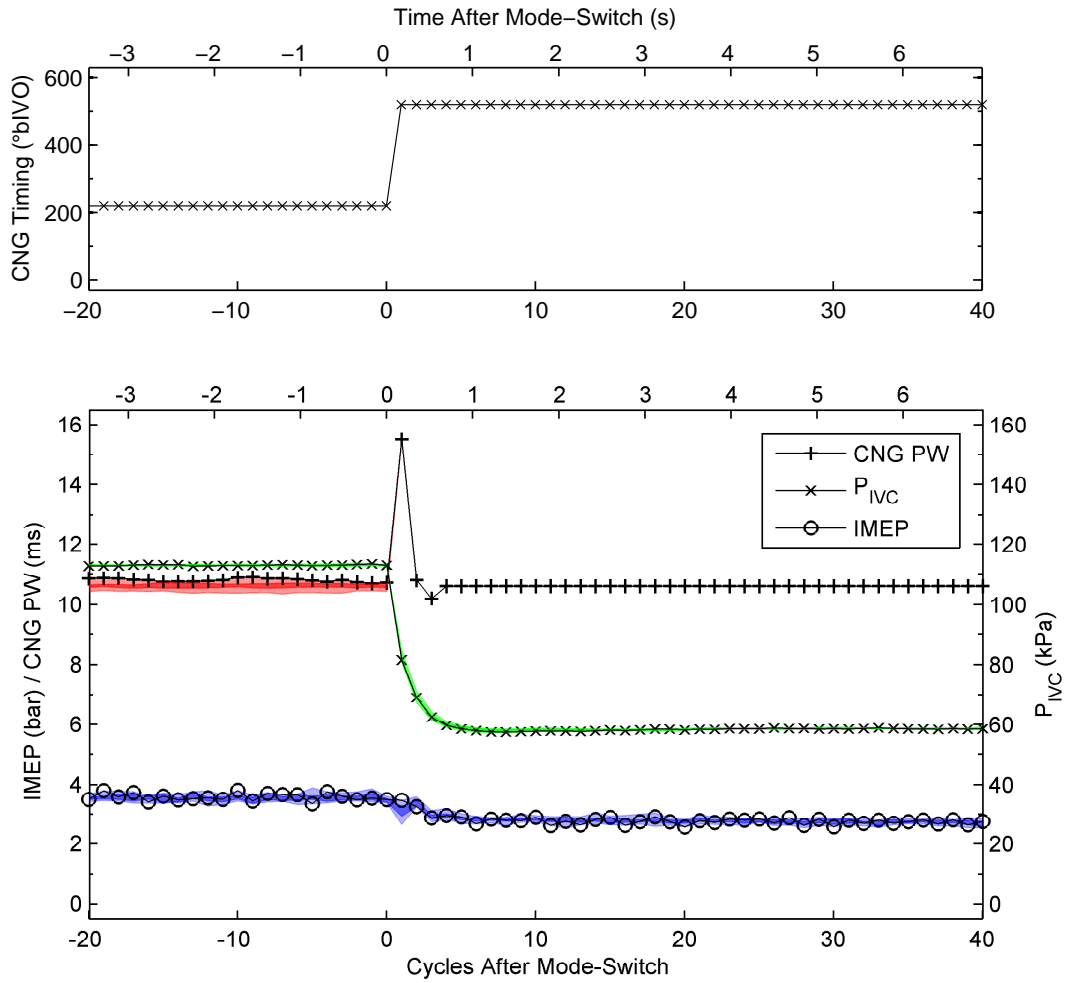
Figure 4.18: HCCI-SI mode-switch with reduced intake manifold volume. ϵ_{IMEP} = 0.06 bar, ϵ_{PIVC} = 2.8 kPa, $\epsilon_{InjectionTiming}$ = 1.1 CAD
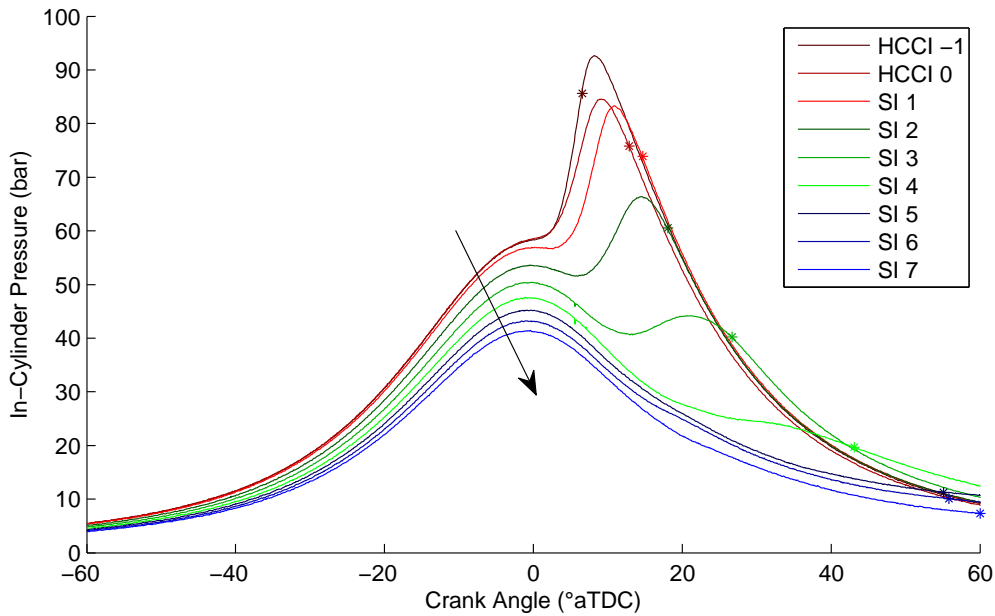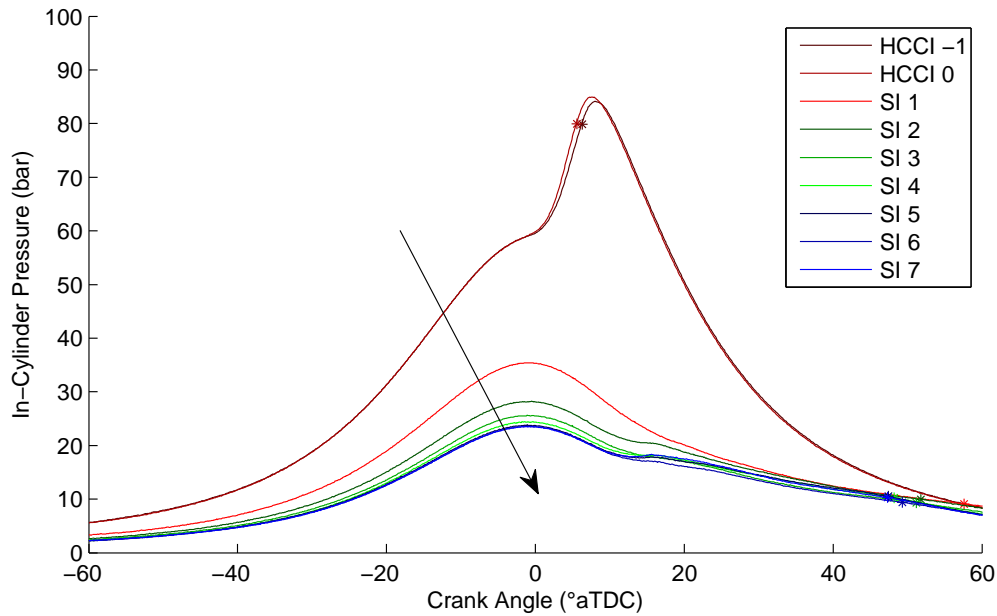
Figure 4.19: In-cylinder pressure traces during HCCI-SI mode-switch with reduced intake manifold volume. The arrow indicates cycle progression. Stars indicate CA50.
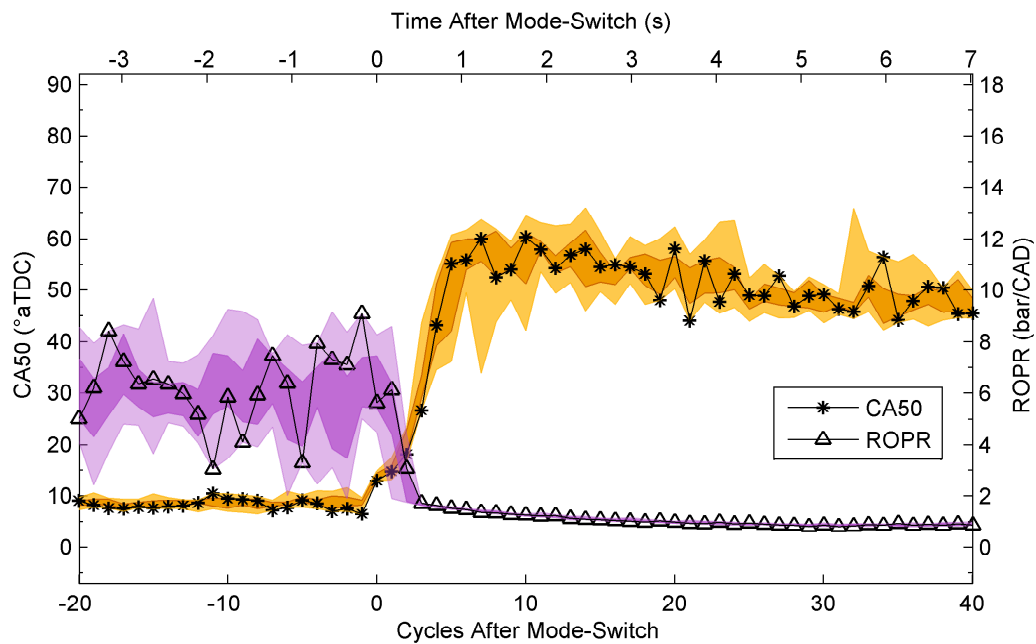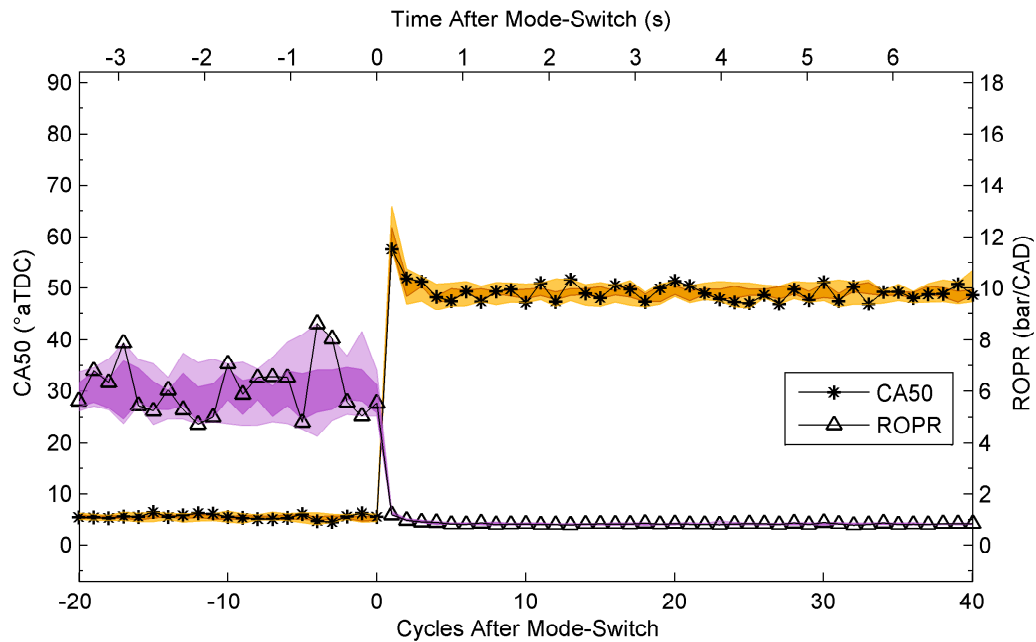

Figure 4.20: CA50 and ROPR during HCCI-SI mode-switch with reduced intake manifold volume. $\epsilon_{CA50} = 3.1/0.89$ CAD (SI/HCCI), $\epsilon_{ROPR} = 0.03$ bar/CAD
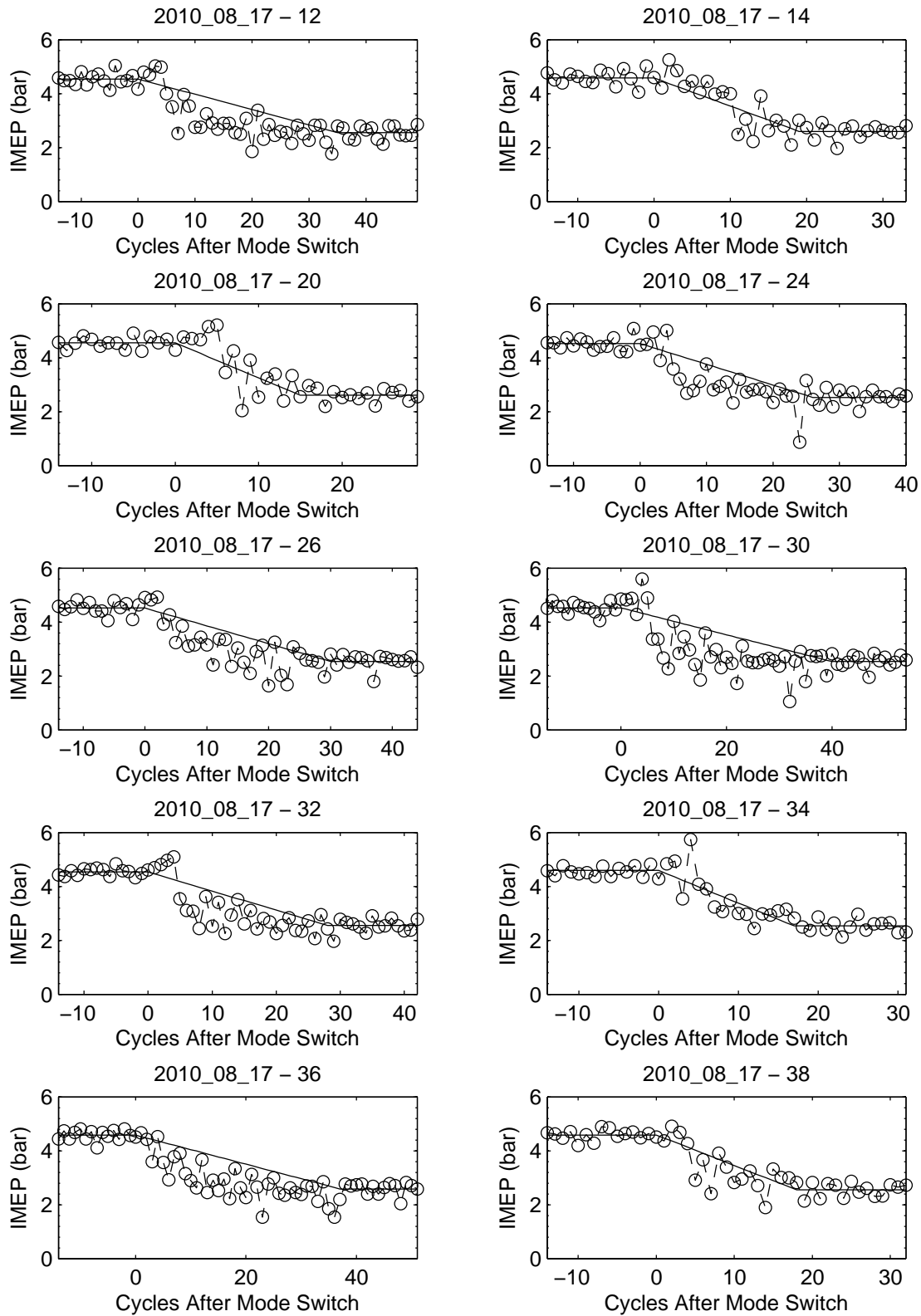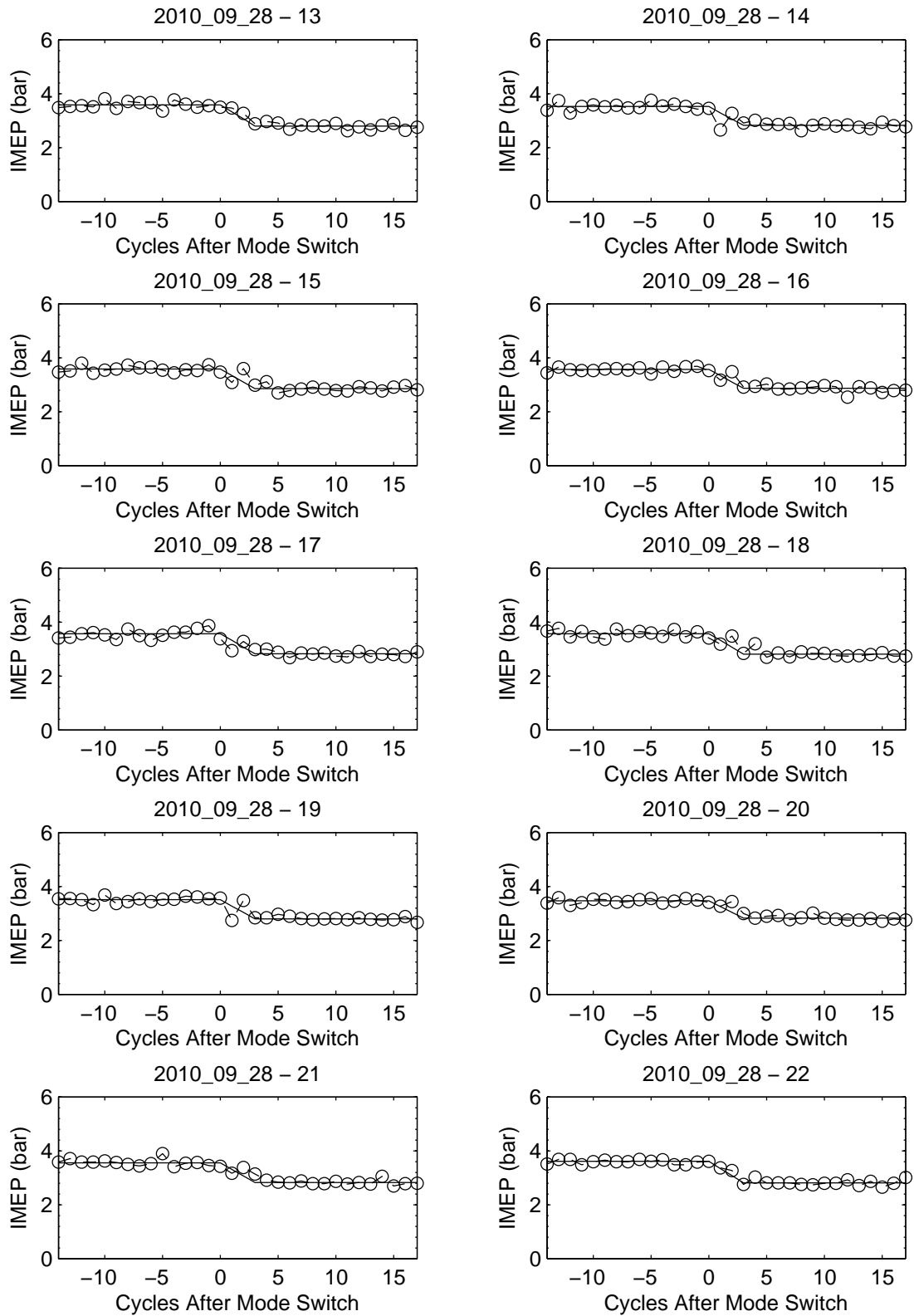
Figure 4.21: IMEP from Section 4.7 to evaluate smoothness for MSPC. Experimental data sets are shown with the desired trend.

Table 4.7: MSPC data for Section 4.7.

Test Date	Test Number										Average	Standard Deviation
2010_09_28	13	14	15	16	17	18	19	20	21	22	Average	Deviation
Duration	3	3	3	3	3	3	3	3	3	3	3.00	0.00
Smoothness	0.00	1.69	1.19	0.43	0.70	0.55	1.86	0.57	0.66	0.00	0.77	0.63
Stabilize	3	3	3	3	3	3	3	3	3	3	3.00	0.00
Knock	0.00	0.00	0.00	0.00	0.00	0.00	0.00	0.00	0.00	0.00	0.00	0.00
MSPC	3.00	4.69	4.19	3.43	3.70	3.55	4.86	3.57	3.66	3.00	3.77	0.63

4.8   SI-HCCI: Optimized Scenario

The small manifold allows for finer control over air induction on individual cycles. Charge mass has the largest influence on ignition timing for HCCI with conventional actuation, especially during the early cycles following an SI-HCCI mode-switch. To improve SI-HCCI mode-switching, air delivery is tailored to meet combustion requirements for individual cycles.

The benefits of this approach can be seen in the test results given in Figure 4.22. A one-cycle step in IMEP to the new steady-state value reduces the duration of the switch to 1 cycle, the ideal case. Controls are adjusted over the subsequent cycles to maintain a nearly constant IMEP output as the engine itself stabilizes to the new operating condition. Figure 4.23 shows the first transition cycle (HCCI 1) occurring with a pressure trend indicative of a hybrid between SI and HCCI combustion. The pressure rise begins at nearly the same location as the steady-state SI cycles (SI -1 and SI 0), but with a more significant pressure rise similar to HCCI combustion (all subsequent cycles). This is a result of the some early SI flame propagation leading to HCCI ignition with the hot SI combustion and residual gases in the combustion chamber. The next cycle (HCCI 2) is not quite at steady-state intake pressure, as indicated by the lower overall cylinder pressure, but shows good HCCI combustion with appropriate combustion timing (CA50). Subsequent cycles have a slowly dropping and retarding peak pressure, but otherwise appear very stable. Figure 4.24 supports these observations with a quick transition from the late SI combustion timing to the earlier HCCI values. ROPR values represent the visible change in combustion severity in the cylinder pressure traces, followed by a smooth transition toward the controlled value of 6 bar/CAD. Again, the two CA50 values shown for cycles 2 and 3 after mode-switch are retarded compared to future cycles due to their evaluation using SI coefficients in the Woschni equations since the spark is still activated.
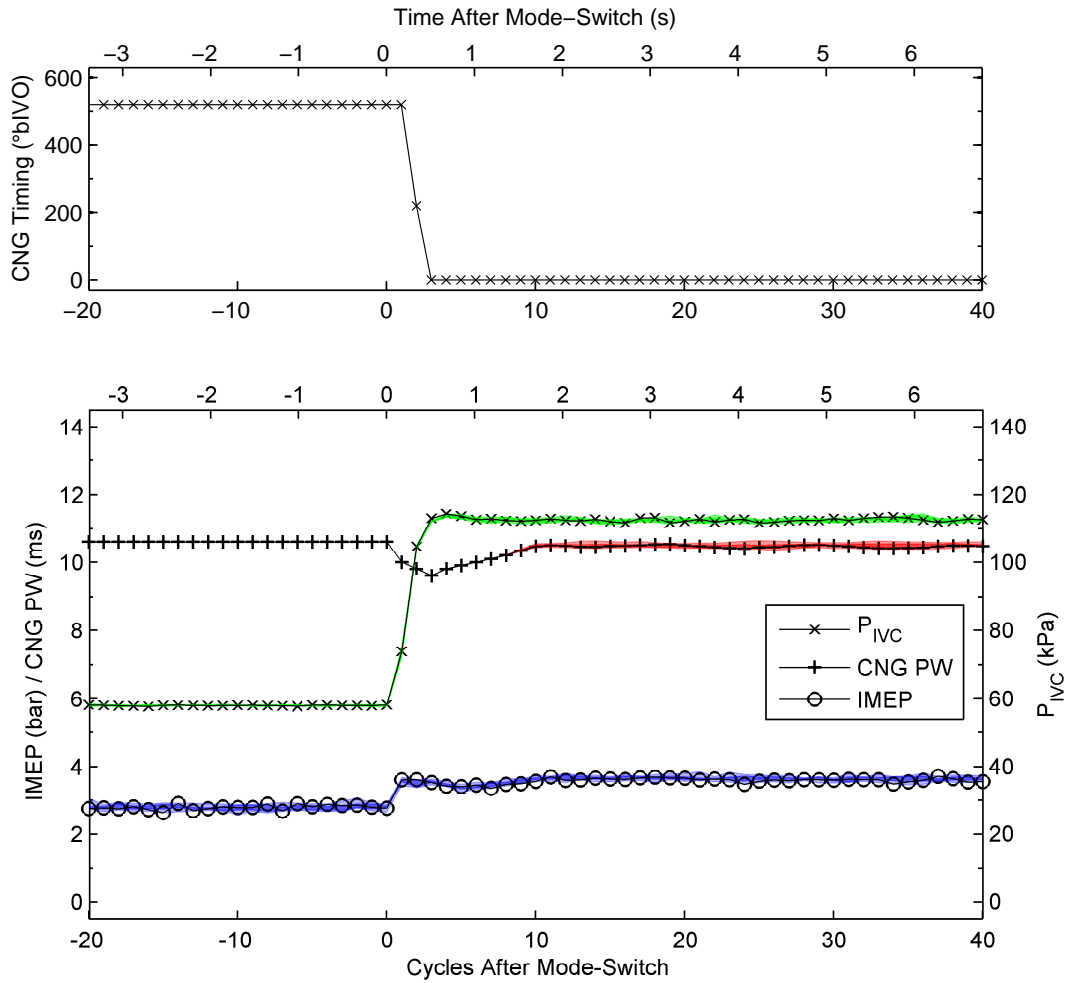
Figure 4.22: SI-HCCI mode-switch with optimized control sequence using relocated throttle. $\epsilon_{IMEP} = 0.06$ bar, $\epsilon_{PIVC} = 2.8$ kPa, $\epsilon_{InjectionTiming} = 1.1$ CAD
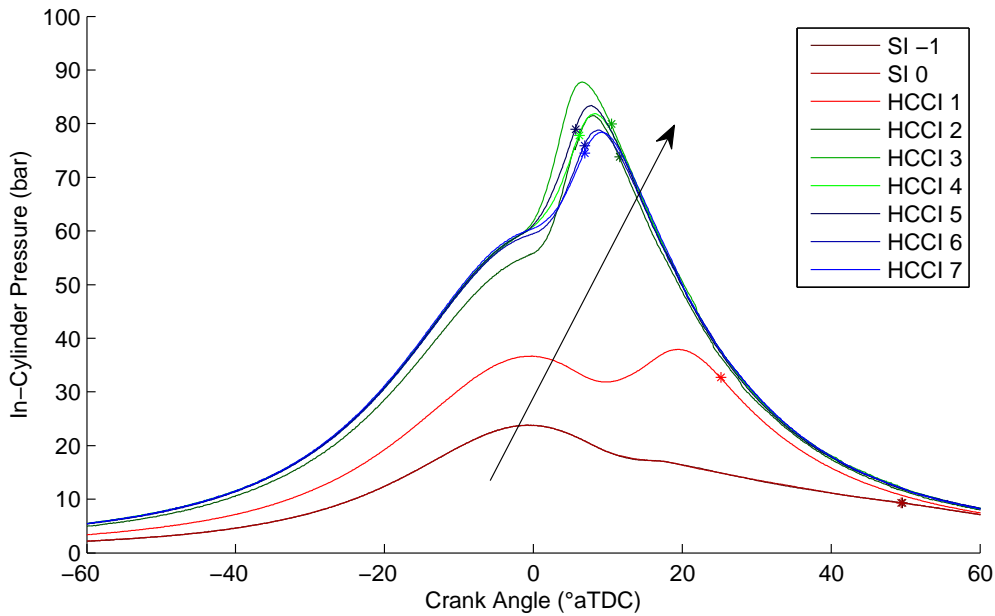
Figure 4.23: In-cylinder pressure traces during SI-HCCI mode-switch with optimized control sequence using relocated throttle. The arrow indicates cycle progression. Stars indicate CA50.
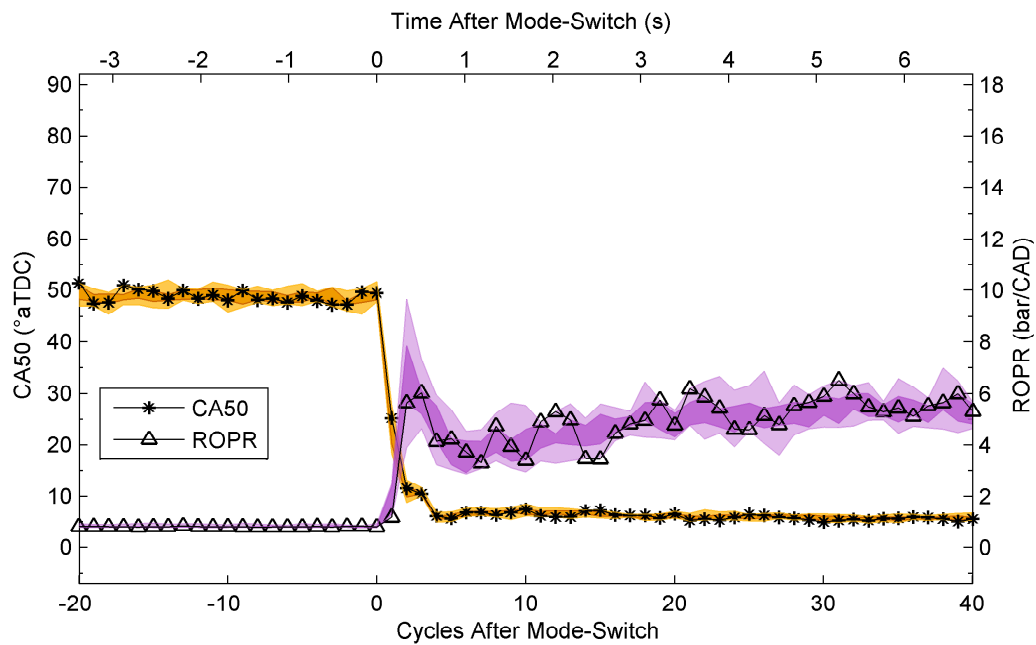
Figure 4.24: CA50 and ROPR during SI-HCCI mode-switch with optimized control sequence using relocated throttle. $\epsilon_{CA50} = 3.1/0.89$ CAD (SI/HCCI), $\epsilon_{ROPR} = 0.03$ bar/CAD

MSPC data for these tests is given in Table 4.8, showing that mode-switch effectiveness based on the developed criteria is ideal. IMEP data in Figure 4.25 supports this with a step change and subsequent smooth operation visible in all tests.
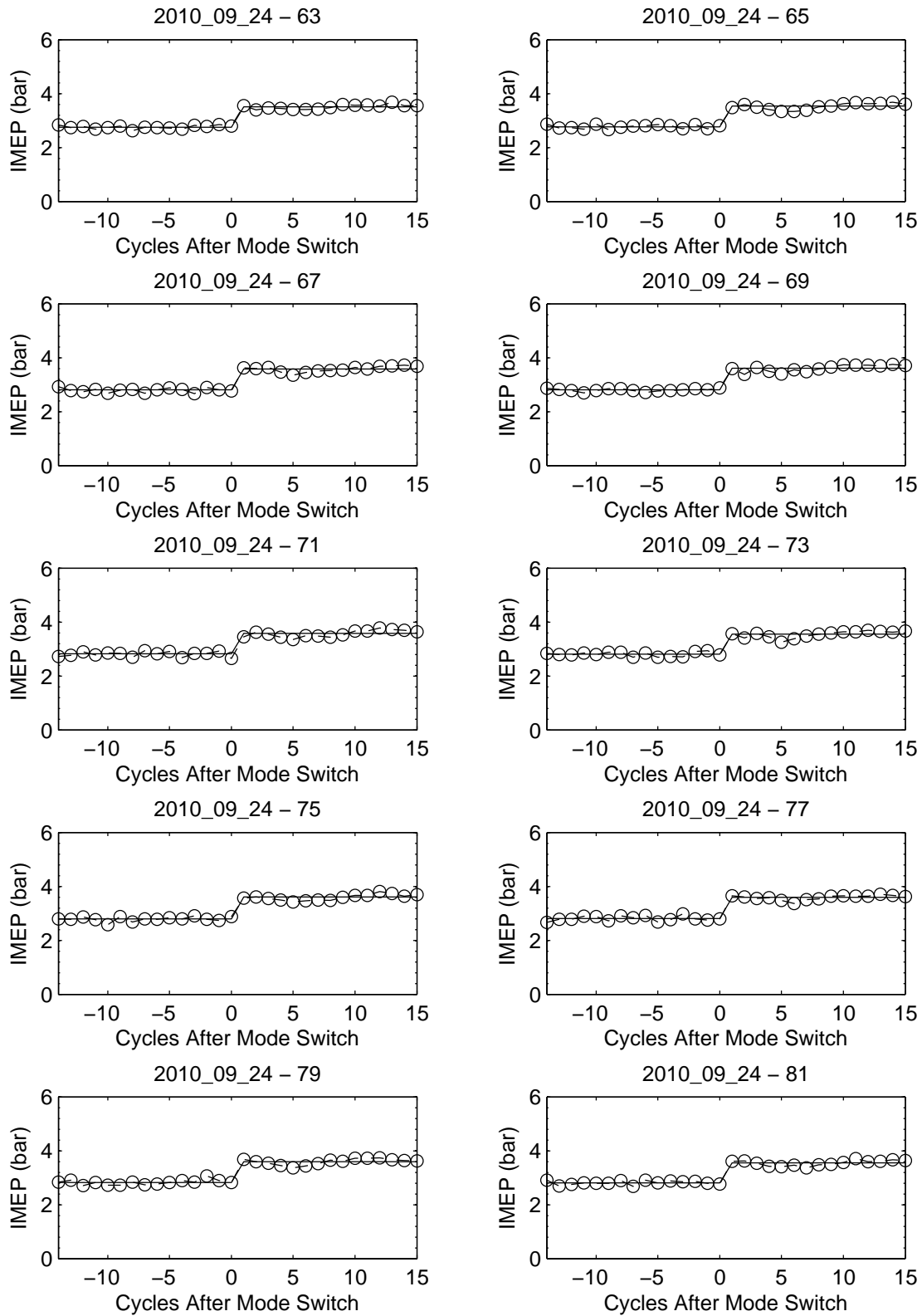
Figure 4.25: IMEP from Section 4.8 to evaluate smoothness for MSPC. Experimental data sets are shown with the desired trend.

Table 4.8: MSPC data for Section 4.8.

Test Date	Test Number										Average	Standard Deviation
2010_09_24	63	65	67	69	71	73	75	77	79	81	**Average**	**Deviation**
Duration	1	1	1	1	1	1	1	1	1	1	1.00	0.00
Smoothness	0.00	0.00	0.00	0.00	0.00	0.00	0.00	0.00	0.00	0.00	0.00	0.00
Stabilize	1	1	1	1	1	1	1	1	1	1	1.00	0.00
Knock	0.00	0.00	0.00	0.00	0.00	0.00	0.00	0.00	0.00	0.00	0.00	0.00
MSPC	1.00	1.00	1.00	1.00	1.00	1.00	1.00	1.00	1.00	1.00	1.00	0.00

4.9   HCCI-SI: Optimized Scenario

A faster transition from HCCI to SI can be achieved by increasing the rate of intake pressure reduction. Instead of stepping the throttle down to the new steady-state value, it is closed for one cycle and then opened to the steady-state value. The lower intake pressure on the first SI cycle results in very infrequent knock. As such, the CNG PW can be adjusted to tailor the power output as desired. If IMEP in SI is not significantly less than in HCCI, it may be possible to reduce the power output to the new steady-state value within one cycle. However, too lean a mixture may experience partial combustion causing undesirable emissions and reduced IMEP. This may be avoided by stepping the IMEP down to an intermediate value between the two steady-state points to maintain a near stoichiometric mixture but results in extending the duration of the mode-switch by one cycle.

Results using this methodology are shown in Figure 4.26. The first SI cycle has a slightly reduced IMEP due to the lean mixture. All following cycles show very consistent SI operation at a constant IMEP. The pressure traces in Figure 4.27 show the progression toward SI operation with stable operation thereafter. Figure 4.28 indicates that the first SI cycle occurs with later than steady-state combustion timing, agreeing with the lean mixture on that cycle, with stable steady-state timing thereafter.

Mode-switching effectiveness using this strategy is nearly ideal based on MSPC as shown in Table 4.9. Five of the tests are less than ideal resulting from variability in IMEP on the first SI cycle after mode-switch shown in Figure 4.29. Overall performance of this mode-switching control strategy is maintained at a low average MSPC of 1.5 with a standard deviation of 1.1.
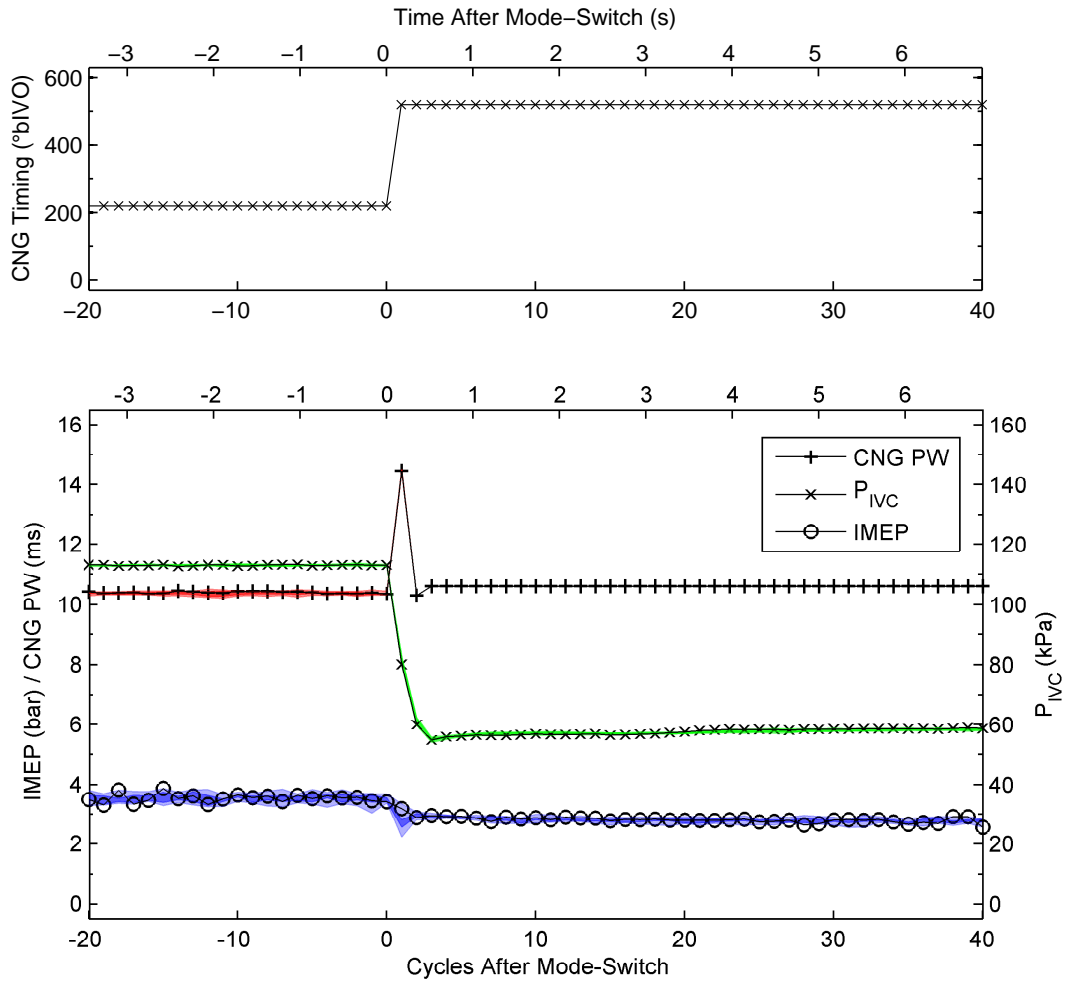
Figure 4.26: HCCI-SI mode-switch with optimized control sequence using relocated throttle. $\epsilon_{IMEP} = 0.06$ bar, $\epsilon_{PIVC} = 2.8$ kPa, $\epsilon_{InjectionTiming} = 1.1$ CAD
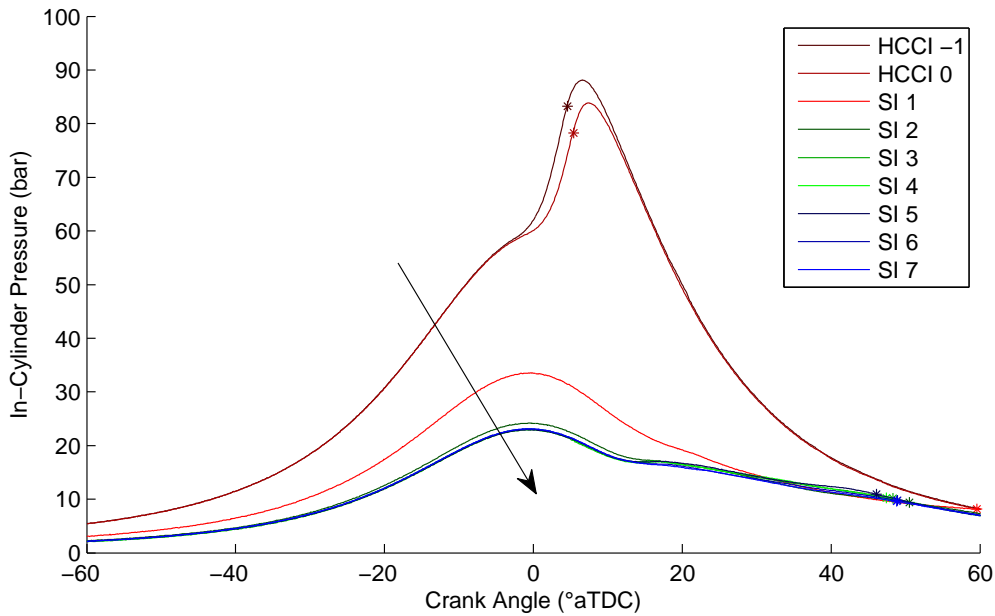
Figure 4.27: In-cylinder pressure traces during HCCI-SI mode-switch with optimized control sequence using relocated throttle. The arrow indicates cycle progression. Stars indicate CA50.
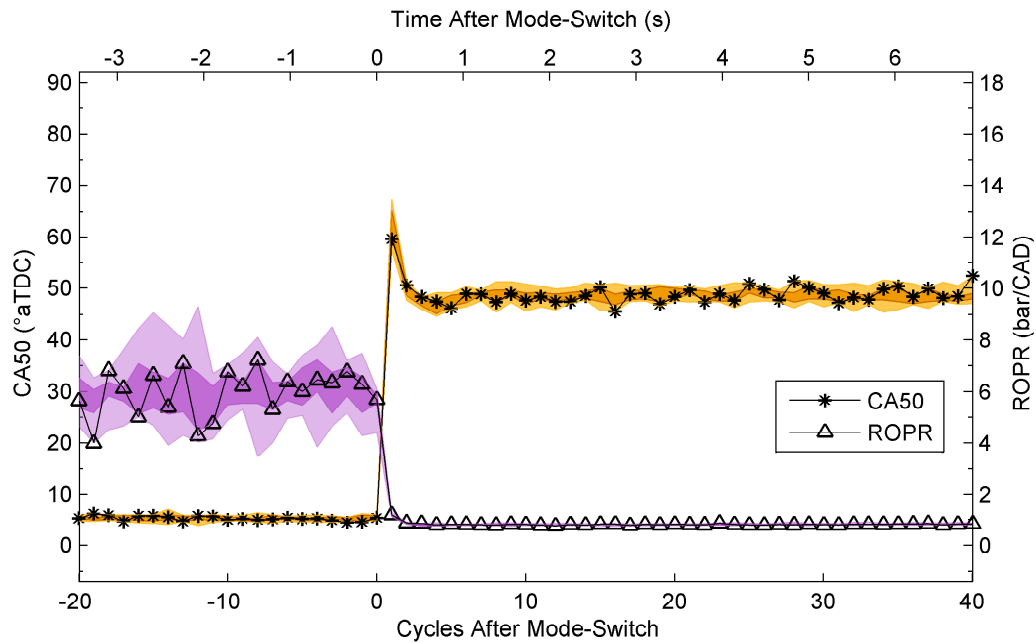
Figure 4.28: CA50 and ROPR during HCCI-SI mode-switch with optimized control sequence using relocated throttle. $\epsilon_{CA50} = 3.1/0.89$ CAD (SI/HCCI), $\epsilon_{ROPR} = 0.03$ bar/CAD
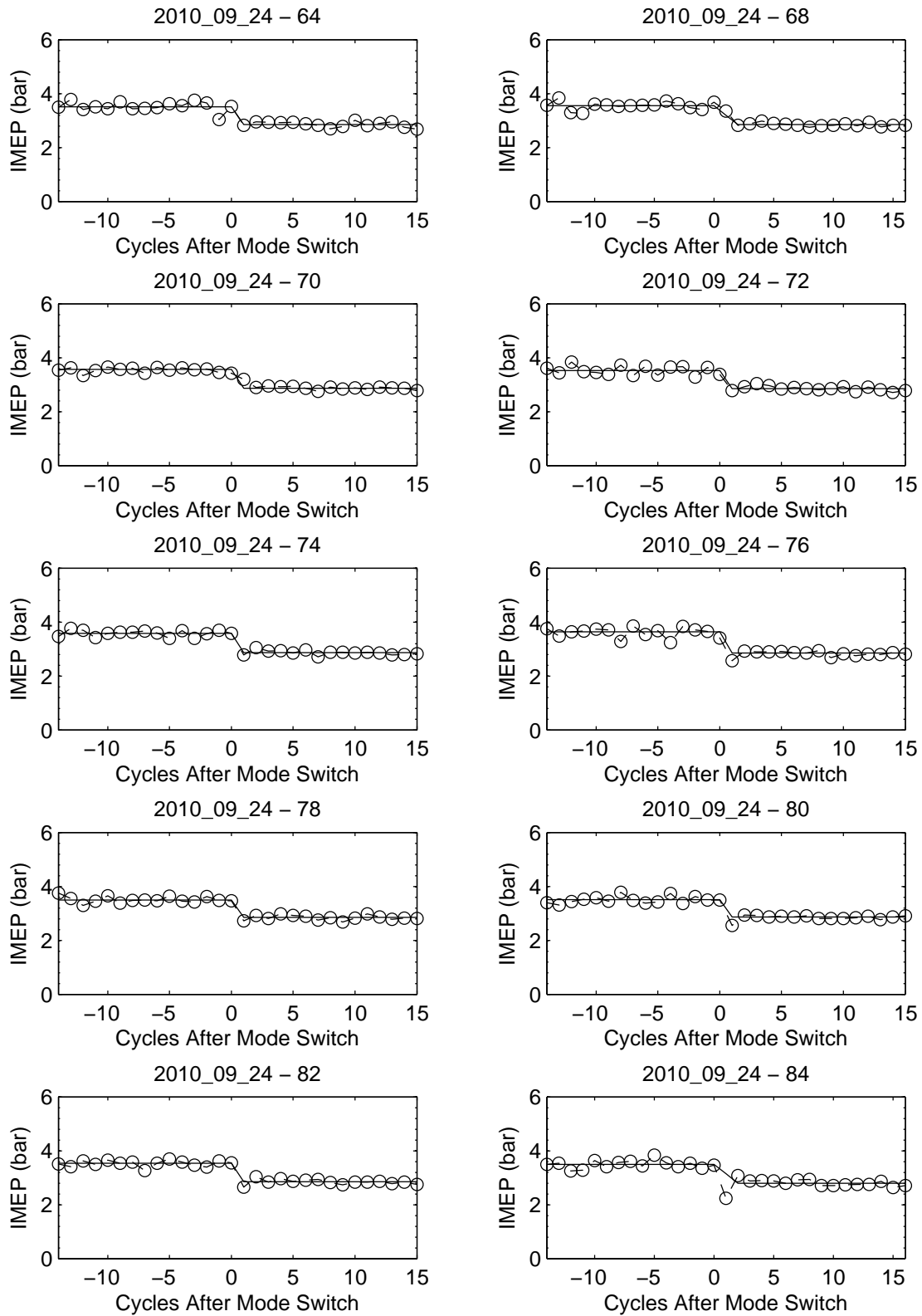
Figure 4.29: IMEP from Section 4.9 to evaluate smoothness for MSPC. Experimental data sets are shown with the desired trend.

Table 4.9: MSPC data for Section 4.9.

Test Date	Test Number										Average	Standard
2010_09_24	64	68	70	72	74	76	78	80	82	84	Average	Deviation
Duration	1	2	1	1	1	1	1	1	1	2	1.20	0.42
Smoothness	0.00	0.00	0.21	0.00	0.00	0.11	0.00	0.20	0.00	2.50	0.30	0.78
Stabilize	1	2	1	1	1	1	1	1	1	2	1.20	0.42
Knock	0.00	0.00	0.00	0.00	0.00	0.00	0.00	0.00	0.00	0.00	0.00	0.00
MSPC	1.00	2.00	1.21	1.00	1.00	1.11	1.00	1.20	1.00	4.50	1.50	1.10

4.10 Mode-Switching Sensitivity - Repeated SI-HCCI-SI Transitions

For real-world applications, it is possible that a need to mode-switch will occur frequently. Depending on the sensitivity of the method used to induce the mode-switch, this may not be possible without elaborate control schemes to adapt to unstable engine conditions. To investigate this aspect, a set of repeat mode-switches are completed using the same optimized open-loop control sequences as in Sections 4.8 and 4.9. No adjustments have been made for the different operating conditions experienced during these quick transitions as opposed to beginning in steady-state. Disturbances exist in engine speed, mixture temperature, and the pressure in the intake buffer tank, with the first two being measured values and presented in Figure 4.32. The limitation in CNG injection timing can not be avoided in this test and one cycle in HCCI must intentionally misfire with no fuel delivered before mode-switching back to SI. This further destabilizes the engine.

Test data are shown in Figures 4.30 and 4.31. Results are encouraging as the mode-switching still completes in both directions with only a few partial burn cycles during the HCCI-SI mode-switches. These are due to a lean mixture implemented in Section 4.9 to smooth IMEP during the transition. Delivering more CNG on the first SI cycle after these HCCI-SI mode-switches would remedy the partial burn cycles experienced in this situation. Again, the first few cycles under HCCI combustion are evaluated using Woschni heat transfer coefficients for SI while the spark is still activated as discussed in Section 3.3.1.
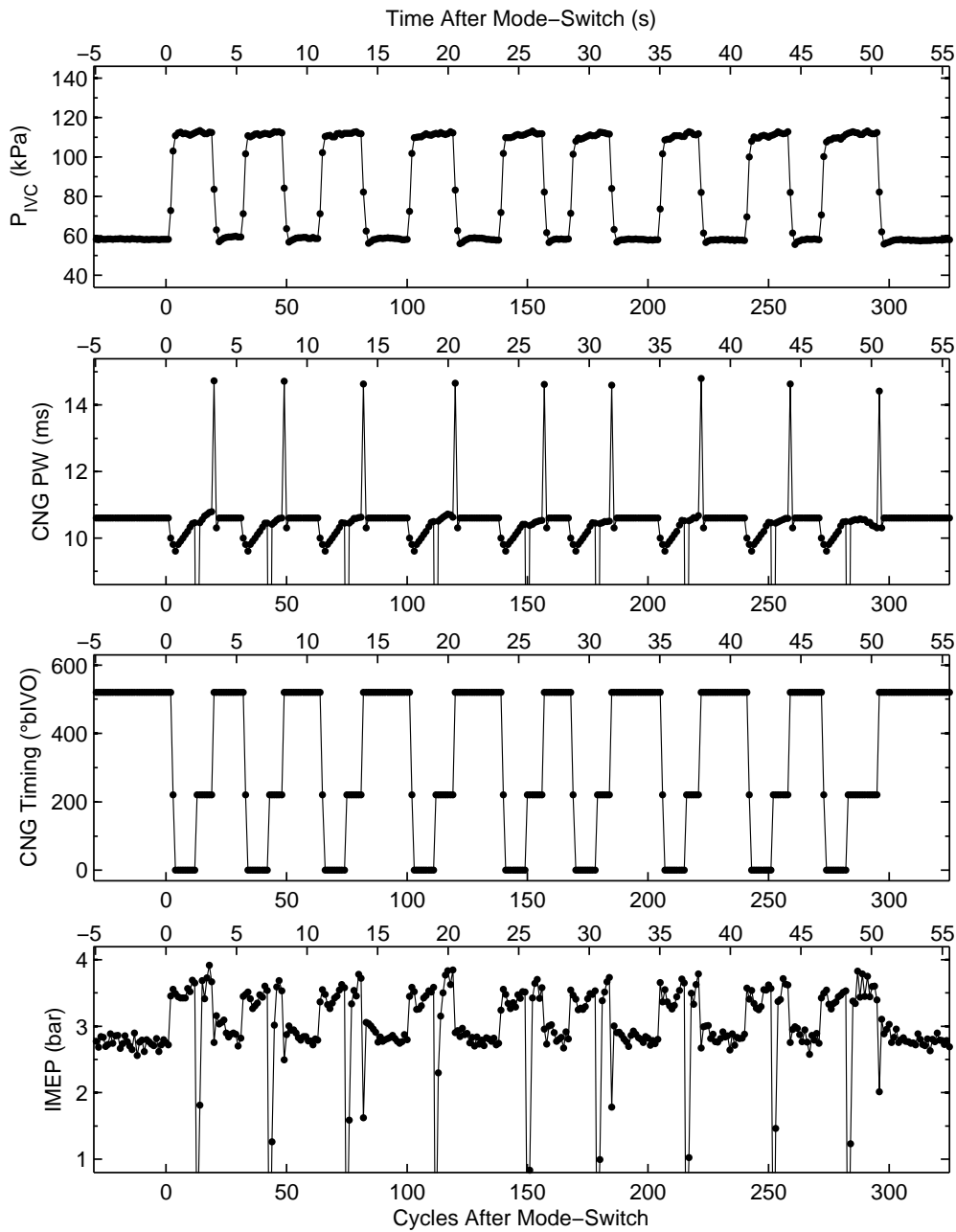
Figure 4.30: Controls and IMEP during repeated SI-HCCI-SI mode-switching. Low P_{IVC} and IMEP values correspond to SI and high values are HCCI. CNG PW and IMEP values falling below the lower edge indicate a misfire resulting from the necessary CNG timing adjustment. $\epsilon_{IMEP} = 0.06$ bar, $\epsilon_{PIVC} = 2.8$ kPa, $\epsilon_{InjectionTiming} = 1.1$ CAD
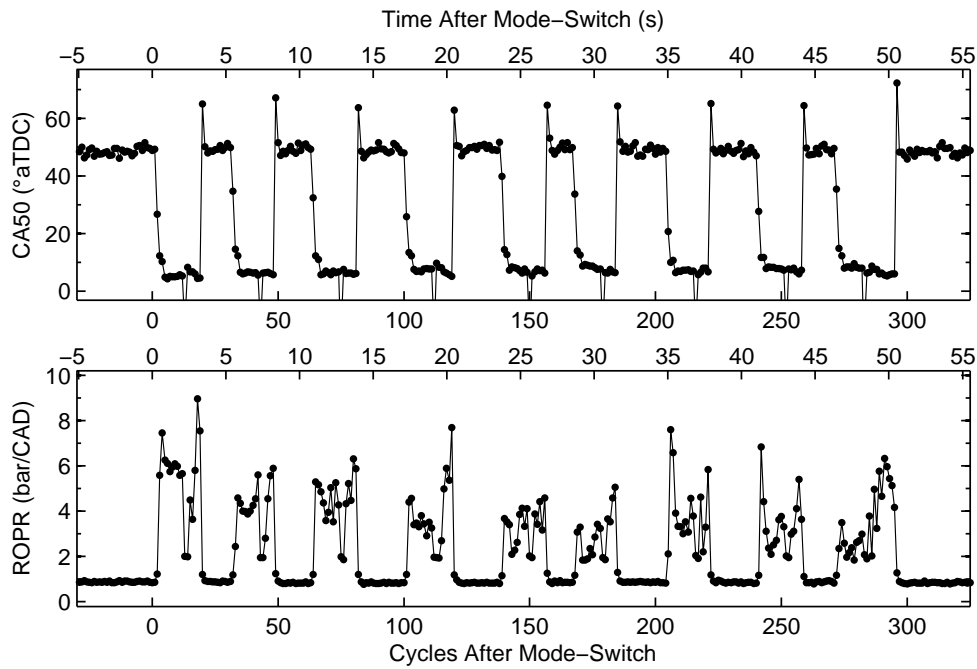
Figure 4.31: Combustion evaluation during repeated SI-HCCI-SI mode-switching. CA50 values falling below lower edge indicate a misfire resulting from CNG timing adjustment. SI and HCCI operation correspond with Figure 4.30. $\epsilon_{CA50} = 3.1/0.89$ CAD (SI/HCCI), $\epsilon_{ROPR} = 0.03$ bar/CAD, $\epsilon_{EquivalenceRatio} = 12\%$
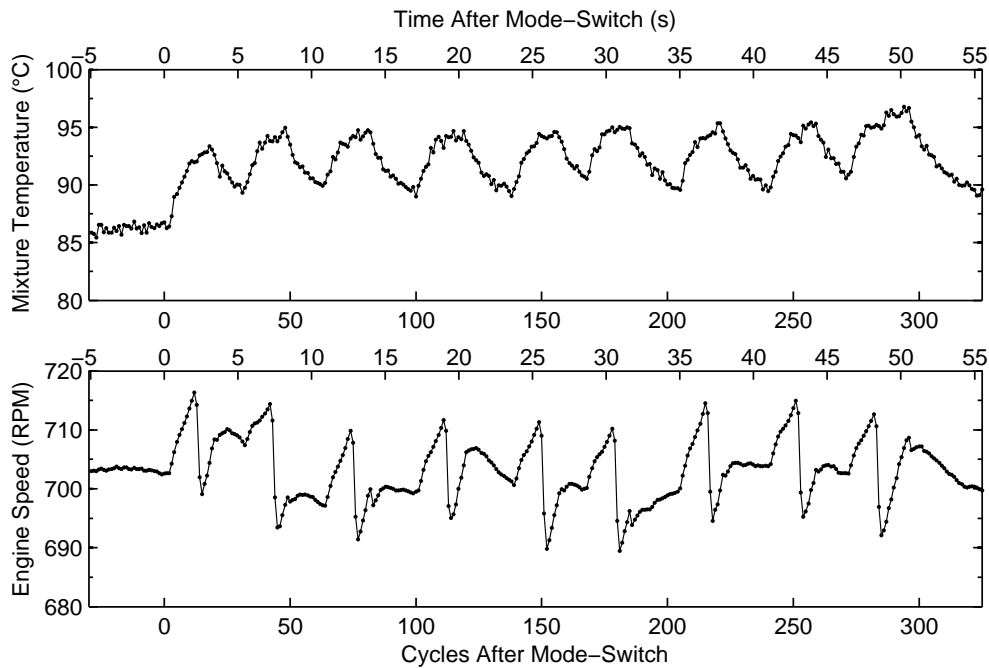
Figure 4.32: Disturbances experienced during repeated SI-HCCI-SI mode-switching that are not considered in the open-loop control sequence. SI and HCCI operation correspond with Figure 4.30.

4.11   Extension to Other Operating Points

In this section, a different operating speed is tested to show mode-switching potential along with variability in IMEP for both SI and HCCI. The focus of this research is directed toward large stationary engines, so a slower engine speed of 500 RPM is chosen. Slower engine speed induces some changes in HCCI combustion, most notable being less memory effect between cycles, and less audible knock at the same ROPR value.

Testing begins with an operating point similar to those presented in previous mode-switching tests, although with cooler intake air temperature and slightly advanced spark timing to increase IMEP in SI. Table 4.10 presents the variations on this operating point to achieve higher and lower IMEP levels in both SI and HCCI. Open-loop control sequences for fuel delivery and throttle positions are developed in the same manner as described in sections 4.8 and 4.9. Figures 4.33, and 4.37 present results for various IMEP levels in SI for both directions of mode-switch, while Figure 4.35 and 4.39 present tests for different levels of IMEP during HCCI operation. Calculated parameters including CA50, ROPR, and equivalence ratio are provided in Figures 4.34, 4.38, 4.36, and 4.40 for the aforementioned test data. Several observations are drawn from this information and are outlined in Sections 5.4 and 5.4.

Mode-switch effectiveness for these tests with varying IMEP is presented in Table 4.11. Most cases are optimized to an ideal case where MSPC is equal to 1; however, four of the tests have some penalty. The only significant penalty occurs for test 3 SI-HCCI due to knock that propagates after the mode-switch as shown in Figure 4.36.

Table 4.10: Steady-state operating conditions between which mode-switching tests occur for Figures 4.33, 4.37, 4.35, and 4.39. All HCCI points operate with an ROPR set point of 6 bar/CAD.

	Test data at steady-state (SI / HCCI)				
	1	**2**	**3**	**4**	**5**
Engine Speed (RPM)	500	500	500	500	500
Intake Temperature (°C)	110	110	110	110	160
Mixture Temperature (°C)	75/83	76/84	74/83	75/85	84/103
Air Mass Flow (g/s)	1.08/2.44	0.94/2.50	0.83/2.50	1.08/2.70	1.05/2.46
CNG Mass Flow (mg/s)	59.1/59.9	45.5/60.2	46.2/61.4	59.2/65.3	60.3/54.4
Volumetric Efficiency (η_{vol})	0.75/0.92	0.73/0.91	0.72/0.92	0.75/0.90	0.75/0.94
Throttle Set Point (%)	20.3/78.7	13.2/79.4	3.4/76.7	18.4/100	19.9/76.0
Equivalence Ratio	0.94/0.41	1.00/0.42	0.96/0.42	0.96/0.42	0.99/0.38
Spark Timing (°aTDC)	3	3	0	3	5
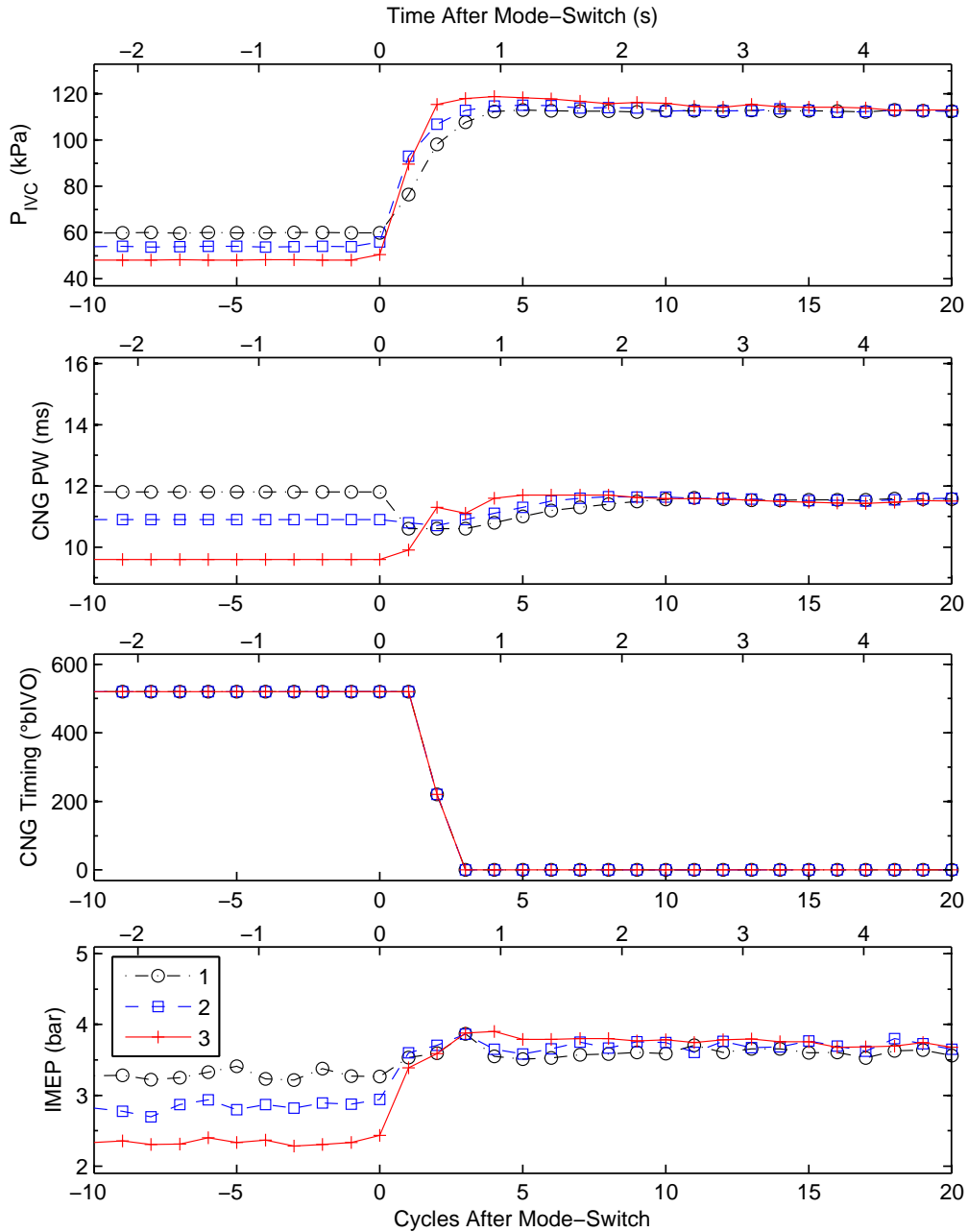
Figure 4.33: SI-HCCI mode-switches showing different power levels during SI operation. $\epsilon_{IMEP} = 0.06$ bar, $\epsilon_{PIVC} = 2.8$ kPa, $\epsilon_{InjectionTiming} = 1.1$ CAD
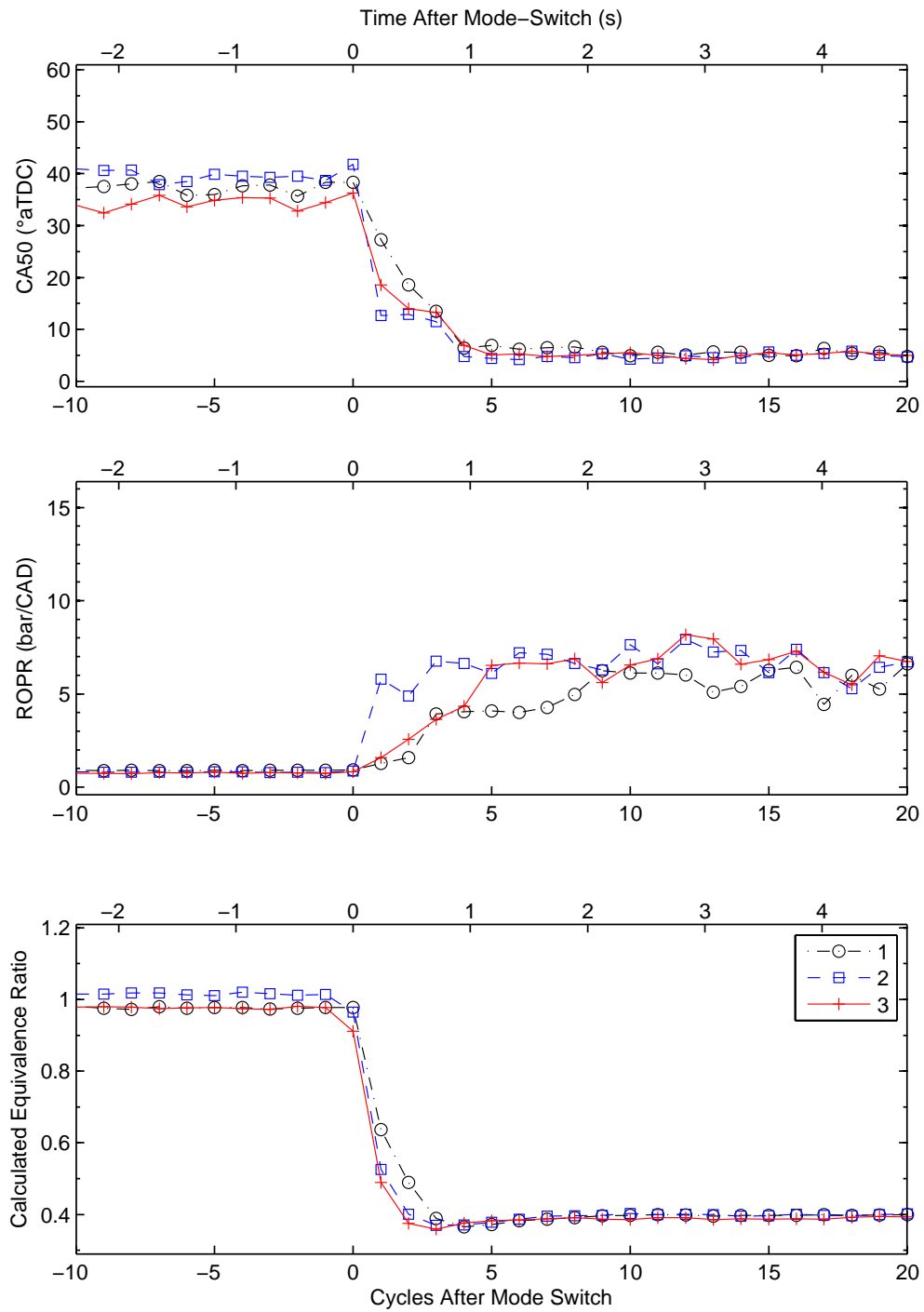
Figure 4.34: CA50, ROPR, and approximate equivalence ratio for SI-HCCI mode-switches presented in Figure 4.33. $\epsilon_{CA50} = 3.1/0.89$ CAD (SI/HCCI), $\epsilon_{ROPR} = 0.03$ bar/CAD, $\epsilon_{EquivalenceRatio} = 12\%$
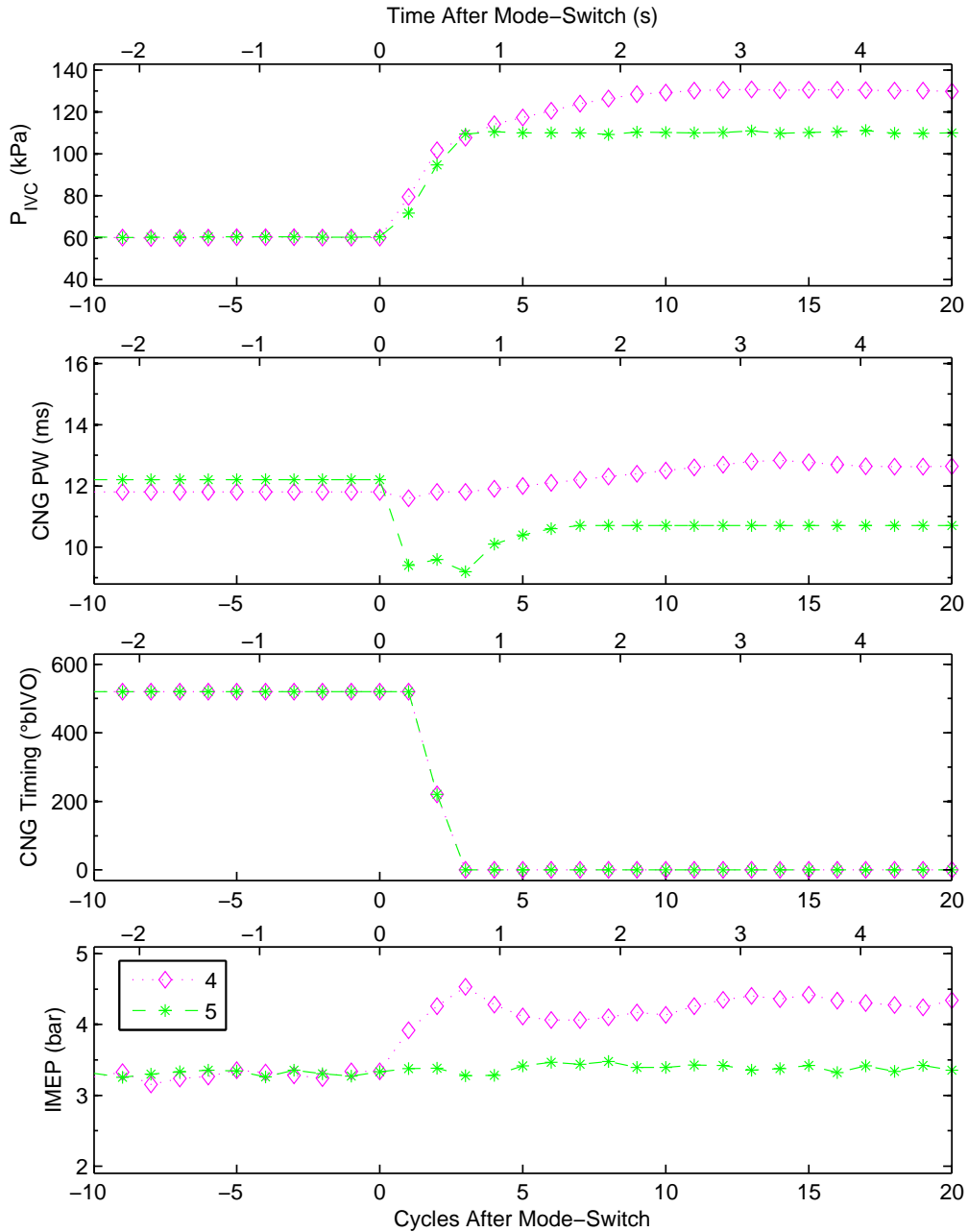
Figure 4.35: SI-HCCI mode-switches showing different power levels during HCCI operation. $\epsilon_{IMEP} = 0.06$ bar, $\epsilon_{PIVC} = 2.8$ kPa, $\epsilon_{InjectionTiming} = 1.1$ CAD
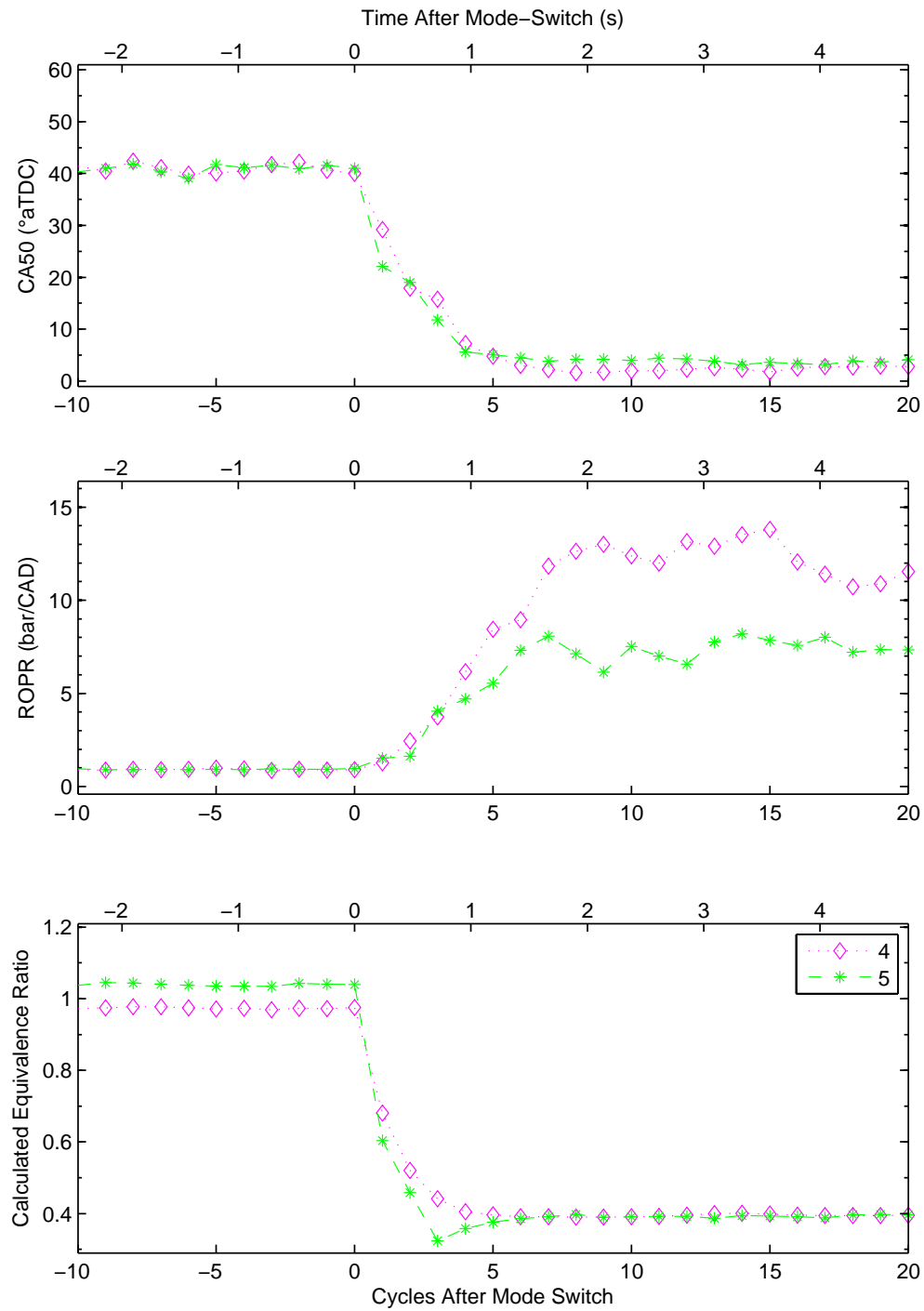
Figure 4.36: CA50, ROPR, and approximate equivalence ratio for SI-HCCI mode-switches presented in Figure 4.35. $\epsilon_{CA50} = 3.1/0.89$ CAD (SI/HCCI), $\epsilon_{ROPR} = 0.03$ bar/CAD, $\epsilon_{EquivalenceRatio} = 12\%$
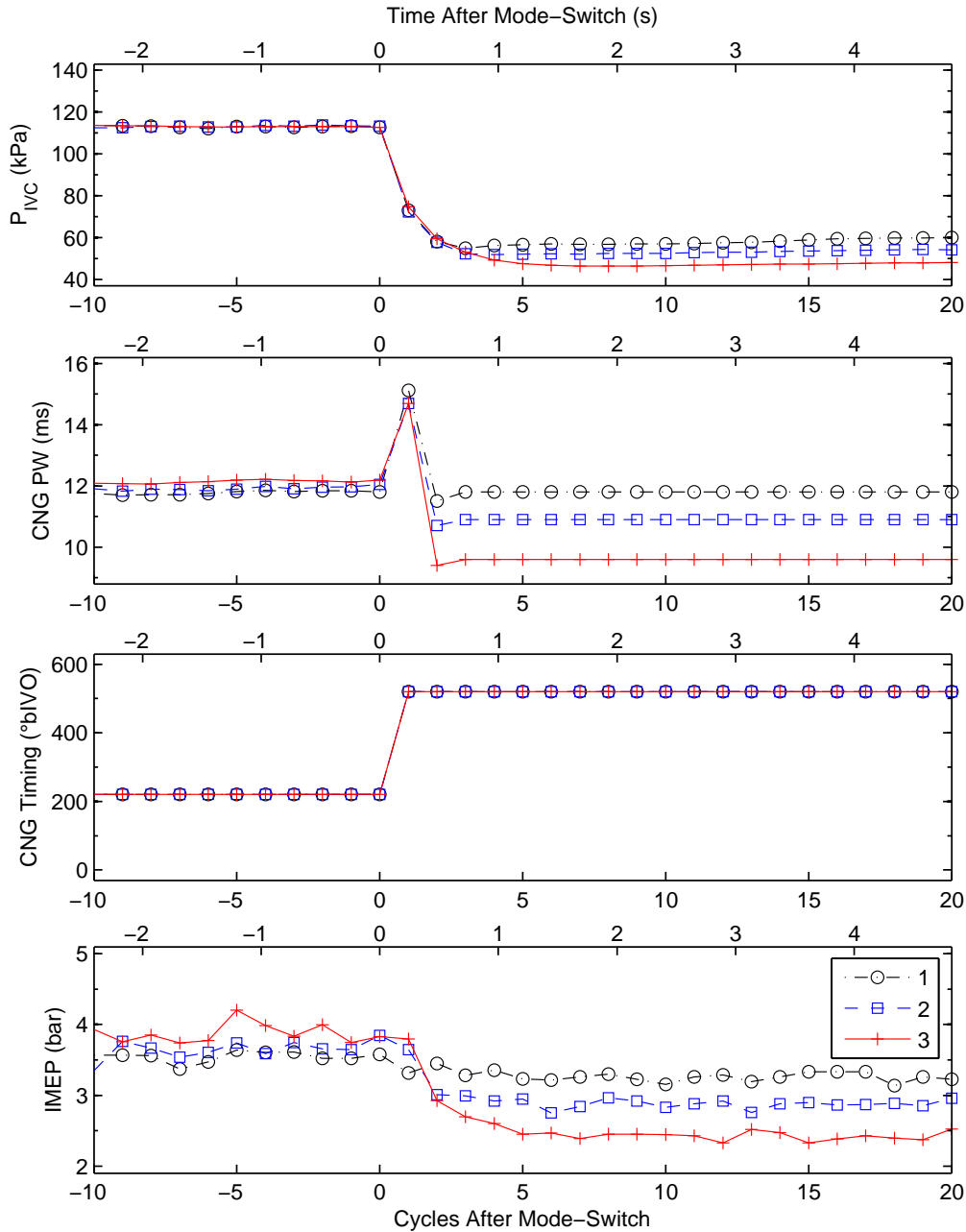
Figure 4.37: HCCI-SI mode-switches showing different power levels during SI operation. $\epsilon_{IMEP} = 0.06$ bar, $\epsilon_{PIVC} = 2.8$ kPa, $\epsilon_{InjectionTiming} = 1.1$ CAD
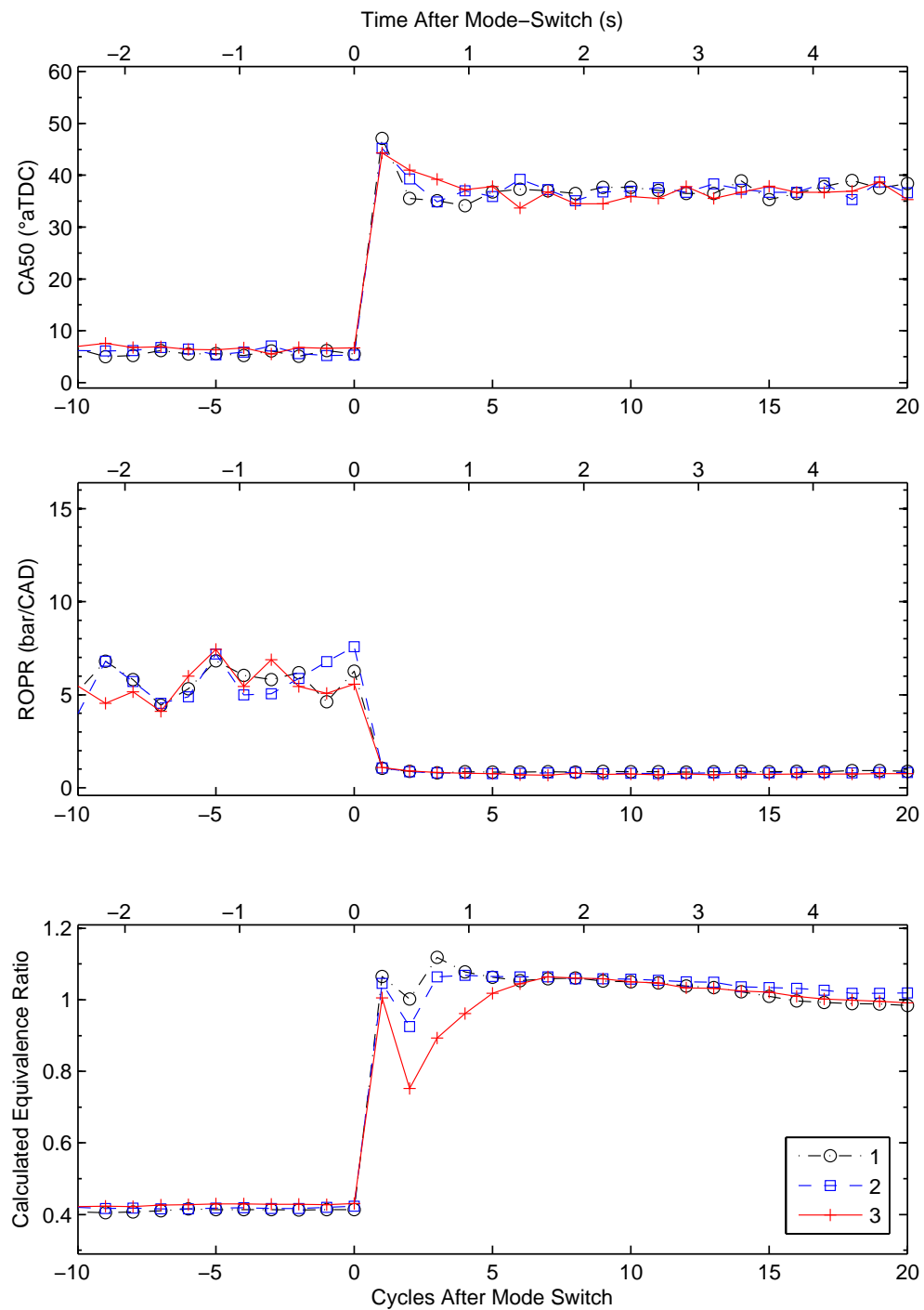
Figure 4.38: CA50, ROPR, and approximate equivalence ratio for HCCI-SI mode-switches presented in Figure 4.37. $\epsilon_{CA50} = 3.1/0.89$ CAD (SI/HCCI), $\epsilon_{ROPR} = 0.03$ bar/CAD, $\epsilon_{EquivalenceRatio} = 12\%$
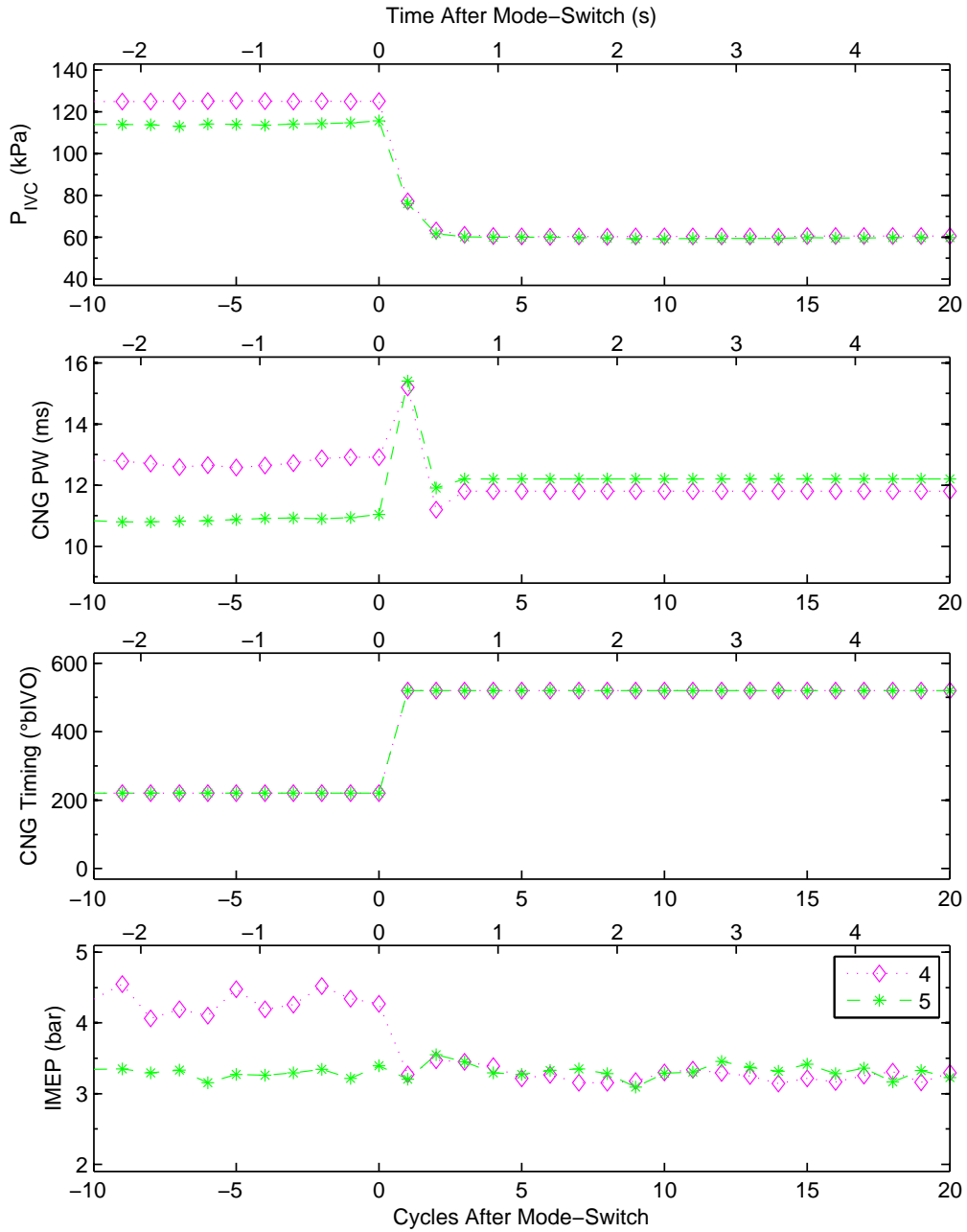
Figure 4.39: HCCI-SI mode-switches showing different power levels during HCCI operation. $\epsilon_{IMEP} = 0.06$ bar, $\epsilon_{PIVC} = 2.8$ kPa, $\epsilon_{InjectionTiming} = 1.1$ CAD
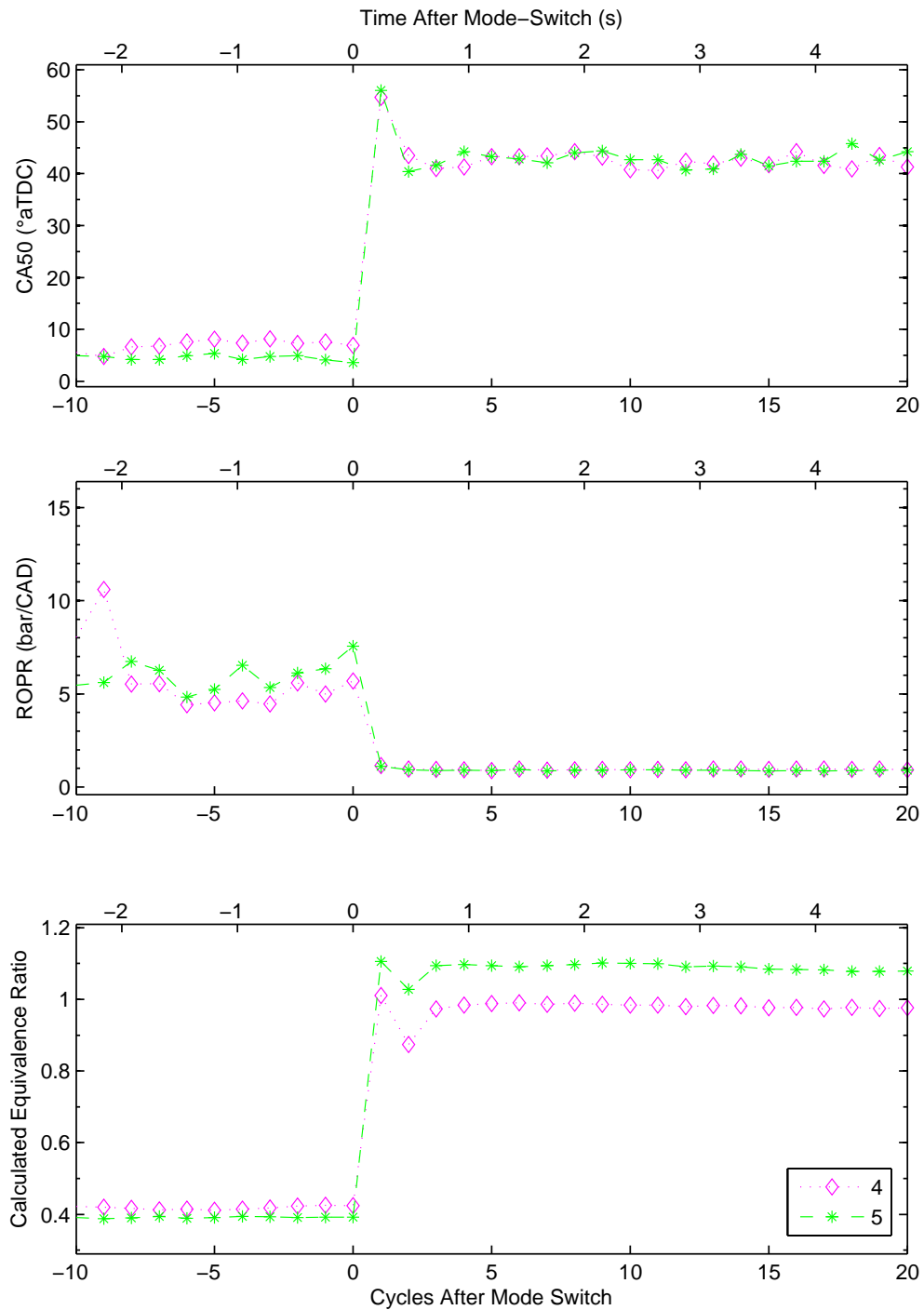
Figure 4.40: CA50, ROPR, and approximate equivalence ratio for HCCI-SI mode-switches presented in Figure 4.39. $\epsilon_{CA50} = 3.1/0.89$ CAD (SI/HCCI), $\epsilon_{ROPR} = 0.03$ bar/CAD, $\epsilon_{EquivalenceRatio} = 12\%$

Table 4.11: MSPC data for Section 4.11.

Year_	Month_Day - Test Number									
2010_	09_27 - 14	09_27 - 13	09_27 - 43	09_27 - 39	09_30 - 95	09_29 - 25	09_29 - 48	09_29 - 47	10_01 - 23	09_30 - 16
Plot Label	1 SI-HCCI	1 HCCI-SI	2 SI-HCCI	2 HCCI-SI	3 SI-HCCI	3 HCCI-SI	4 SI-HCCI	4 HCCI-SI	5 SI-HCCI	5 HCCI-SI
Duration	1	1	1	2	1	3	1	1	1	1
Smoothness	0.00	0.00	0.00	0.38	0.39	0.71	0.14	0.00	0.00	0.00
Stabilize	1	1	1	2	1	3	24	1	1	1
Knock	0.00	0.00	0.00	0.00	0.00	0.00	17.11	0.00	0.00	0.00
MSPC	1.00	1.00	1.00	2.38	1.39	3.71	18.25	1.00	1.00	1.00

CHAPTER 5

DISCUSSION

This chapter discusses the results presented in Chapter 4 for a better understanding of engine response during SI-HCCI-SI mode-switching.

5.1 SI-HCCI-SI Mode-Switching With Conventional Actuators

Conventional actuators, throttle and CNG injection, are used in this study to enable SI-HCCI mode-switching between two steady-state operating points. The effects of adjusting these controls during a mode-switch are summarized in Figure 5.1. Higher P_{IVC} resulting from larger throttle openings increases the tendency toward knock, while lower P_{IVC} increases the tendency toward misfire. CNG pulse width has a similar response, while CNG injection timing promotes knock by more advanced combustion timing. Achieving the desired IMEP for a smooth mode-switch requires a balance between suitable combustion (no misfire or knock) and the mass of CNG available during a combustion cycle for sufficient heat release. For example, initial experiments in Section 4.2 avoid knock by reducing CNG PW, but with an associated drop in IMEP; the later work in Section 4.8 achieves the correct balance of actuators to avoid knock while still achieving the desired IMEP.

P_{IVC} and CNG pulse width adjustments for HCCI-SI mode-switching follow a similar response, as shown in Figure 5.2, with higher values having higher tendency
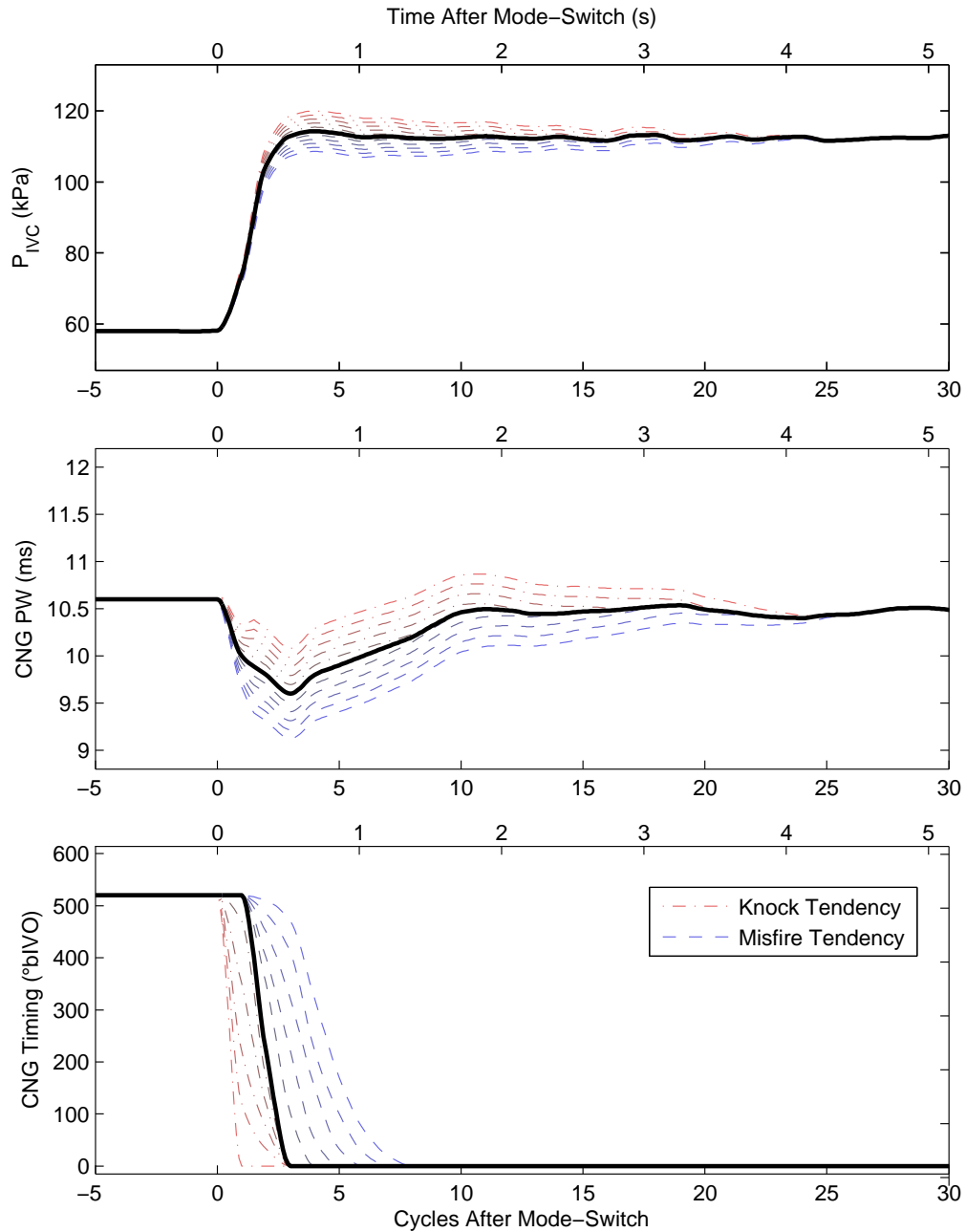
Figure 5.1: SI-HCCI mode-switching map showing actuator adjustments to tend toward knock and misfire.

toward knock. CNG timing, however, tends toward knock by retarding more slowly over a greater number of cycles. These effects must be considered to avoid unexpected knock; however, mixture quality and spark timing during early SI operation dictate IMEP and are controlled to achieve a smooth transition while avoiding misfire. Leaner mixtures by reducing CNG PW at a given P_{IVC} can be used to reduce IMEP, but increase the likeliness of misfire; greater charge mass near stoichiometric conditions increases IMEP with a higher tendency toward knock.

5.1.1 Redevelopment of Mode-Switching Control Sequences for Another Engine

The mode-switching strategies developed in this work provide a methodology to develop open-loop control using only convention actuation for a candidate engine. A more direct means of developing the control sequences is possible using experience obtained from testing. These steps are outlined below.

First, compatible operating points must be found where stable operation in both SI and HCCI combustion modes is possible with the same intake air temperature. Tables 4.1, 4.6, and 4.10 indicate the operating points used in this study and may be used for reference.

Throttle control values can be determined while motoring the engine without fuel. The goal is to transition between the steady-state levels of P_{IVC} and achieve the same trend as demonstrated in Figures 4.22 or 4.26 depending on the direction of mode-switch. P_{IVC} values should be slightly lower than the steady-state values determined above since CNG is not being injected in the intake manifold while motoring. The amount lower can be determined by motoring the engine at the same speed and throttle opening as the steady-state operating points found above and measuring the reduced P_{IVC} for both operating modes.

Develop the open-loop CNG injection parameters similar to the values in Fig-
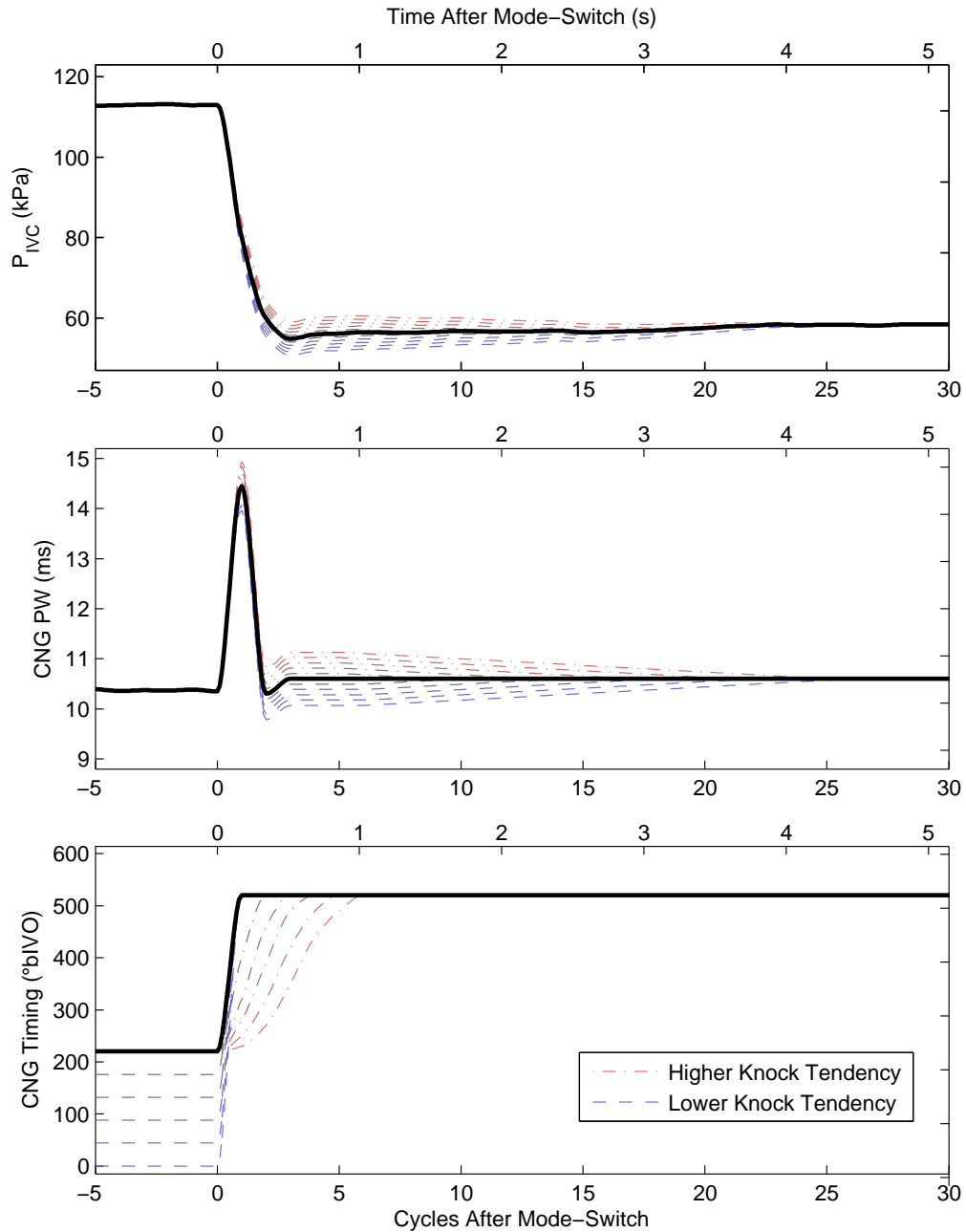
Figure 5.2: HCCI-SI mode-switching map showing actuator adjustments to tend toward knock and misfire.

ures 4.22 or 4.26 but scaled based on the new experimental setup (for instance, if using a higher CNG injection pressure the pulse widths will have to be scaled down to achieve a similar mass of CNG delivery per cycle). Reduce the mass delivered for all cycles during and following the mode-switch by 10-20% to initially approach misfire as opposed to knock.

Start the engine and operate in SI mode until steady-state (see Section 3.4) is achieved at the desired mode-switch operating conditions. Attempt the mode-switch using the developed throttle and fuel control sequences simultaneously. Note that synchronization of input response on each cycle is essential. Increase fuel delivery gradually on successive runs, starting with the early cycles in the mode-switch, until IMEP and ROPR approach the target values. Figures 5.1 and 5.2 can then be used to tune the control sequences and achieve the desired IMEP while avoiding misfire and knock.

5.2 Repeated SI-HCCI-SI Mode-Switching

HCCI is sensitive to operational disturbances under normal operation, and this is reflected in repeat mode-switches. ROPR following the first SI-HCCI transition, shown in Figure 4.31, quickly approaches the target value of 6 bar/CAD since the engine is under the intended conditions for mode-switching. Successive SI-HCCI mode-switches experience a reduction in ROPR indicating reduced stability. Higher variability in the IMEP results support this observation. Deviation increases as engine conditions drift further from the steady-state values for which the mode-switch sequence is developed. Even with degrading combustion, all mode-switches successfully achieve on-going HCCI operation. CA50 approaches the steady-state value quickly following all SI-HCCI mode-switches, taking only 2-3 cycles to transition.

Based on this test, the open-loop control being implemented can handle some level of disturbance while still completing the mode-switch properly. Further devi-

ation from the design conditions would eventually lead to misfire or knock, which could be addressed with some form of feedback or adaptive control. Profiling additional operating points to map a range of expected conditions may also provide a means of adapting to disturbances through interpolation [34]. Additional consideration of environmental conditions (air temperature, humidity, etc.) and operating variables (fuel composition, oil temperature, etc.) will require further investigation to determine their influence on mode-switching and the degree of control necessary to accommodate them.

5.3   Variation in Steady-State IMEP for SI-HCCI Mode-Switching

In Figures 4.33 and 4.35, the CNG PW is commanded to respond in a manner proportional to the difference in steady-state IMEP levels. Having a small IMEP increase from SI to HCCI suggests that lower values of CNG PW are needed during the initial HCCI cycles. This is likely due to the relatively hotter residual gases and combustion chamber surfaces, promoting earlier ignition timing and more efficient combustion.

Similarly in Figure 4.33, intake pressure must be increased at a faster rate when starting at a lower IMEP level in SI and stepping up to the same IMEP in HCCI. The calculated equivalence ratios in Figure 4.34 show an obvious trend with the first three cycles corresponding to the differences in fuel and intake pressure as discussed above, with all tests approaching the same steady-state level as HCCI combustion stabilizes.

Observing IMEP data for SI-HCCI transitions in Figures 4.33 and 4.35, it is evident that the third cycle after the mode-switch shows a sudden increase for most tests. This is related to advancing CNG injection timing directly to IVO causing combustion timing to advance. The sudden decrease in fuel on this cycle for test 3 in Figure 4.33 is an attempt to counteract this effect; however, it appears

that a greater reduction in CNG PW is necessary. Test 5 in Figure 4.35 uses a more significant reduction in fuel for this cycle, successfully removing the IMEP increase for a smoother transition. An alternative approach could be to advance the injection timing more slowly at this cycle, which as discussed in Chapter 3 is a limitation of this experimental setup.

SI-HCCI mode-switching to higher levels of IMEP in HCCI are found to be more prone to knock, as demonstrated by test 4 in Figure 4.36. Further tuning of this point may remove this condition by increasing intake pressure at a slower rate, or by overcoming the injection timing limitation and advancing the injection event toward IVO at a slower rate than the 2 cycle step implemented here. Leaner mixtures by reducing CNG mass delivery during the knock period could also remedy the situation, but likely at the expense of a longer transition to the steady-state IMEP in HCCI. Addition of external EGR could also be employed to mitigate knock in this scenario, but with careful consideration necessary due to the significant change in exhaust gas flow rate, temperature, and composition during the mode-switch. Another alternative would be to reduce the engine compression ratio to achieve higher IMEP in HCCI through greater supercharging pressure [23]; however, for a conventionally controlled engine, this adjustment would not be possible during operation and would be restricted to an initial design decision.

5.4   Variation in Steady-State IMEP for HCCI-SI Mode-Switching

For mode-switching from HCCI to SI, most notable for discussion is the fuel delivery during early SI operation. CNG PW must be increased significantly on the first SI cycle, as demonstrated in Figures 4.37 and 4.39, to allow SI ignition with the greater air mass. The objective is to keep the mixture stoichiometric or slightly lean to avoid an increase in IMEP by retarding combustion past the steady-state CA50 value. Calculated equivalence ratios in Figures 4.38 and 4.40 suggest that

near stoichiometric conditions are experienced during this first SI cycle, with the exception of test 5 that appears to be running slightly rich and yet still exhibits a similarly late CA50. Ongoing rich mixtures are calculated for SI in test 5 as operation stabilizes. Comparing these with the equivalence ratio provided in Table 4.10, which instead is derived from average mass flow measurements of air and CNG, the rich tendency shown in Figure 4.40 is believed to be an artifact of the per-cycle equivalence ratio calculations outlined in Section 3.1.4. The higher intake air temperature is the likely cause for the deviation. Note that the 12% error in this parameter still includes stoichiometric operation for these cycles.

Moving forward, the second SI cycle in Figures 4.37 and 4.39 following an HCCI-SI mode-switch reduces CNG PW to slightly below the steady-state level for smoother IMEP response. All following cycles are held at the steady-state level. In all tests, there are some fluctuations in the calculated equivalence ratio during cycles 2-4, shown in Figures 4.38 and 4.40, as P_{IVC} and other conditions stabilize. A more consistent equivalence ratio during early SI operation could be achieved by tailoring the inputs based on these results, although the smoothness of IMEP and the other calculated parameters suggest that re-testing would provide little visible benefit. Only test 3 shows a significant deviation from stoichiometric operation, where leaner mixtures during cycles 2-4 help reduce IMEP more quickly as the intake pressure continues to decrease to the desired steady-state level. CA50 data in Figure 4.38 supports this with a smoother yet longer transition toward steady-state ignition timing.

Test 5 in Figures 4.35 and 4.39 presents a constant load mode-switch that is useful for applications where it is desirable to achieve HCCI combustion without disturbing power output. A higher intake temperature is necessary under the conditions tested in order to reduce HCCI power sufficiently for this purpose, as IMEP in SI could not be increased without experiencing knock at these high intake

temperatures. This demonstrates the potential limits in the ability of the engine to respond to a broad range of power requirements at the mode-switch boundary using only fast conventional actuators. On the other hand, it is interesting to know that a constant load SI-HCCI-SI mode-switch is possible using only conventional actuation.

5.5   Mode-Switching Performance Criterion (MSPC)

The performance of this parameter is explored by evaluating all of the mode-switching done in this study and comparing the results qualitatively relative to one another, as is the current standard procedure. Individual components (duration, smoothness, and knock) and the overall average and standard deviation of each set of data correlates well with the subjective observations regarding the different methods.

Subjective observations for each section correlate well with the the individual components of MSPC (duration, smoothness, and knock) as well as the overall average and standard deviation for the 10 tests in each set.

For instance, Section 4.2 provided a rough modes-switch with a large drop in IMEP for several cycles, but is fairly repeatable; whereas Section 4.3 is generally a better switch but with more variability between tests with some containing partial burn or knock cycles. Correspondingly, Section 4.2 provides a much higher average MSPC than Section 4.3, but with a lower standard deviation between tests. Other sections compare similarly with the qualitative discussion presented in the associated sections. Values follow the expected trend with less refined tests from the earlier sections providing much higher (less desirable) MSPC values than the optimized scenarios.

5.5.1 Weight Factor Justification

With no other criteria to judge the performance of the MSPC, a comparison is made with alternate weight factors that have been considered. The selected values are provided in Table 5.1 with MSPC data re-evaluated from Sections 4.2 - 4.9 given in Table 5.2. A visual comparison is presented in Figure 5.3 for the development of SI-HCCI mode-switching from Sections 4.2 (Intake pressure step), 4.3 (Throttle step), 4.4 (Injection timing adjustment), and 4.8 (Optimized). It is important to note that the trends in Figure 5.3 remain the same despite the changes in weight factors. This indicates that the MSPC criterion appears to be a robust measure of mode-switching effectiveness.

Table 5.1: Alternate MSPC weight factors.

	Proposed Method	Option 1	Option 2
Duration	1	1	0
Smoothness	Duration/2	2	Duration
Stabilize	0	0	0
Knock	0.5	0.25	0.5
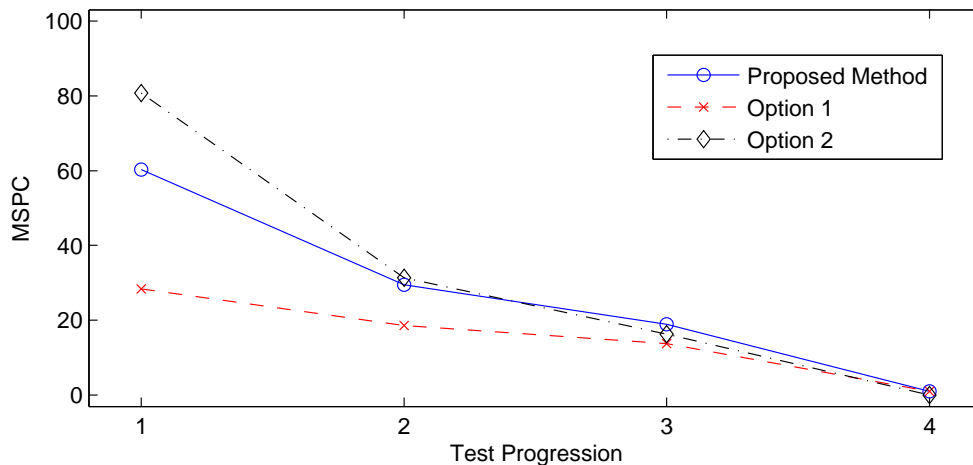
Figure 5.3: MSPC weight factor comparison for SI-HCCI mode-switching development tests.

Table 5.2: MSPC data calculated with alternate weight factors given in Table 5.1. Average values for all 10 tests in each section are provided.

SI-HCCI: Intake pressure step	Proposed Method	Option 1	Option 2
Duration	19.90	19.90	0.00
Smoothness	40.30	8.46	80.60
Stabilize	20.90	20.90	20.90
Knock	0.10	0.05	0.10
MSPC	60.30	28.41	80.71

SI-HCCI: Throttle step	Proposed Method	Option 1	Option 2
Duration	11.60	11.60	0.00
Smoothness	13.47	4.75	26.95
Stabilize	20.20	20.20	20.20
Knock	4.41	2.20	4.41
MSPC	29.48	18.55	31.36

SI-HCCI: Injection timing adjustment	Proposed Method	Option 1	Option 2
Duration	10.30	10.30	0.00
Smoothness	7.70	3.01	15.41
Stabilize	12.30	12.30	12.30
Knock	0.94	0.47	0.94
MSPC	18.95	13.78	16.35

HCCI-SI: Large manifold	Proposed Method	Option 1	Option 2
Duration	26.50	26.50	0.00
Smoothness	40.95	5.81	81.90
Stabilize	26.50	26.50	26.50
Knock	0.00	0.00	0.00
MSPC	67.45	32.31	81.90

HCCI-SI: Small manifold	Proposed Method	Option 1	Option 2
Duration	3.00	3.00	0.00
Smoothness	0.77	1.02	1.53
Stabilize	3.00	3.00	3.00
Knock	0.00	0.00	0.00
MSPC	3.77	4.02	1.53

SI-HCCI: Optimized	Proposed Method	Option 1	Option 2
Duration	1.00	1.00	0.00
Smoothness	0.00	0.00	0.00
Stabilize	1.00	1.00	1.00
Knock	0.00	0.00	0.00
MSPC	1.00	1.00	0.00

HCCI-SI: Optimized	Proposed Method	Option 1	Option 2
Duration	1.20	1.20	0.00
Smoothness	0.30	0.71	0.61
Stabilize	1.20	1.20	1.20
Knock	0.00	0.00	0.00
MSPC	1.50	1.91	0.61

5.5.1.1 Option 1

Smoothness in this alternative is weighted with a constant value that is not dependent on the duration. The drawback of this approach is most notable in Figure 5.3 where only a small difference exists between the first two SI-HCCI tests, intake pressure step and throttle step. Experimental observations of IMEP data from the intake pressure step tests experienced a significant drop for early HCCI cycles that was eliminated in the following throttle step tests. The proposed method more accurately demonstrates this improvement with its duration-dependent weight factor for smoothness.

The knock penalty is also reduced in this alternative by one half. The result is that all knock values scale down by a factor of 2 for a similar relative influence on the final MSPC as in the proposed method. The linear relationship between knock intensity and ROPR has been assumed for the evaluation of MSPC and can not be verified further without a detailed investigation.

5.5.1.2 Option 2

Another method to evaluate mode-switch performance is to consider duration only as the weight factor for smoothness. The improvement in IMEP smoothness between the intake pressure step and throttle step tests is accurately represented by MSPC, as demonstrated in Figure 5.3. For the tests presented in Table 5.2, it is not evident why this option is less desirable than the proposed method, but can be discussed in a theoretical sense.

The objective of mode-switching is to achieve the new steady-state IMEP level in a quick and smooth manner. The developed smoothness criterion only evaluates deviation from a linear trend between the initial and final IMEP levels with no direct indication of the number of cycles involved in this calculation. In the case where the engine responds very close to this linear trend and $COV_{\text{IMEP\_trans}}$ is less

than 5%, smoothness is assigned a value of 0 and the duration weight factor has
no effect. This case should only be considered ideal if the linear trend occurs over
a single cycle as well, or the requirement for a "quick" mode-switch has not been
met. The proposed method takes this into account by considering an independent
duration penalty.

5.5.2   Extension of MSPC to Other Scenarios

As presented thus far, MSPC is useful for evaluating mode-switching on a single-
cylinder engine between two arbitrary IMEP levels. Moving toward real-world
applications, other issues arise requiring attention: transition of slow actuators,
power demand, and multiple cylinders. With minor modifications, the MSPC can
cover these scenarios as well.

5.5.2.1   Power Demand

Adapting MSPC to a dynamic power demand is easily accomplished. Instead of
finding the steady-state IMEP in the final combustion mode, the target values con-
sist of the demand for the engine as it is being controlled. Equations 3.10, 3.11, and
3.12 still apply and the mode-switch is considered complete when COV_{IMEP_trans},
comprised of a running 15 cycles, drops below 5%. This scenario will become more
prominent as mode-switching controllers are developed and performance must be
evaluated while responding to an unknown input from an operator.

5.5.2.2   Transition of Slow Actuators

Mode-switching is evaluated between two steady-state points in this study with nei-
ther representing typical operation in either SI or HCCI. Under normal operation,
the engine will be required to transition slow actuators, such as intake tempera-
ture, to a region able to support a mode-switch, initiate the mode-switch itself,

then transition to the final operating point. Engine operation during these slow transitions may or may not require a penalty depending on whether the engine can respond to demand.

The variable power demand discussed above can be evaluated during this transition with any deviation from the target IMEP causing a COV_{IMEP_trans} greater than 5% or knock cycles leading to penalties similar to during the mode-switch itself. If IMEP deviation and knock reduce to an acceptable level before the entire transition is complete, penalties will not be necessary until the mode-switch itself or the engine deviates again. This incorporates the benefit of mode-switching strategies incorporating more comprehensive actuators, such as variable valve technology, that can adjust cylinder conditions sufficiently with all fast actuators and avoid transition time of any slow actuators. On the other hand, applications where power demand does not change instantaneously or can be predicted may not need the capibility to mode-switch without slow actuation first, and may benefit more from a mechanically simpler solution.

For this study, slow actuation is not tested or considered. The engine operates steady-state in both modes at the selected operating conditions, so a transition of slow actuators is unnecessary. Intake air temperature responds with a very long time constant in the existing setup, so the feasibility of repeating mode-switches for development is further time limited. Modifications could be made to improve response time by installing an electric air heater or exhaust gas heat exchanger with improved air contact surface area and reduced thermal mass, or by implementing a fast thermal management system (mixing air from hot and cold streams). This would allow for investigation of the transition between mode-switching operating conditions and more typical operating points for SI and HCCI.

5.5.2.3   Multiple Cylinders

Mode-switching with multiple cylinders adds the complication of deciding how to combine the data in a representative and suitable manner. A few alternatives are considered:

- First, averaging the data (IMEP and ROPR) from all cylinders on each cycle provides an indication of overall engine performance during the mode-switch. Analysis is simple and can be carried out in the same manner as presented; however, misfire, partial burn, and knock cycles may occur on individual cylinders simultaneously, with the averaging causing the stability of the engine to be mis-represented.

- Another approach is to consider each combustion event sequentially across all cylinders. Cycles with poor combustion are evaluated properly, but the duration and smoothness of the mode-switch analysis may be compromised if certain cylinders take longer to stabilize than others.

- Finally, each cylinder could be considered individually and evaluated as presented in this study. Cylinders may progress through the mode-switch at different rates based on operating conditions and the control scheme being used, and each cylinder would also account for undesirable knock or misfire.

The last option offers the most representative evaluation and is discussed further. For example, assume that all tests in one of the mode-switching development sections in Chapter 4 are individual cylinders in a 10-cylinder engine. The average MSPC would describe the engine's overall mode-switch performance for that single test, while the standard deviation of MSPC represents the variability between cylinders for the same test. The only necessary adaptation to the presented definition of MPSC is a method to combine results from several tests in a representative manner of performance and repeatability:

- The average MSPC for each test ($MSPC_i$) could be combined to provide the overall performance of the mode-switching method (μ_{MSPC}).

- The standard deviation between $MSPC_i$ evaluates the stability of the mode-switching method for the engine as a whole (σ_{MSPC}).

- Averaging the standard deviation of MSPC between cylinders for each test represents the typical variability between cylinders ($\sigma_{\text{MSPC\_cyl}}$).

Together, these three values should provide a good indication of the overall performance of a mode-switching strategy on a multiple-cylinder engine. Written expressions for these definitions are summarized here:

$$\mu_{\text{MSPC}} = \frac{1}{J} \sum_{i=1}^{J} MSPC_i \tag{5.1a}$$

$$\sigma_{\text{MSPC}} = \sqrt{\frac{1}{J} \sum_{i=1}^{J} (MSPC_i - \mu_{MSPC})^2} \tag{5.1b}$$

$$\sigma_{\text{MSPC\_cyl}} = \frac{1}{J} \sum_{i=1}^{J} \sqrt{\frac{1}{M} \sum_{j=1}^{M} (MSPC_{\text{cyl(j)}} - MSPC_i)^2} \tag{5.1c}$$

$$J = Number\ of\ Tests$$

$$M = Number\ of\ Cylinders$$

CHAPTER 6

CONCLUSIONS

The objective of this study is to investigate SI-HCCI-SI mode-switching through conventional actuation and establish a means of quantitatively evaluating mode-switching performance. Accomplishments are summarized in the following sections. Potential avenues to further this strategy of mode-switching are also presented.

6.1 SI-HCCI-SI Mode-Switching Through Conventional Actuation

A modified CFR engine operating with port-injected CNG is utilized to explore SI-HCCI-SI mode-switching with conventional actuation. Late spark timing and throttling are implemented to avoid knock during SI with heated intake air. Testing explores the influence of intake pressure, CNG injection mass, and CNG injection timing on mode-switching between SI and HCCI in both directions. Slow actuators such as intake air temperature are not adjusted during the transition. The large intake manifold fitted on the engine initially is determined to be a limiting factor and reduced from 10L to approximately one engine displacement, or 0.5 L, to increase control over air delivery.

Open-loop control is developed experimentally for each sequence of actuator inputs used to mode-switch. Repeatability is explored during development by running open-loop sequences 10 times under the same conditions. Optimized scenar-

ios for mode-switching in both directions are achieved where the new steady-state IMEP is achieved within 1 engine cycle and maintained.

Sensitivities to disturbances are explored by quickly repeating several mode-switches over a one minute period using the same open-loop control sequences as developed for steady-state conditions. Stability in HCCI following an SI-HCCI mode-switch is reduced later in the sequence, but still successfully achieves HCCI combustion in a quick and relatively smooth manner without knock or misfire. In some instances, the first SI cycle following an HCCI-SI mode-switch experiences partial combustion due to the slightly lean mixtures used to limit IMEP. More fuel on this cycle could correct the issue by potentially adding one cycle to the transition duration at an intermediate IMEP.

Initial profiling of the mode-switching region is carried out under various conditions at a slower engine speed of 500 RPM. A range of IMEP is demonstrated in both SI and HCCI steady-state regions surrounding a mode-switch with modified open-loop control sequences achieving relatively smooth transitions in both directions. This proves that mode-switching using conventional actuation is possible at more than a single operating point.

6.2 Mode-Switching Performance Criterion (MSPC)

Mode-switching is evaluated using the developed quantitative measure of duration, smoothness, and knock. This single value, MSPC, can describe the overall effectiveness of a mode-switch under any means of actuation. Comparing with qualitative observation, the current standard, MSPC and its components correlate very well with experimental data in this study. Adaptation of MSPC analysis for situations with variable power demand, necessary transitions of slow actuators, and multiple-cylinder engines is forecast to require only minor adjustments beyond the method presented.

6.3 Future Work

Several possibilities exist as potential areas of research to further develop these two topics:

- Test the influence of other common actuators for their ability to assist and control combustion during a mode-switch. Some possibilities include variable spark timing and exhaust back pressure (such as from a turbocharger). External EGR is commonly used to stabilize HCCI operation and reduce emissions, but offers complications due to variable exhaust composition, temperature, and mass flow during the mode-switch that will have to be accounted for.

- Valve timing more suitable to HCCI operation may be desirable for an engine designed to operate primarily in HCCI, but potential for knock during SI operation will have to be explored. Compression ratio may also be adjusted to shift operating conditions for mode-switching based on the relationship between intake temperature, boost pressure, and heat rise during compression.

- Profile the range of possible mode-switching points for different engine speeds, power levels, and states of slow actuators. A method to determine mode-switching control sequences at intermediate operating points may be possible similar to [34], or model-based controllers capable of adapting to measurable engine conditions and disturbances could be developed. Detailed modeling of the mode-switching with conventional actuators would improve the understanding of conditions necessary to achieve the desired combustion, making controller design more robust and comprehensive.

- Adapt this mode-switching method to multi-cylinder operation. Since individual throttle control for each cylinder is unlikely due to cost and complexity, a range of intake pressures will be experienced during transition through the

unstable region between combustion modes. Other actuators will have to be adjusted to maintain suitable combustion.

- Evaluating COV_{IMEP} over a limited number of engine cycles for MSPC could be explored in greater detail to validate that 15 cycles represents a suitable approximation of engine stability defining the end of a mode-switch.

- Apply MSPC evaluation to mode-switching data from a multiple cylinder engine to validate the proposed summary parameters.

Bibliography

[1] John B. Heywood. *Internal Combustion Engine Fundamentals.* McGraw-Hill, Inc., 1988.

[2] Hua Zhao, editor. *HCCI and CAI engines for the automotive industry.* Woodhead Publishing Limited, 2007.

[3] Shigeru Onishi, Souk Hong Jo, Katsuji Shoda, Pan Do Jo, and Satoshi Kato. Active Thermo-Atmosphere Combustion (ATAC) - A New Combustion Process For Internal Combustion Engines. *SAE Technical Paper Series*, 790501.

[4] Paitoon Kongsereeparp. *Chemical Kinetic Based Simulation for an HCCI Engine and its Combustion.* PhD thesis, University of Alberta, 2008.

[5] Paitoon Kongsereeparp and David Checkel. Study of Reformer Gas Effects on n-Heptane HCCI Combustion Using a Chemical Kinetic Mechanism Optimized by Genetic Algorithm. *SAE Technical Paper Series*, 2008-01-0039.

[6] Mingfa Yao, Zhaolei Zheng, and Haifeng Liu. Progress and Recent Trends in Homogeneous Charge Compression Ignition (HCCI) Engines. *Progress in Energy and Combustion Science*, 35(5):398 – 437, 2009.

[7] Junseok Chang, Orgun Gralp, Zoran Filipi, Dennis Assanis, Tang-Wei Kuo, Paul Najt, and Rod Rask. New Heat Transfer Correlation for an HCCI Engine Derived from Measurements of Instantaneous Surface Heat Flux. *SAE Technical Paper Series*, 2004-01-2996.

[8] Jessica Marshall. Clean-burn engine dodges ever tighter regulations. *New Scientist*, 189(2534):26 – 27, 2006.

[9] Hailin Li, W. Stuart Neill, Wally Chippior, Lisa Graham, Trevor Connolly, and Joshua D. Taylor. An Experimental Investigation on the Emission Characteristics of HCCI Engine Operation Using N-Heptane. *SAE Technical Paper Series*, 2007-01-1854.

[10] Rudolf H. Stanglmaier, Thomas W. Ryan III, and Jason S. Souder. HCCI Operation of a Dual-Fuel Natural Gas Engine for Improved Fuel Efficiency and Ultra-Low NOx Emissions at Low to Moderate Engine Loads. *SAE Technical Paper Series*, 2001-01-1897.

[11] Mahdi Shahbakhti and Charles Robert Koch. Physics Based Control Oriented Model for HCCI Combustion Timing. *Journal of Dynamic Systems, Measurement and Control, Transactions of the ASME*, 132:021010, 1–12, 2010.

[12] Adrian D. Audet. Closed Loop Control of HCCI using Camshaft Phasing and Dual Fuels. Master's thesis, University of Alberta, 2008.

[13] J. Bengtsson, P. Strandh, R. Johansson, P. Tunestl, and B. Johansson. Hybrid modelling of homogeneous charge compression ignition (HCCI) engine dynamics - A survey. *International Journal of Control*, 80(11):1814 – 1848, 2007.

[14] Robert Anthony William Lupul. Steady State and Transient Characterization of a HCCI Engine with Varying Octane Fuel. Master's thesis, University of Alberta, 2008.

[15] Zhi Wang, Jian-Xin Wang, Guo hong Tian, Shi-Jin Shuai, Zhifu Zhang, and Junwei Yang. Research on Steady and Transient Performance of an HCCI

Engine with Gasoline Direct Injection. *SAE Technical Paper Series*, 2008-01-1723.

[16] Vahid Hosseini. *Reformer Gas Application in HCCI Combustion Engine*. PhD thesis, University of Alberta, 2008.

[17] Daniel L. Flowers, Nick J. Killingsworth, Francisco Espinosa-Loza, Joel Martinez-Frias, Salvador M. Aceves, Miroslav Krstic, and Robert Dibble. Demonstrating Optimum HCCI Combustion with Advanced Control Technology. *SAE Technical Paper Series*, 2009-01-1885.

[18] Gran Haraldsson, Jari Hyvonen, Per Tunestl, and Bengt Johansson. HCCI Closed-Loop Combustion Control Using Fast Thermal Management. *SAE Technical Paper Series*, 2004-01-0943. Collection.

[19] Daniel I. Handford. Direct Injection Assisted HCCI Combustion of Natural Gas. Master's thesis, University of Alberta, 2009.

[20] Adrian Audet and Charles Robert Koch. Actuator comparison for closed loop control of HCCI combustion timing. *SAE Technical Paper Series*, 2009-01-1135.

[21] Sotirios Mamalis, Vishnu Nair, Peter Andruskiewicz, Dennis Assanis, Aristotelis Babajimopoulos, Nicole Wermuth, and Paul Najt. Comparison of Different Boosting Strategies for Homogeneous Charge Compression Ignition Engines - A Modeling Study. *SAE Technical Paper Series*, 2010-01-0571.

[22] D. I. Handford and M. D. Checkel. Extending the Load Range of a Natural Gas HCCI Engine using Direct Injected Pilot Charge and External EGR. *SAE Technical Paper Series*, 2009-01-1884.

[23] Yuuichi Kodama, Izumi Nishizawa, Takumi Sugihara, Norihiko Sato, Tadashi Iijima, and Tatsuya Yoshida. Full-Load HCCI Operation with Variable Valve Actuation System in a Heavy-Duty Diesel Engine. *SAE Technical Paper Series*, 2007-01-0215.

[24] Hiroshi Kuzuyama, Masahiro Machida, Kazuhiro Akihama, Kazuhisa Inagaki, and Matsuei Ueda. A Study on Natural Gas Fueled Homogeneous Charge Compression Ignition Engine - Expanding the Operating Range and Combustion Mode Switching. *SAE Technical Paper Series*, 2007-01-0176.

[25] Wen Zeng and Maozhao Xie. A novel approach to reduce hydrocarbon emissions from the HCCI engine. *Chemical Engineering Journal*, 139(2):380 – 389, 2008.

[26] Shazam Williams, Linjie (Robin) Hu, Tohru Nakazono, Hiroyuki Ohtsubo, and Miwa Uchida. Oxidation Catalysts for Natural Gas Engine Operating under HCCI or SI Conditions. *SAE Technical Paper Series*, 2008-01-0807.

[27] Magnus Christensen, Bengt Johansson, and Patrik Einewall. Homogeneous Charge Compression Ignition (HCCI) Using Isooctane, Ethanol and Natural Gas - A Comparison with Spark Ignition Operation. *SAE Technical Paper Series*, 972874.

[28] Joel Hiltner, Scott Fiveland, Rey Agama, and Martin Willi. System Efficiency Issues for Natural Gas Fueled HCCI Engines in Heavy-Duty Stationary Applications. *SAE Technical Paper Series*, 2002-01-0417.

[29] Jim Iverson. EPA emissions regulations: What they mean for standby, prime and distributed power systems. Technical report, Cummings Power Generation, 2006.

[30] H. M. Cho and B.-Q. He. Combustion and Emission Characteristics of a Lean Burn Natural Gas Engine. *International Journal of Automotive Technology*, 9(4):415–422, 2008.

[31] Patrik Einewall, Per Tunestl, and Bengt Johansson. Lean Burn Natural Gas Operation vs. Stoichiometric Operation with EGR and a Three Way Catalyst. *SAE Technical Paper Series*, 2005-01-0250.

[32] Ruonan Sun, Rick Thomas, and Charles L. Gray Jr. An HCCI Engine: Power Plant for a Hybrid Vehicle. *SAE Technical Paper Series*, 2004-01-0933.

[33] Alasdair Cairns and Hugh Blaxill. The Effects of Two-Stage Cam Profile Switching and External EGR on SI-CAI Combustion Transitions. *SAE Technical Paper Series*, 2007-01-0187.

[34] Jonathan Etheridge, Sebastian Mosbach, Markus Kraft, Hao Wu, and Nick Collings. A Fast Detailed-Chemistry Modelling Approach for Simulating the SI-HCCI Transition. *SAE Technical Paper Series*, 2010-01-1241.

[35] Guohong Tian, Zhi Wang, Qiangqing Ge, Jianxin Wang, and Shijin Shuai. Mode Switch of SI-HCCI Combustion on a GDI Engine. *SAE Technical Paper Series*, 2007-01-0195.

[36] Hiromu Kakuya, Shiro Yamaoka, Kengo Kumano, and Shinya Sato. Investigation of a SI-HCCI Combustion Switching Control Method in a Multi-Cylinder Gasoline Engine. *SAE Technical Paper Series*, 2008-01-0792.

[37] Nebojsa Milovanovic, Dave Blundell, Stephen Gedge, and Jamie Turner. SI-HCCI-SI Mode Transition at Different Engine Operating Conditions. *SAE Technical Paper Series*, 2005-01-0156.

[38] Nebojsa Milovanovic, Dave Blundell, Stephen Gedge, and Jamie Turner. Cam Profile Switching (CPS) and Phasing Strategy vs Fully Variable Valve Train (FVVT) Strategy for Transitions between Spark Ignition and Controlled Auto Ignition Modes. *SAE Technical Paper Series*, 2005-01-0766.

[39] Hao Wu, Nick Collings, Simon Regitz, Jonathan Etheridge, and Markus Kraft. Experimental Investigation of a Control Method for SI-HCCI-SI Transition in a Multi-Cylinder Gasoline Engine. *SAE Technical Paper Series*, 2010-01-1245.

[40] Yan Zhang, Hui Xie, and Hua Zhao. Investigation of SI-HCCI Hybrid Combustion and Control Strategies for Combustion Mode Switching in a Four-stroke Gasoline Engine. *Combustion Science and Technology*, 181:782–799, 2009.

[41] Matthew J. Roelle, Gregory M. Shaver, and J. Christian Gerdes. Tackling the Transition: A Multi-mode Combustion Model of SI and HCCI for Mode Transition Control. *International Mechanical Engineering Conference and Exposition*, IMECE2004-62188, November 2004.

[42] Halim Santoso, Jeff Matthews, and Wai K. Cheng. Managing SI/HCCI Dual-Mode Operation. *SAE Technical Paper Series*, 2005-01-0162.

[43] Jari Hyvnen, Gran Haraldsson, and Bengt Johansson. Operating Conditions Using Spark Assisted HCCI Combustion During Combustion Mode Transfer to SI in a Multi-Cylinder VCR-HCCI Engine. *SAE Technical Paper Series*, 2005-01-0109.

[44] YaPing Peng, ManZhi Tan, Liang Guo, FaFa Liu, Hua Li, and YingNan Guo. Study the ethanol SI/HCCI combustion mode transition by using the fast thermal management system. *Chinese Science Bulletin*, 52(19):2731–2736, 2007.

[45] Waukesha CFR. *Operation & Maintenance Manual*, second edition edition, 2003.

[46] Emiliano Pipitone, Alberto Beccari, and Stefano Beccari. The Experimental Validation of a New Thermodynamic Method for TDC Determination. *SAE Technical Paper Series*, 2007-24-0052.

[47] E. Corti, D. Moro, and L. Solieri. Real-Time Evaluation of IMEP and ROHR-related Parameters. *SAE Technical Paper Series*, 2007-24-0068.

[48] G. Woschni. A Universally Applicable Equation for the Instantaneous Heat Transfer Coefficient in the Internal Combustion Engine. *SAE Technical Paper Series*, 670931.

[49] M. Iida, M. Hayashi, D. E. Foster, and J. K. Martin. Characteristics of Homogeneous Charge Compression Ignition (HCCI) Engine Operation for Variations in Compression Ratio, Speed, and Intake Temperature While Using n-Butane as a Fuel. *ASME Journal of Engineering for Gas Turbines and Power*, 125:472–478, April 2003.

[50] P. Attard and J. Micallef. Ion current combustion technology for controlled auto-ignition gasoline engines. *International Journal of Engine Research*, 8:429–437, 2007.

[51] Yiqun Huang and Darius Mehta. Investigation of an In-cylinder Ion Sensing Assisted HCCI Control Strategy. *SAE Technical Paper Series*, 2005-01-0068.

[52] Petter Strandh, Magnus Christensen, Johan Bengtsson, Rolf Johansson, Andreas Vressner, Per Tunestl, and Bengt Johansson. Ion Current Sensing for HCCI Combustion Feedback. *SAE Technical Paper Series*, 2003-01-3216.

[53] B. M. Belyaev and V. G. Patrikeev. Influence Of Variations Of The Composition Of Natural Gas From Different Fields On The Results Of Mass And Volumetric Flowrate Measurement Under Standard Conditions In Gas Distribution Organizations. *Measurement Techniques*, 46(5):462–465, 2003.

[54] David Dyntar, Christopher Onder, and Lino Guzzella. Modeling and Control of CNG Engines. *SAE Technical Paper Series*, 2002-01-1295.

[55] William J. Glewen, Robert M. Wagner, K. Dean Edwards, and C. Stuart Daw. Analysis of cyclic variability in spark-assisted HCCI combustion using a double Wiebe function. *Proceedings of the Combustion Institute*, 32:2885–2892, 2009.

[56] Yunus A. Cengel and Michael A. Boles. *Thermodynamics: An Engineering Approach.* McGraw-Hill, fifth edition, 2006.

[57] J. R. Roebuck. The Joule-Thomson Effect in Air. *Proceedings of the National Academy of Sciences of the United States of America*, 12(1):55–58, 1926.

[58] Yunus A. Cengel. *Heat and Mass Transfer: A Practical Approach.* McGraw-Hill, third edition edition, 2007.

[59] Damorn Bundhurat. Uncertainty Analysis of Flow and Emission Measurement for Engine Testing. Unpublished manuscript, May 2008.

[60] Robert J. Moffat. Describing the Uncertainties in Experimental Results. *Experimental Thermal and Fluid Science*, 1:3–17, 1988.

Appendix A

Effective Compression Ratio

Geometric engine compression ratio is difficult to measure given the small clearance volumes and the optical research head being used. A method is adopted similar to previous work [16, 19] in which the effective compression ratio is estimated from the motored pressure trace.

Cylinder pressure is curve fitted to a third-order polynomial in the region surrounding top dead center (TDC) to determine peak pressure while avoiding noise. This is evaluated for each of the 100 cycles in a typical motoring test and the results averaged. In the original method, the average motoring peak pressure along with intake air temperature is compared to simulated values from a single-zone engine model to determine an effective compression ratio. During testing it was found that changes in barometric pressure had a noticeable effect on the output due to variation in cylinder charge mass. To account for this, a pressure ratio between peak motoring cylinder pressure and intake manifold pressure at IVC (P_{IVC}) is used instead of peak pressure alone.

Both methods are tested on the engine to investigate their dependency on barometric pressure. The intake air bypass is sealed and air is supplied through the compressed building air supply. Using a pressure regulator, the flow is adjusted to provide different levels of intake manifold pressure to approximate changes in

barometric pressure, thus allowing the throttle to remain fully open as in normal motoring tests. With intake pressure set at one of the desired values, a test using the old method (CR4) is run and immediately followed by a test using the new method (CR5 P_{IVC}). The engine's geometric compression ratio was not adjusted during these tests, so the desired result is a constant value for all tests at different pressures. As shown in Figure A.1, the new method provides much more consistent results with changes in absolute intake manifold pressure.
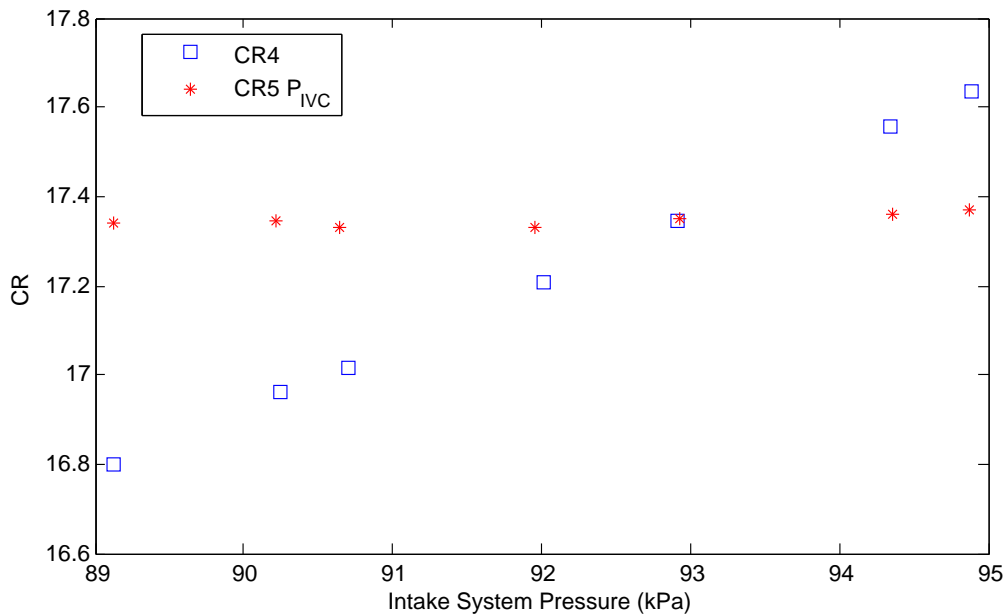
Figure A.1: Effective compression ratio evaluation using old (CR4) and new (CR5 P_{IVC}) methods.

Appendix B

Thermodynamic Loss Angle

Accurately indexing the engine crankshaft position in the engine operating software is necessary to compute parameters accurately. It has been noted that a 1 degree error in TDC location can produce errors as large as 10% in IMEP and 25% in heat release [46]. Determining the location of peak pressure in a motoring trace is a relatively simple process, but does not directly correlate to the position of TDC on the engine due to heat transfer away from the working fluid. This heat loss causes the peak pressure to shift back from TDC by an amount referred to as the thermodynamic loss angle (TDLA). A series of tests are performed to emperically measure TDLA on the test engine to account for this effect.

First, the flywheel is indexed to geometric TDC using a dial indicator. The flywheel is rotated past TDC in both forward and reverse directions until the piston drops a certain distance, at which point the crank position on the flywheel is read. Deviation of the flywheel reading from TDC is calculated, the marker adjusted, and re-tested. The final index position is determined to be at 0.01 ± 0.09 CAD with 95% confidence.

Next, the engine is warmed up and motored at 1000 RPM with the spark activated. After adjusting spark timing to TDC, a set of cylinder pressure cycles are logged. The region surrounding the recorded peak pressure is fitted with a

3rd order polynomial and subtracted from the measured pressure. As visible in Figure B.1, the point of maximum deviation is found as a result of spark noise in the system. The mode of all such positions for a test is selected as the position of geometric TDC. When repeated over a range of compression ratios, a rough linear trend is observed as shown in Figure B.2.

An outlier is apparent at a compression ratio of 17 causing a low correlation coefficient of 0.493 when assuming a linear response. This point is explored through Chauvenet's Criterion to reveal if it is reasonable to exclude. The probability of this measurement occurring (assuming a normal distribution) is multiplied by the 5 test points taken at each compression ratio. The resulting value of 0.079 falls well below the criterion threshold of 0.5 to be considered a valid point; therefore, this point is excluded to provide the data set shown in Figure B.3 for an improved linear fit that falls within error at all other test points. Future compression ratio tests use the relation given in Equation B.1 to locate geometric TDC in relation to the pulse-per-cycle (PPC) index and the peak motoring cylinder pressure.
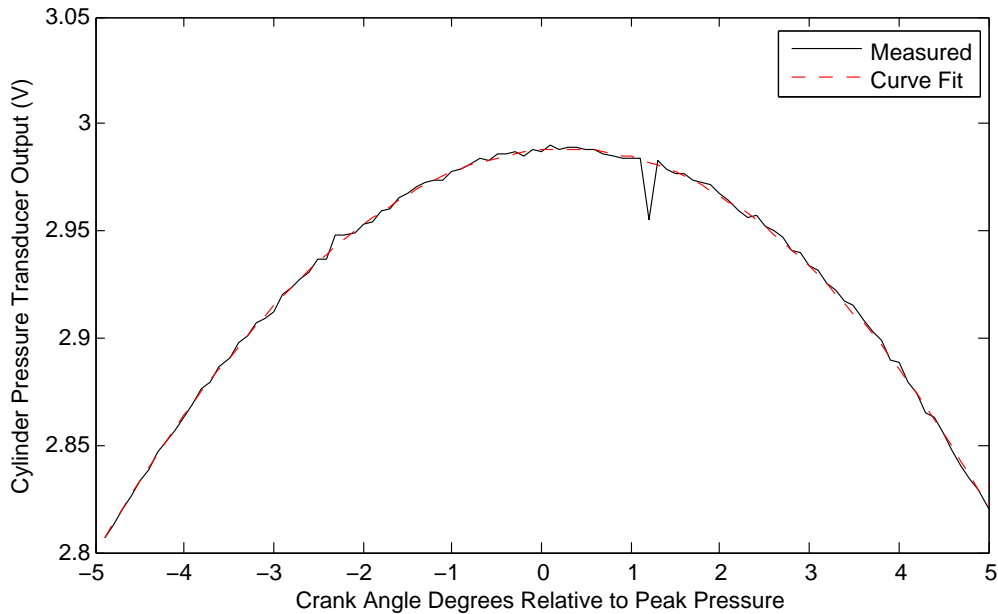
Figure B.1: Spark noise in cylinder pressure trace is used to locate geometric TDC.
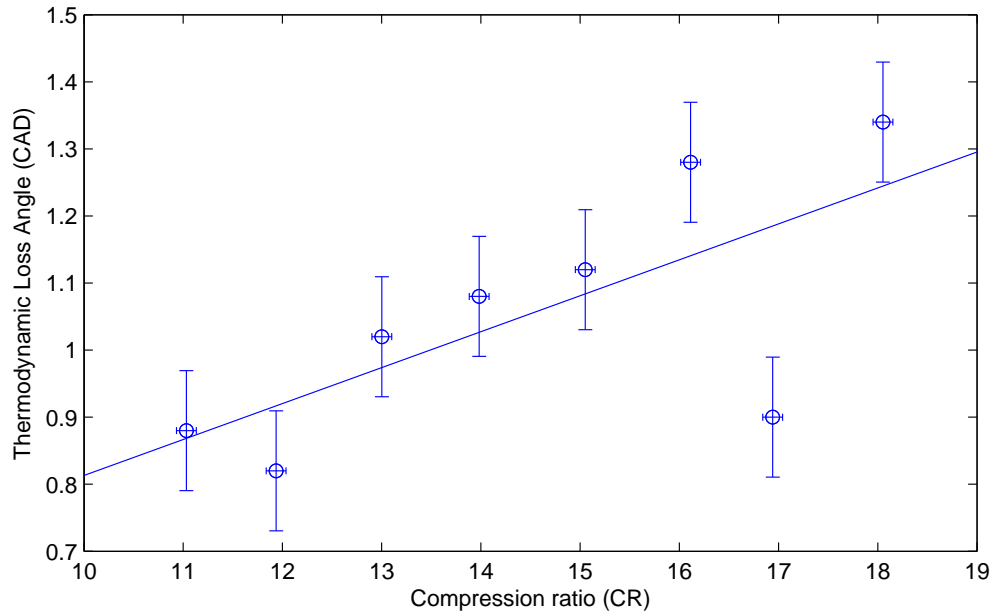
Figure B.2: Thermodynamic loss angle as determined using spark noise while motoring. Correlation Coefficient is 0.493
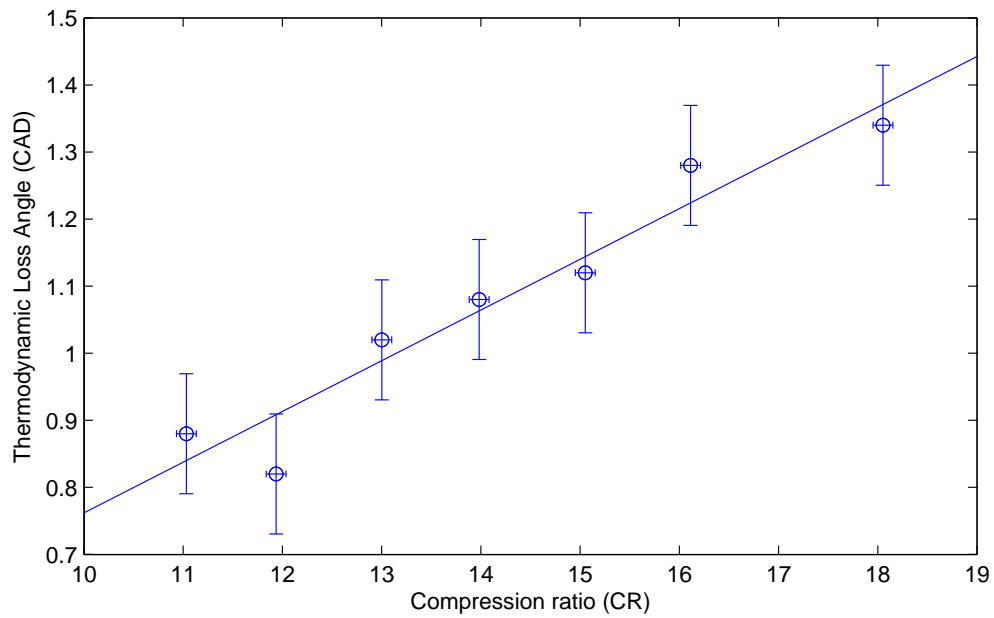
Figure B.3: Thermodynamic loss angle again, but with outlier point removed. Correlation Coefficient is 0.931

$$TDLA = 0.0756\,CR - 0.0059\,CAD \tag{B.1}$$

Appendix C

Intake Heat Loss Calculation

This appendix investigates the thermodynamic effects with the modified intake manifold system that lead to a greater air temperature reduction than the original large intake manifold setup. Consider temperature gradients in the heater manifold pipe, polytropic expansion, the Joule-Thomson effect, heat transfer to the throttle cooling lines, dilution cooling from the injected room-temperature CNG, intake blow-back, and convection heat loss from the additional outside surfaces.

C.1 Heater Manifold Temperature Gradient

Air flow in the heater manifold pipe changes between SI and HCCI operation when the throttle is located downstream. The intake system upstream of the throttle is charged using building air and a pressure regulator. When the throttle is closed to decrease the intake manifold pressure, the flow rate in the heater manifold is reduced. By measuring the temperature profile immediately downstream of the air heater, shown in Figure C.1, it becomes apparent that a shift in flow characteristics exists between the two modes of operation. The visible temperature gradient in SI suggests laminar flow with reduced mixing, while HCCI shows a more consistent temperature across the diameter indicative of turbulent flow. Lower temperatures at the top and bottom of the pipe in both scenarios suggest that these measurement

points are within the boundary layer with lower flow rates and significant heat loss to the pipe. Average temperatures of 127.5 °C for SI and 130.8 °C for HCCI are measured 5 cm upstream of the throttle where flow converges in a 2.54 cm (1") diameter pipe section. Note that the intake temperature controller thermocouple is located slightly above the mid-point in the pipe where the temperature during SI in Figure C.1 is being controlled to 140 °C.
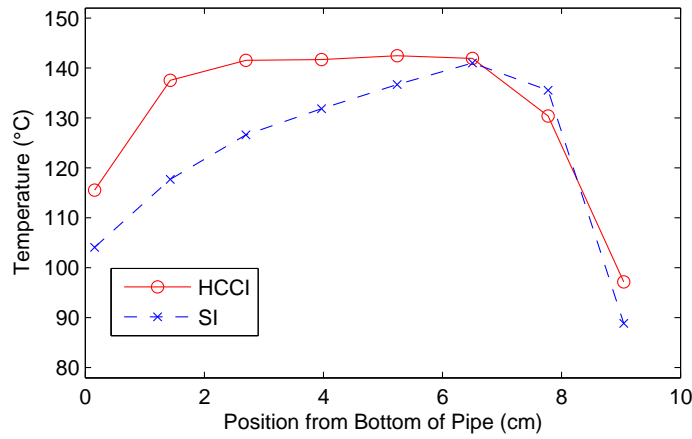
Figure C.1: Air temperature gradient measured downstream of the electric air heater.

C.2 Polytropic Expansion

Temperature change occurs as a gas expands to a lower pressure through the process of polytropic expansion [56]. The basic relation is

$$P V^n = C \tag{C.1}$$

where P is pressure, V is volume, n and C are constants. Using the ideal gas law to replace the volume term and equating two states before and after the throttle,

the correlation between pressure and temperature is

$$\frac{T_2}{T_1} = \left(\frac{P_1}{P_2}\right)^{\frac{n-1}{n}} \tag{C.2}$$

The constant n depends on operating conditions and may vary between isothermal ($n = 1$) and isentropic ($n = k = 1.4$ for air). Adiabatic conditions are assumed as reasonable in the small vicinity around the throttle plate where the pressure drop occurs.

Pressure measurements upstream and downstream of the throttle are presented in Figures C.2 and C.3 at 700 RPM for SI and HCCI operation, respectively. For choked flow during SI operation, air is moving past the throttle throughout the cycle as indicated by the pressure difference. Considering the average of the two states, the pressure upstream of the throttle is 125 kPa while being 70 kPa downstream. HCCI operation shows that significant flow only occurs during and slightly after the intake stroke, corresponding with the pressure drop during the intake stroke. The pressure drop for polytropic expansion in this instance is considered only in this region, being 114 kPa upstream and 106 kPa downstream of the throttle. Evaluating Equation C.2 with these pressures and the average air temperatures measured above in Section C.1 results in Table C.1 for several values of n. The true value of n is difficult to predict and would require temperature measurements in close vicinity of the throttle plate.

C.3   Joule-Thomson Effect

The Joule-Thomson effect is based on non-ideal properties of a gas as its pressure is reduced [56]. Depending on the initial temperature of the gas in relation to its inversion temperature, the gas temperature may either increase, decrease, or
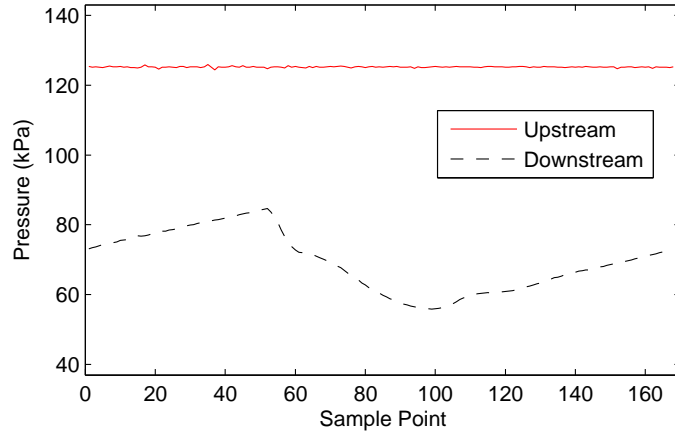
Figure C.2: Intake pressure trends both upstream (heater manifold) and downstream (intake manifold) of the throttle during SI operation given in Table 4.6.
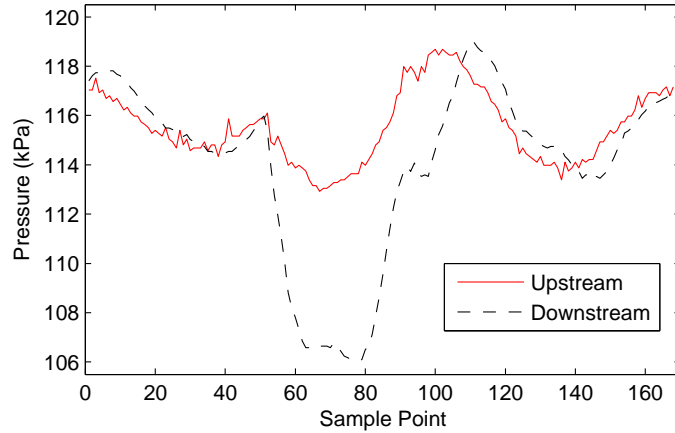
Figure C.3: Intake pressure trends both upstream (heater manifold) and downstream (intake manifold) of the throttle during HCCI operation given in Table 4.6.

Table C.1: Temperature reduction due to polytropic expansion across the throttle for several values of n.

	Temperatures ($^\circ$C)	
Case	**SI**	**HCCI**
Upstream Air	127.5	130.8
$n = 1.0$	127.5	130.8
$n = 1.1$	106.7	128.1
$n = 1.2$	90.2	125.9
$n = 1.3$	76.8	124.1
$n = 1.4$	65.7	122.5

remain constant after throttling based on the relation

$$\mu_{JT} = \left(\frac{\partial T}{\partial P} \right)_h \tag{C.3}$$

where μ_{JT} is the Joule-Thomson coefficient equated with the change of temperature with pressure at constant enthalpy [56]. With a pressure of 1 atmosphere and temperature of 150 °C, the Joule-Thomson coefficienct for air is 0.0927 °C/bar [57]. This indicates that the contribution of this effect is minimal since the pressure drop across the throttle is less than 1 atmosphere.

C.4   Throttle Cooling Lines

Water cooling lines are installed to prevent throttle actuator overheating when located downstream of the intake heater, leading to heat loss from the air being throttled. Using the temperature change and flow rate of the cooling water, the amount of heat transfer is determined as shown in Table C.2. The base case is tested on a different day with the throttle on, but the engine off and intake manifold at room temperature. Taking the difference between the operating points and the base case, the heat loss from the intake air is 25.0 W for SI and 24.2 W for HCCI. SI operation maintains approximately the same heat transfer to the throttle cooling lines as HCCI with lower air flow rate but increased contact area and turbulence with the throttle in a more closed position.

Table C.2: Heat loss measurements for water cooling lines on throttle actuator. The engine is off for the base case, then run at the conditions given in Table 4.6 for SI and HCCI data.

Case	T_1 (°C)	T_2 (°C)	Time (s)	Volume (L)	Heat Transfer (W)
Base	6.7	8.0	32.1	0.1	16.9
SI	3.0	6.4	33.9	0.1	42.0
HCCI	3.0	6.3	33.6	0.1	41.1

C.5   Convection

Heat loss from the outer surface of the throttle and additional aluminum fittings, as visible in Figure 3.3, to the room air is evaluated by approximating these surfaces as a cylinder with 3" diameter and 10" length [58]. Surface temperature of the throttle and additional fittings are measured at four points and averaged to 79.5 °C and 84.3 °C during SI and HCCI operation, respectively, at the operating conditions in Table 4.6. The higher temperature in HCCI is due to the higher mass flow rate and air temperature for greater heat transfer from the hot manifold air to the throttle and aluminum fittings.

The relations used to approximate convection heat loss to the room air are summarized as follows:

$$\text{Gr}_D = \frac{g\,\beta(T_\text{s} - T_\infty)\,L_c^3}{\nu^2} \tag{C.4a}$$

$$\text{Ra}_D = \text{Gr}_D\,\text{Pr} \tag{C.4b}$$

$$\text{Nu} = \left(0.6 + \frac{0.387\,\text{Ra}_D^{1/6}}{[1 + (0.559/\text{Pr})^{9/16}]^{8/27}}\right)^2 \quad (horizontal\ cylinder) \tag{C.4c}$$

$$h = \frac{k\,\text{Nu}}{L_c} \tag{C.4d}$$

$$Q_\text{conv} = h\,A_\text{conv}\,(T_\text{s} - T_\infty) \tag{C.4e}$$

where

$\text{Gr}_D = Grashof\ Number\ [-]$

$g = Gravitational\ Acceleration\ [m/s^2]$

$\beta = Volumetric\ thermal\ expansion\ coefficient,$

$approximated\ as\ 1/T\ for\ ideal\ fluids\ [1/\text{K}]$

$T_\text{s} = Surface\ Temperature\ [\text{K}]$

$T_\infty = Room\ Temperature\ [\text{K}]$

$L_c = Characteristic\ Length\ [m];\ Diameter\ for\ horizontal\ cylinder)$

$\nu = Kinematic\ viscosity\ of\ the\ fluid\ [m^2/s]$

$\text{Ra}_D = Rayleigh\ Number\ [-]$

$\text{Pr} = Prandtl\ Number\ [-]$

$\text{Nu} = Nusselt\ Number\ [-]$

$h = Average\ Convection\ Coefficient\ [W/m^2\ {}^\circ\text{C}]$

$k = Thermal\ Conductivity\ [W/m\ {}^\circ\text{C}]$

$Q_\text{conv} = Convection\ Heat\ Transfer\ [W]$

$A_\text{conv} = Area\ for\ Convection\ Heat\ Transfer\ [m^2]$

Using the room temperature of 22 °C, the average convection coefficients are calculated to be 6.10 W/m^2 °C for SI operation and 6.22 W/m^2 °C for HCCI. The resulting convection heat transfer rates are 21 W for SI and 24 W for HCCI.

C.6   Temperature Downstream of Throttle

Air temperature is experimentally measured 5cm downstream of the throttle as 96.3 °C for SI and 111.3 °C for HCCI operation. Considering the above factors for polytropic expansion, heat loss through the throttle cooling lines, and convection to air in the room, air temperature downstream of the throttle is calculated as shown in Table C.3. To match the calculated values with experimental data, HCCI operation requires an n value of approximately 1.2, while SI can not achieve a high enough temperature even with isothermal operation having an n of 1.0. The influence of CNG injection and backflow may induce mixing in the intake manifold to influence the temperature downstream of the throttle and are discussed next.

Table C.3: Calculated air temperatures downstream of throttle combining all discussed effects for a range of n values.

	Temperatures (°C)	
Case	SI	HCCI
Upstream Air	127.5	130.8
$n = 1.0$	91.1	116.3
$n = 1.1$	70.3	113.6
$n = 1.2$	53.8	111.4
$n = 1.3$	40.4	109.6
$n = 1.4$	29.3	108.0

C.7   CNG Injection

Room temperature CNG is injected into the hot throttled air upstream of the intake valve. The CNG induces a cooling effect as the mixture reaches thermal

equilibrium. The final temperature is calculated using a thermodynamic balance

$$T_{\text{mix}} = \frac{(T_{\text{air}} \, \dot{m}_{\text{air}} \, C_{p\_\text{air}} + T_{\text{res}} \, \dot{m}_{\text{res}} \, C_{p\_\text{res}})}{(\dot{m}_{\text{air}} \, C_{p\_\text{air}} + \dot{m}_{\text{res}} \, C_{p\_\text{CNG}})} \tag{C.5}$$

where T is temperature, C_p is the constant pressure specific heat capacity, and $\dot{m}$ is the mass flow rate for the indicated constituents. Temperature reduction in Table C.4, compared with Table C.3 without CNG injection, is greater during SI operation due to the larger mass fraction of CNG (stoichiometric as opposed to lean in HCCI).

Table C.4: Calculated mixture temperatures after CNG injection for a range of n values.

	Temperatures (°C)	
Case	**SI**	**HCCI**
Upstream Air	127.5	130.8
$n = 1.0$	83.3	112.0
$n = 1.1$	64.9	109.4
$n = 1.2$	50.2	107.3
$n = 1.3$	38.3	105.6
$n = 1.4$	28.5	104.0

C.8   Backflow

Combustion products from the previous engine cycle can influence the intake mixture temperature when the residual gas in the cylinder is at a higher pressure than the intake manifold at IVO [1]. Hot exhaust gases may backflow into the intake manifold during throttled operation in SI once the intake valve opens. With slow engine speed and IVC occurring past BDC (see Table 3.3), there is potential for gases to backflow into the intake manifold at the end of the intake stroke as well. While the interaction occurring here is complex and depending on many variables, a simplified approach is adopted to consider this effect.

First, cylinder volume at EVC is calculated using the slider-crank relation given

in Equation 3.6. Assuming this volume consists of complete combustion products (stoichiometric SI operation) at exhaust pressure and temperature, a thermodynamic balance is carried out with the incoming air similar to Equation C.5. Although this approach neglects heat loss from the residual gas to the combustion chamber and mixing characteristics, the accuracy is considered sufficient for this rudimentary analysis. The intake manifold temperatures incorporating backflow are summarized in Table C.5 including all other effects discussed above.

Table C.5: Calculated intake manifold temperatures including backflow for a range of n values.

Case	Temperatures ($^\circ$C)	
	SI	HCCI
Upstream Air	127.5	130.8
$n = 1.0$	117.2	112.0
$n = 1.1$	100.4	109.4
$n = 1.2$	87.1	107.3
$n = 1.3$	76.2	105.6
$n = 1.4$	67.3	104.0

C.9   Discussion

The target mixture temperatures through this analysis are 85 and 102 $^\circ$C for SI and HCCI, respectively, as measured in Table 4.6. The calculated values support the measured SI value at $n = 1.22$, but there is no value of n to drop the mixture temperature sufficiently for HCCI. There are a few possibilities to explain this discrepancy:

- The black injection fitting downstream of the aluminum fitting and connected to the engine block (see Figure 3.3) may remove additional heat from the gas mixture; however, the combination of convection to the air and conduction to the block make it difficult to approximate this effect.

- Convection heat loss from all surfaces may be higher than calculated. The exposed surface area is approximated by a cylinder, which is not the actual surface area. Further, convection from the non-cylindrical geometry may deviate from the empirical relations for natural convection from a horizontal cylinder.

- Air movement in the room from exhaust fans may induce some forced convection to increase heat transfer away from the throttle and additional fittings.

With the small difference between the measured and calculated mixture temperatures, this analysis validates the need for a higher intake air set point of $140\,^\circ\mathrm{C}$ with the throttle position downstream of the intake heater for the small intake manifold.

Appendix D

Sensor Calibrations

All sensors used during engine testing are calibrated on a regular basis. Following are detailed descriptions of the equipment and procedures used along with the resulting calibrations. Note that in some figures the error bars are small enough to fall inside the data point markers.

Error is presented in the calibration plots using 95% confidence intervals. A single error value is selected for each instrument by comparing the average of the 95% confidence interval with two standard deviations of the residual. The two values generally fall very close to one another with any significant differences discussed for the specific case.

D.1 Air Mass Flow

The TSI 42350101 hot wire anemometer is calibrated using a 5 cubic foot Bell Prover made available in the Chemical Engineering Department at the University of Alberta. Air is supplied through the same regulator and 0.5" ID rubber hose as on the engine. Air flow first passes through the TSI meter and then into the Bell Prover. All connections are leak tested prior to calibrating.

Using the same DAQ computer and hardware as on the engine, a series of tests are run. First, the regulator is set to the desired rate as defined by a given voltage

output on the TSI meter. After closing the Bell Prover bypass valve, a LabVIEW program is started at the 0.5 cubic foot marking, which simultaneously start a counter and data logging of the TSI meter output. The program is stopped at the 4.5 cubic foot marking and the output voltage is averaged over the duration of the test. Taking into account air temperature and the slight differential pressure in the Bell Prover, the mass flow rate can be calculated. As flow rate increases, it becomes more difficult to start and stop the program at the desired points. To keep error down to a reasonable amount, the number of tests run at each point is increased from 6 to 10 for the upper three flow rates. A resulting calibration is shown in Figure D.1.
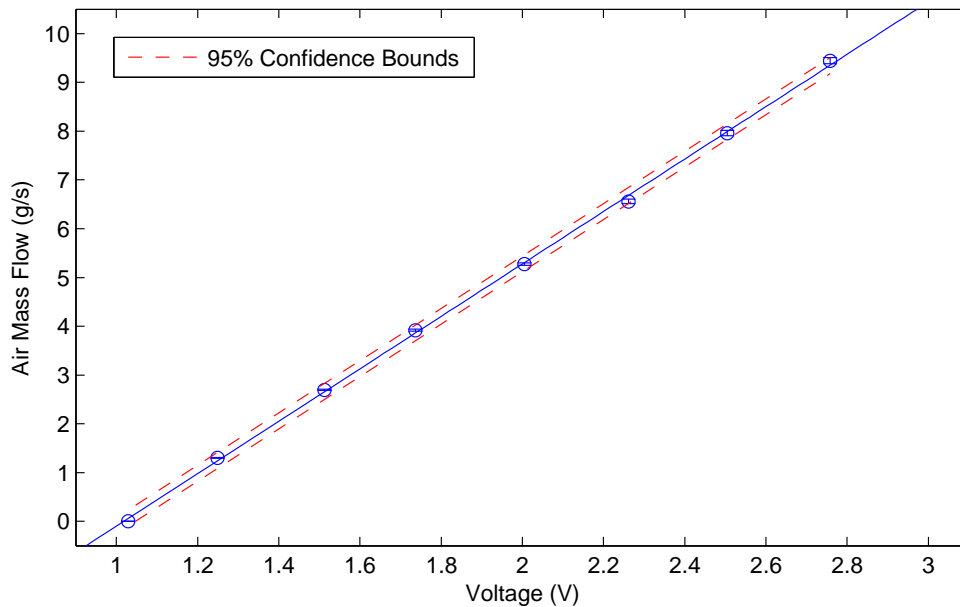
Figure D.1: Air mass flow calibration. Linear Fit: AirMF = 5.376*Volts - 5.475 $\pm$ 0.16 g/s (20:1); Correlation Coefficient: 0.99975

D.2 Compressed Natural Gas (CNG) Mass Flow

The Omega FMA-A2117 flow meter is calibrated using a gravimetric method. The CNG tank is placed on a calibrated GSE 550 scale while the engine is run at various

speeds and loads. Output from the Omega meter is logged over the duration, averaged, and compared with the mass of fuel burned over the time period. Figure D.2 shows a calibration result.

Estimating error in this sensor produces a high value of 6 mg/s using the 95% confidence interval method, primarily resulting from the small number of test points. More calibration tests are not completed as the run time for each point ranges from 20-60 minutes to reduce mass error. With the high correlation coefficient suggesting that the linear fit is very close to the test data, and with typical operation occuring only in the central region, it is reasonable to assume error for the CNG mass flow meter is equal to $\pm$ 4 mg/s as determined by twice the standard deviation of the residuals.
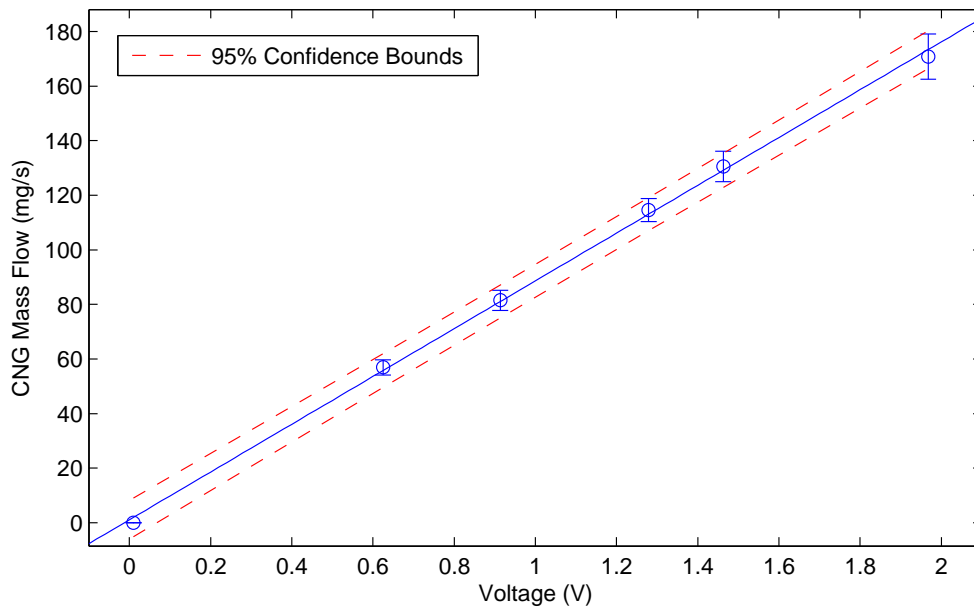
Figure D.2: CNG mass flow calibration. Linear Fit: y = 87.60*Volts + 1.032 $\pm$ 4 mg/s (20:1); Correlation Coefficient: 0.99955

D.3   Piezoelectric Cylinder Pressure Transducer

The Kistler 6043A pressure transducer is calibrated using a hydraulic Budenburg dead weight pressure calibrator. Since this sensor is designed to measure relative changes in pressure, the calibration must be dynamic in nature. Using the same Kistler 507 charge amplifier and DAQ computer as on the engine, the output of the sensor is logged as a pressure step is applied. A small amount of air trapped in the system could not be removed, so there is a constraint on the pressure step possible without bottoming out the dead weight calibrator. With this in mind, a series of pressure steps at various average pressures are carried out in both increasing and decreasing directions. Processing of this data is done similar to Handford, where the slope of the output is calculated before and after the pressure step and the sensitivity determined at the mid-point. Figure D.3 shows a sample of the procedure with the resulting calibration shown in Figure D.4.
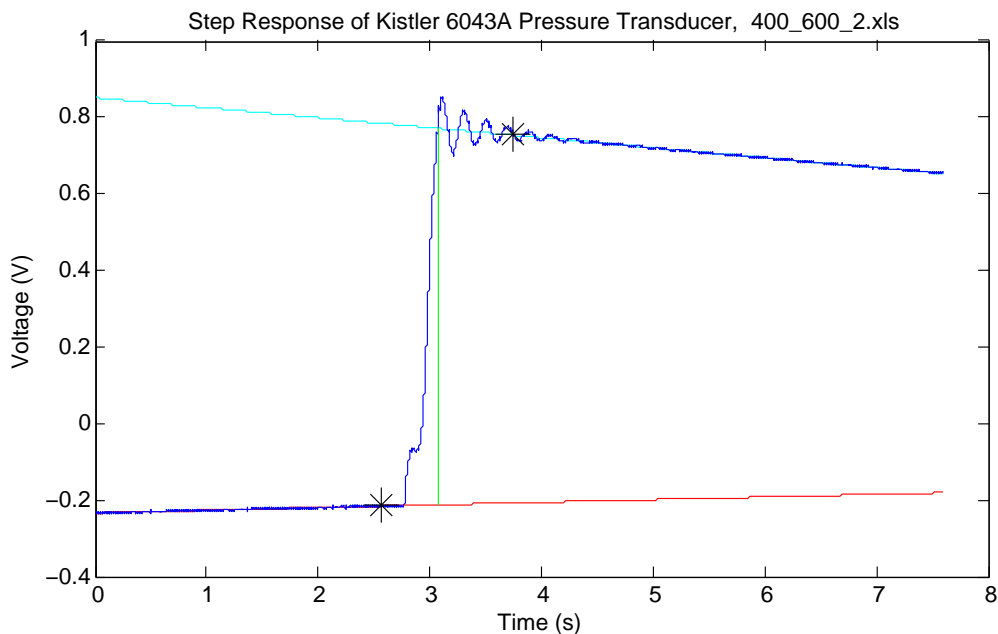
Figure D.3: Dynamic pressure calibration for piezoelectric pressure transducer.
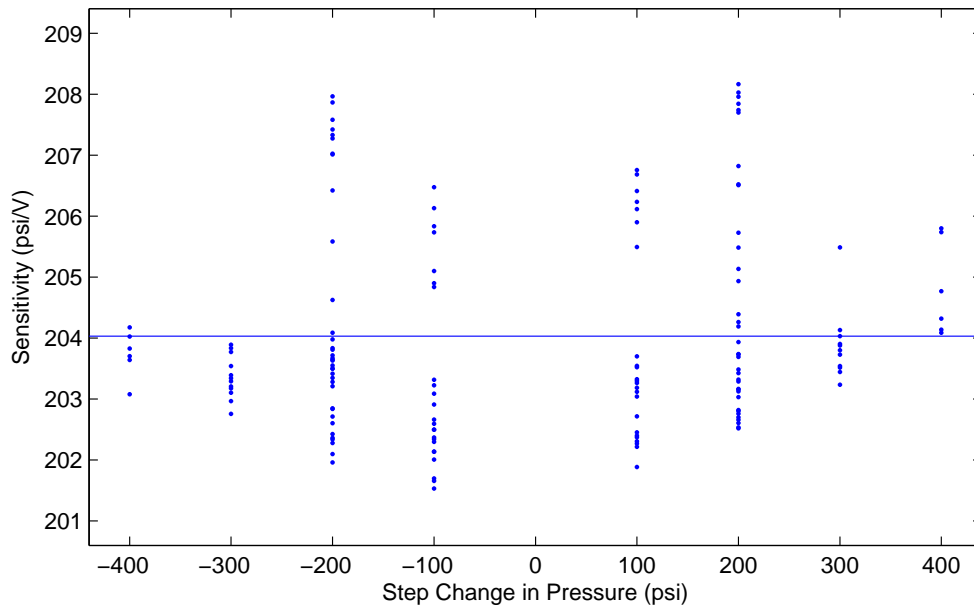
Figure D.4: Piezoelectric cylinder pressure transducer calibration. Average sensitivity is 204.0 ± 3.3 psi/V (20:1).

D.4   Gauge Pressure Transducers

An Omega DPI 610 pressure calibrator is used to provide a reference air pressure between -14 and +30 psig for the two Valedyne DP15 pressure transducers. The output is conditioned using a signal demodulator with adjustable zero and span. Voltage output is recorded at several points while ramping pressure from atmospheric to each extremum and back. Some hysteresis is visible in the readings and is taken into account in the error analysis by not averaging the two measurements at each pressure level. Calibrations for the intake and exhaust pressure transducers are shown in Figures D.5 and D.6.

D.5   Thermocouples

A Fluke 9173 Metrology Well is used to provide reference temperatures between 50 and 600 °C; an ice bath provides 0 °C. Thermocouples are run through their expected range of temperatures while recording the output readings at each point.
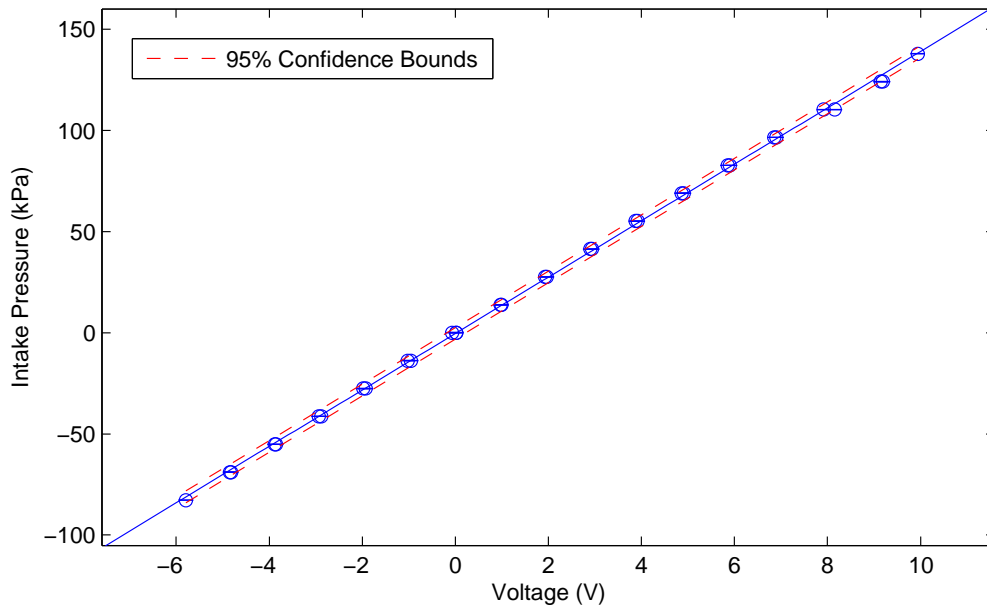
Figure D.5: Intake pressure transducer calibration. Linear Fit: y = 13.94*Volts - 0.3921 ± 2.7 kPa (20:1); Correlation Coefficient: 0.99978
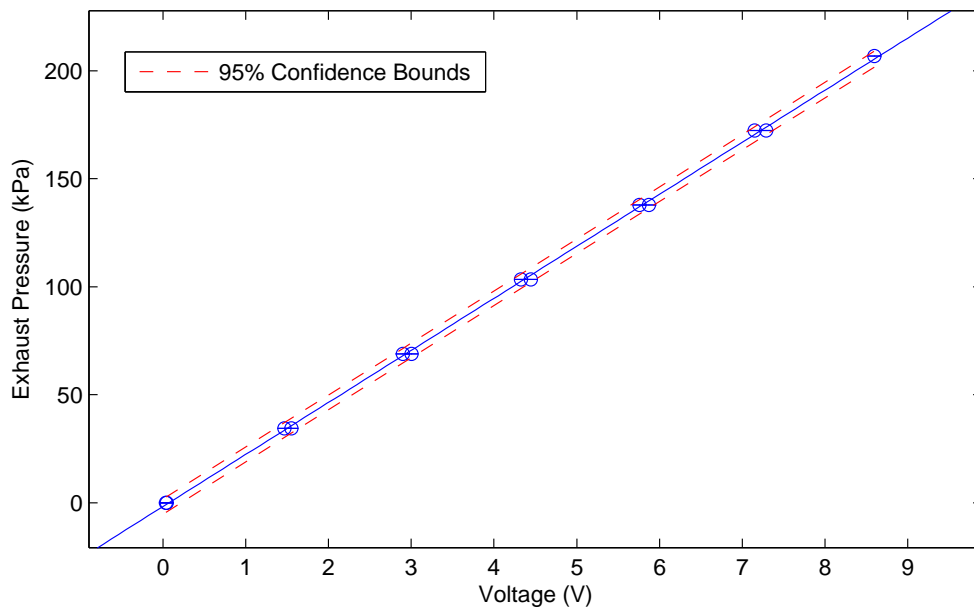
Figure D.6: Exhaust pressure transducer calibration. Linear Fit: y = 24.08*Volts - 1.666 ± 3.4 kPa (20:1); Correlation Coefficient: 0.99979

Due to the deep wells in the metrology calibrator, most thermocouples are unable to be inserted to the bottom (the calibrated point in the metrology well) leading to some error in the reference point. Kaowool insulation is placed at the top of the calibrator to reduce convective heat loss and minimize the temperature gradient in the calibrator wells. Errors found in the measurements are presented in Figure D.7.

The temperature controller is the only long thermocouple inserted to the bottom of the well and provides a typical error distribution around the reference temperatures. The mixture thermocouple, although shorter, shows similar error around the reference temperature likely due to its thinner 1/32" size reducing heat loss due to conduction. All other short thermocouples exhibit the expected behavior of consistently falling below the reference temperature. As such, the thermocouples have been confirmed to be operating properly, but no calibration will be applied to the readings. Temperatures are used directly as measured along with an uncertainty of $1\,°C$.
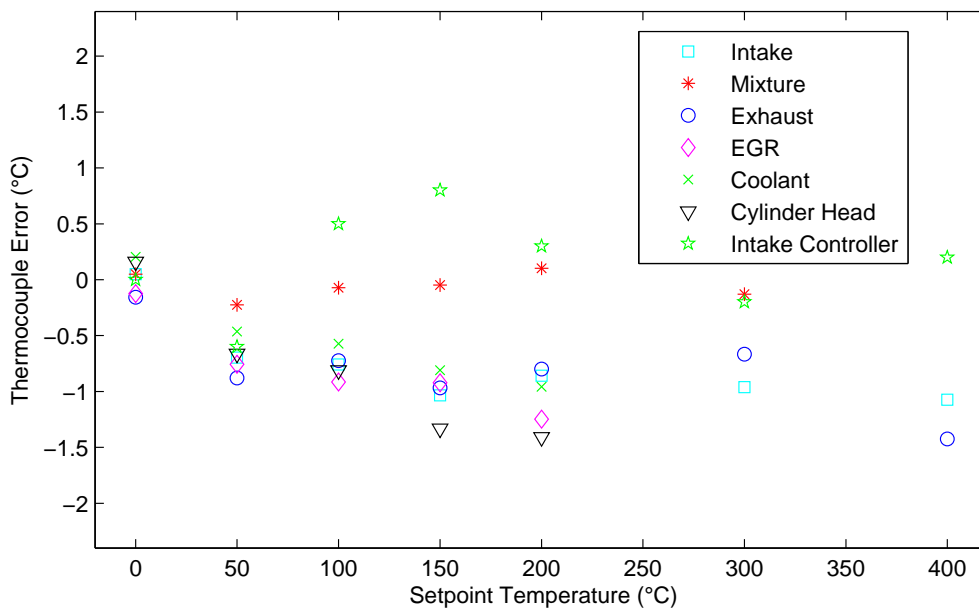
Figure D.7: Thermocouple calibration.

D.6 Exhaust Emissions

Damorn Bundhurat, a visiting researcher from Chiang Mai University in a prior year, developed the exhaust emissions system and calibration procedure [59]. Similar to work by Handford [19], the same setup and procedures are used in this study. Instruments being used are presented in Table D.1 and calibration gases are shown in Table D.2.

Table D.1: California Analytical Instruments emissions analyzers.

Instrument	Measured Gas	Range
300-CLD	NO_x	0-4000 ppm
300M-HFID	HC	0-10,000 ppm (CH_4)
300	CO_2	0-20 %
300 (Infrared)	CO	0-2.5 %
100P	O_2	0-25 %

Table D.2: Emissions calibration gases.

Composition	Zero Gas For:	Span Gas For:
2000 ppm NO, bal. N_2	CO_2, CO, O_2	NO_x
Compressed Air (20.9% O_2, bal. N_2)	NO_x, HC	O_2
5000 ppm CH_4, 5100 ppm CO, 5 % CO_2, bal. N_2	-	HC, CO_2, CO
20 % CO_2, 25 % CO, bal. N_2	-	CO_2

Appendix E

Uncertainty Analysis

The uncertainty associated with measured and calculated parameters are evaluated in this appendix.

E.1 Average Intake Pressure

Error in this cyclical measurement is calculated by considering both the accuracy of the calibrated intake pressure sensor and the variability in the measurement. During a motoring test, the engine is held at steady-state conditions while 100 cycles are recorded. Observing the variability in the recorded values gives an indication of uncertainty in to measurement.

For the instance of intake pressure, a standard deviation of 0.023 kPa is observed. Since greater than 30 samples are considered, the uncertainty due to variability is taken as twice the standard deviation. Combining this value with the calibration uncertainty is accomplished using a root sum of the squares (RSS) approach [60] using

$$\delta R = \sqrt{\sum_{i=1}^{Num} \delta X_i^2} \tag{E.1}$$

where δR is the uncertainty in the result, δX_i is the uncertainty of each component being considered, and Num is the number of uncertainty components. The total

uncertainty for intake pressure is thus found to be 2.7 kPa. As expected, the low variability of the measurement does not have a significant influence on the total uncertainty as dictated by the calibration uncertainty.

E.2 P_{IVC}

Pressure at IVC is determined by averaging 5% of the intake pressure measurements immediately prior to IVC as discussed in Section 3.1.2.1. Using the same approach as described above for intake pressure, the standard deviation in P_{IVC} while motoring is found to be 0.71 kPa. Since only 8 samples are used in this measurement, a Student's t-test is applied to determine uncertainty due to variability. Combining the result with calibrational uncertainty using a RSS results in a total uncertainty in P_{IVC} of 2.8 kPa with 95% confidence.

One aspect of error that can not be easily evaluated is the correlation between average intake pressure or P_{IVC} and air mass flow during fast changes in throttle position. Without the proper equipment to measure air mass induction on each engine cycle, the effect can only be speculated upon.

With a large change in throttle position, the air pressure on both sides of the throttle experience conditions not representative of steady-state operation. The manifold pressure is likely to drift up or down throughout the engine cycle as the intake system tends toward stability. Conditions present while the intake valve is open may not correlate with the average throughout the cycle; however, P_{IVC} should provide a more representative value of the engine conditions due to its shorter duration and specific location relative to IVC. This capability allows for a more accurate prediction of cycle specific equivalence ratio during mode-switching when using P_{IVC} as opposed to average intake pressure.

E.3   CNG Injection Timing and P_{IVC} Sample Location

Uncertainty in CNG injection timing and P_{IVC} sample location is primarily a result of error in RPM. The rotational speed of the engine is not constant throughout the cycle as demonstrated in Figure E.1. Only the average value is recorded and used to determine the location of the injection event. The error is found by cumulatively integrating the time error throughout the engine cycle, resulting in a maximum of 0.98 ± 0.08 CAD when running in SI at 700 RPM for 100 cycles. Quantization error in the RPM measurements are negligible with the DAQ timebase of 80 MHz (0.05% for each of the 7200 measurements), so the total error in CNG injection timing and P_{IVC} sample location is accepted as 1.1 CAD.
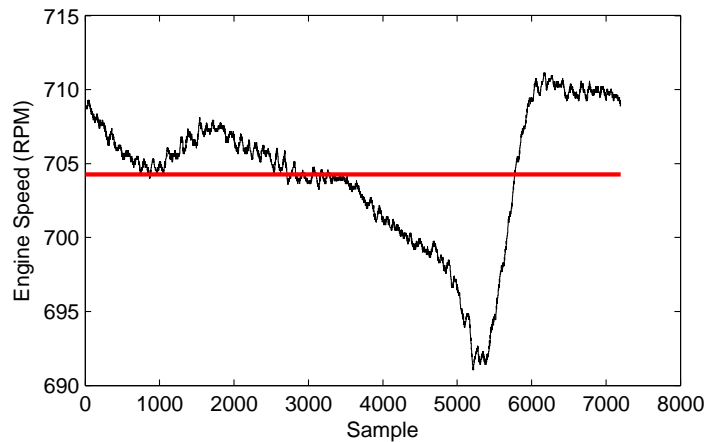
Figure E.1: Variation in RPM throughout one engine cycle. The horizontal line shows the average value that would be recorded for this cycle.

E.4   CNG Injection Pulse Width

Injection duration carries an error associated with the internal timing in the DAQ hardware. With a timebase of 20 MHz, the quantization error is 0.05 microseconds. Since this is minuscule compared to the typical injection timings of 9-15 milliseconds, the error in injection pulse width is assumed to be negligible.

E.5 IMEP

Indicated mean effective pressure is calculated using the recorded in-cylinder pressure trace. The piezoelectric pressure transducer that samples cylinder pressure carries a quoted accuracy of 8.8% for each individual measurement. Since IMEP is evaluated as the integral of pressure over volume throughout one engine cycle, the total error is reduced by dividing by the square root of the number of samples per cycle, which in this study is 7200. The resulting calculation error for IMEP is 0.1%.

Variability from cycle to cycle generally contributes a larger error than the calculated error, but this will depend on the stability of the operating point. Since the focus of this study is observing cycles individually, measurement variability must be evaluated independently. Data obtained while motoring is used as this constitutes very stable engine operation to observe measurement uncertainty as opposed to operational variability. A standard deviation of 0.03 bar for IMEP is found among the 100 cycles. With the calculation error being significantly lower than the variability for the approximate IMEP range of 3-5 bar experienced in this study, the total error in IMEP is taken as 0.06 bar with 95% confidence.

E.6 CA50

The location of 50% fuel mass burned is determined from the rate of heat release, which in turn is calculated using the cylinder pressure trace. Handford investigated the error in this calculation by applying a Monte Carlo algorithm that varied the heat transfer coefficienct by $\pm$ 50% resulting in an error of 0.83 CAD in CA50 with 95% confidence [19]. For this study, the same procedures is implemented during HCCI operation, but the original Woschni heat transfer coefficients are implemented during SI operation. Table E.1 lists the results of applying a Monte

Carlo algorithm to the different combinations of heat transfer coefficients and combustion types. Note that the uncertainty of evaluating CA50 for HCCI combustion with HCCI heat transfer coefficients is very close to the value obtained by Handford.

Table E.1: Monte Carlo algorithm applied to CA50 calculation using SI and HCCI heat transfer coefficients for SI and HCCI combustion cycles. Values are given in °aTDC.

Heat Transfer Coefficients	**SI**		**HCCI**	
Combustion Type	SI	HCCI	SI	HCCI
Average CA50	48.29	38.54	10.14	4.86
95% Uncertainty in CA50	3.05	1.91	0.69	0.89

E.7   ROPR

The maximum rate of pressure rise is determined from the cylinder pressure trace after applying a low-pass butterworth filter with a normalized cutoff frequency of 0.10. The filter reduces noise in the measurements to provide a more appropriate value for maximum slope, but complicates a numerical evaluation of this error. Variability of this parameter with the system during stable operation should provide a representative value. While motoring, the standard deviation in ROPR is found to be 0.016 bar/CAD over 100 cycles. Using this to support the assumption that the low-pass filter sufficiently dampens out cylinder pressure measurement fluctuations, the error in ROPR is taken as 0.03 bar/CAD with 95% confidence.

E.8   Equivalence Ratio

Equivalence ratio is calculated based on the mass of CNG and air inducted during each engine cycle as presented in Equation 3.1. As discussed in Section 3.1.4, these two quantities are determined from correlations of CNG mass flow rate with CNG injection pulse width, and air mass flow rate with P_{IVC}.

E.8.1   CNG Mass Per Cycle

Figure 3.9 shows the relationship between CNG mass flow rate and injection pulse width. Considering two standard deviations of the residuals, the error in the CNG mass per cycle is 0.15 milligrams with 95% confidence. The strong linear trend in the data leads to this low error in the best fit line; however, the uncertainty in each of the measurements should be carried through for future calculations. Starting with the CNG mass flow error of 4 mg/s, the error in CNG mass per injection is converted to 0.68 mg/cycle with 95% confidence. Combining this with the residual error through a RSS, the total error becomes 0.7 mg/cycle with 95% confidence.

E.8.2   Air Mass Per Cycle

Initially, the volumetric efficiency of the engine at various P_{IVC} values is determined as discussed in Section 3.1.4. The error in the resulting values is determined through a means of perturbing the inputs individually and taking the RSS of all contributing factors [60]. When using the absolute errors associated with the measurements as calculated in Appendix D, the absolute error in volumetric efficiency becomes 0.07 with 95% confidence. This error is large relative to the observed trend in volumetric efficiency values. The uncertainty is reduced significantly when considering only the variability in the test runs and not the bias error associated with calibration. This is reasonable for the characterization of volumetric efficiency with P_{IVC} as these values are only intended for use on this engine with the current measurement system; however, the benefit of this approach is limited to differentiatng between volumetric efficiencies during this characterization. The total uncertainty of 0.07 must be considered in successive calculations using volumetric efficiency based on this data.

Next, the air mass is calculated for individual cycles during mode-switching. Volumetric efficiency is determined from the measured P_{IVC} based on Figure 3.12

before solving for air mass flow rate through an iterative approach. Engine speed is used to determine the mass of air induced on a single cycle as opposed to an average air mass flow rate. Error throughout these calculations is again determined by perturbing the inputs by their associated uncertainties, resulting in an overall uncertainty of 12% in the calculated equivalence ratio with 95% confidence.

Appendix F

Engine Control Program Details

The LabVIEW control program developed for this study is introduced in Chapter 3. Greater detail and a discussion of functionality are provided in this appendix.

F.1 Channel Configuration

Four National Instruments DAQ cards are used to accommodate all functions of this program, including data acquisition and actuator control. DAQmx drivers allow multiple operations to be carried out with each card within a single program, including analog input, analog output, digital output, and counter operations. The specific channels used in this study are outlined in Tables F.1, F.2, F.3, and F.4.

Table F.1: National Instruments PCI-MIO-16E-1 (1) input/output description.

Channel	Pins	Range	Description
AI2	65 (+)	0 - 5 V	CNG Mass Flow
AI10	31 (-)		
AI3	30 (+)	0 - 5 V	Air Mass Flow
AI11	63 (-)		
AI4	28 (+)	-10 - 10 V	Dyno Torque
AI12	61 (-)		
AI6	25 (+)	-10 - 10 V	Intake Pressure
AI14	58 (-)		
AI7	57 (+)	-10 - 10 V	Exhaust Pressure
AI15	23 (-)		

Table F.2: National Instruments PCI-MIO-16E-1 (2) input/output description.

Channel	Pins	Range	Description
AI0	68 (+)	-	CJC
AI8	34 (-)		
AI2	65 (+)	0 - 200 °C	Intake Mixture Thermocouple
AI10	31 (-)		(1/32", Type J)
AI3	30 (+)	0 - 400 °C	Intake Air Thermocouple
AI11	63 (-)		(1/16", Type J)
AI4	28 (+)	0 - 200 °C	EGR Thermocouple
AI12	61 (-)		(1/16", Type J)
AI5	60 (+)	0 - 200 °C	Coolant Thermocouple
AI13	26 (-)		(1/16", Type T)
AI6	25 (+)	0 - 600 °C	Exhaust Thermocouple
AI14	58 (-)		(1/16", Type J)
AI7	57 (+)	0 - 200 °C	Cylinder Head Thermocouple
AI15	23 (-)		(1/8", Type T)
CTR0	3 (+)	-	Cam Signal
DGND	36 (GND)		
CTR0_Out	2 (+)	0 - 5 V	CNG Injector Signal
DGND	36 (GND)		

Table F.3: National Instruments PCI-MIO-16E-4 input/output description.

Channel	Pins	Range	Description
AI2	65 (+)	0 - 10 V	NOx Emissions
AI10	31 (-)		
AI3	30 (+)	0 - 10 V	HC Emissions
AI11	63 (-)		
AI4	28 (+)	0 - 10 V	TPS Feedback
AI12	61 (-)		
AI5	60 (+)	0 - 10 V	CO_2 Emissions
AI13	26 (-)		
AI6	25 (+)	0 - 10 V	CO Emissions
AI14	58 (-)		
AI7	57 (+)	0 - 10 V	O_2 Emissions
AI15	23 (-)		
AO0	22 (+)	0 - 5 V	Throttle Control
AOGND	55 (GND)		
DIO0	52 (+)	0 - 5 V	Spark Solenoid
DGND	18 (GND)		

Table F.4: National Instruments PCI-6220 input/output description.

Channel	Pins	Range	Description
AI1	33 (+)	-10 - 10 V	In-Cylinder Pressure
AI9	66 (-)		
AI2	65 (+)	-10 - 10 V	Cam Signal
AI10	31 (-)		
AI7	57 (+)	-10 - 10 V	Pulse Per Cycle (gated
AI15	23 (-)		pulse per revolution)
PFI0	11 (+)	-	Pulse Per Cycle (gated
DGND	44 (GND)		pulse per revolution)
PFI3	42 (+)	-	BEI 0.1 CAD Encoder
DGND	18 (GND)		
CTR0	3 (+)	-	BEI 0.1 CAD Encoder
DGND	18 (GND)		

F.2   Program Indexing

As discussed in Appendix B, the engine flywheel is indexed to TDC and testing is
carried out to determine the thermodynamic loss angle. The result is that geometric
top dead center can be determined in the program from a known reference point in
the cycle. The BEI encoder produces a pulse for every 0.1 CAD of rotation, along
with a single pulse per revolution (PPR) of the crankshaft. To ensure that the
same point is referenced in each cycle (2 revolutions), a hall effect cam sensor is
used to gate one of the two PPR pulses to produce a pulse per cycle (PPC) signal.
In addition to gating the PPR signal, the rising edge of the cam signal also acts as
the reference point for fuel injection timing. The location of these signals relative
to a pressure trace is shown below in Figure F.1. Both the rising cam edge and the
PPC are located during a compression ratio test, which occurs every day before
any data is logged. This corrects for any drift over time or manual adjustment of
these sensors on the engine.

The location of these index signals is not chosen arbitrarily. They determine
when in the cycle on-line calculations occur, which affects when the results are
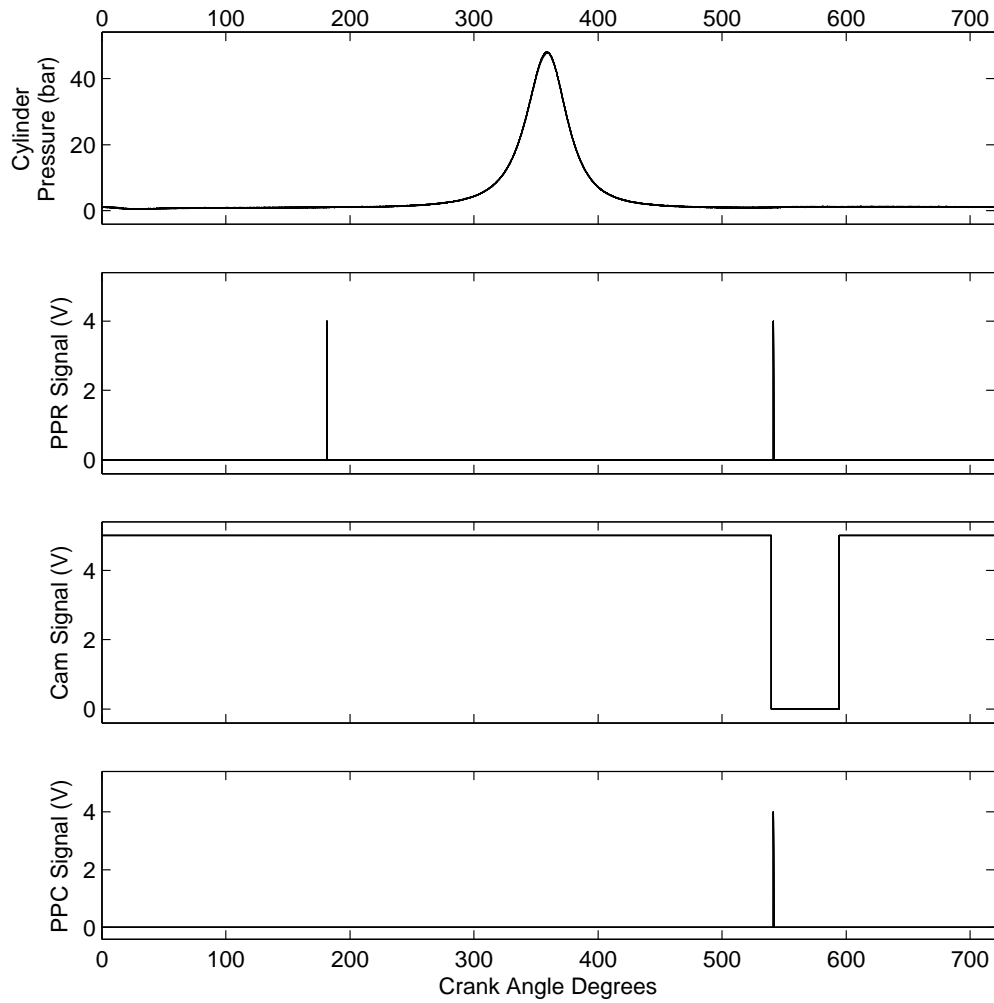available for feed-back control. For this study, it is desired to develop open-loop

Figure F.1: Index signals used for fuel injection timing and to locate TDC during a compression ratio test.

control sequences to control mode-switching, so it is important to have a system capable of producing repeatable actuator response. PI feed-back is implemented following the mode-switch to maintain stable operation in HCCI because of the relatively low intake temperatures being used. Since variable fuel injection timing is used during this study, it is also important to understand how the system responds to changes throughout the engine cycle.

The cam signal must be set in relation to the PPR signal, as it must gate one of the two PPR pulses to create the PPC signal using discrete logic TTL circuitry. After setting the desired PPR pulse timing, the cam signal is adjusted so the falling edge occurs slightly ahead of the PPR signal. This provides the greatest time before the rising edge occurs from which the fuel injection timing is referenced.

The PPC signal determines the point at which data transfer occurs for all DAQ signals. By setting this to occur just after EVO, all useful information from the previous cycle is recorded and available for calculation. The compression and expansion phases of the cylinder pressure trace are available for combustion analysis, and the intake measurements correlate with the recorded pressure trace to ensure data synchronization. The exhaust stroke provides sufficient time for the program to run all on-line computations for feedback control of the next cycle.

There is a limitation to achieve next cycle fuel control such that fuel injection must occur slightly before or during the intake stroke. If injection timing is set after IVC, then the fuel injection event will only affect the following cycle's combustion as it will remain in the intake manifold until that time. Injection during the calculation time is not possible as the system "skips" every second cycle due to the extended time delay associated with the fuel signal. An external fuel controller may remedy this situation, but would not receive the new fuel parameters until the combustion calculations are completed, thus preventing next cycle fuel control in this region.

This concern is handled by restricting injection timing to the stable region, thus excluding the injection from 220° bIVO to IVO (during the exhaust stroke). Injection during the later portion of the intake stroke is avoided to ensure all CNG is induced on a single cycle, so only injection at IVO is used for next cycle fuel control. As a result, advancing the injection timing from anywhere between IVC and 220° bIVO (which fuels the following cycle) to IVO (which fuels the current cycle) must be completed while commanding one cycle of no fuel delivery to avoid double-fueling the next engine cycle. Conversely, adjusting injection timing in the opposite direction from IVO to anywhere between IVC and 220° bIVO inherently provides one cycle without fuel, causing a mis-fire. This is relegated by avoiding this type of injection timing adjustment during a mode-switch as would be desirable during HCCI-SI. Instead, the injection timing is advanced to 220° bIVO and the engine allowed to stabilize before initiating the mode-switch. Further control programming could allow for a double-injection when this type of adjustment is made, but the added complexity was deemed unnecessary for this study.

Appendix G

MATLAB Code for MSPC Analysis

This appendix provides the MATLAB code used to calculate the mode-switching

performance criterion (MSPC).

```matlab
function [results] = MSPC(IMEP,ROPR,switch_point,varargin)
% This function takes cycle data from an SI to HCCI mode-switch (or vice
% versa) and evaluates the performance of the transition quantitatively.
%
% MSPC = Mode-Switch Performance Criterion
% IMEP = vector of IMEP data from consecutive engine cycles
% ROPR = vector of ROPR associated with IMEP data
% switch_point = cycle number where mode-switch is initiated (the last
%                cycle in the initial combustion mode)
% varargin = additional variables; see below for assignments
%
% Written by Jason Boddez on Mar. 19, 2010
% Modified by Jason Boddez on Oct. 22, 2010

if nargin < 4
    COV_IMEP_SS = 0.05;  % Default steady-state value for coefficient of
            % variation of IMEP used to define the end of the mode-switch
else
    COV_IMEP_SS = varargin{1};  % Adjust this value if using a less stable
                                % operating point
end


num = length(IMEP);  % Number of engine cycles in the provided data
COV_IMEP = 1;  % Initialize; transient coefficienct of variation of IMEP
trans = 0;     % Initialize; defines the length of transient for the
               % mode-switch to occur (# of cycles)
while switch_point+trans < num-15 && COV_IMEP > COV_IMEP_SS
    trans = trans + 1;
    COV_IMEP = std(IMEP((switch_point+trans):(switch_point+trans+14)))...
        /mean(IMEP((switch_point+trans):(switch_point+trans+14)));
end


% Calculate the steady-state IMEP in first region (assumed to be SI)
```

```matlab
if switch_point > 15
    IMEP_SI = mean(IMEP(switch_point-15:switch_point-1));
else
    IMEP_SI = mean(IMEP(1:switch_point-1));
    fprintf('Insufficient SI cycles provided; use what is available.\n');
end

% Calculate the steady-state IMEP in second region (assumed to be HCCI)
if COV_IMEP > COV_IMEP_SS
    fprintf(['Engine does not stabilize in the cycles ' ...
        'provided, but assume it does.\n']);
    trans = num-switch_point-14;
    IMEP_HCCI = mean(IMEP(num-14:num));
else
    IMEP_HCCI = mean(IMEP(switch_point+trans+1:switch_point+trans+15));
end


 % Calculate the COV_IMEP during the transition between steady-state
 % operating points by assuming a linear trend between the two levels over
 % the duration of the mode-switch determined above.
IMEP_switch = (IMEP_SI+((IMEP_HCCI-IMEP_SI)/(trans)):...
                    ((IMEP_HCCI-IMEP_SI)/(trans)):IMEP_HCCI)';
IMEP_error = IMEP_switch-IMEP(switch_point+1:switch_point+trans);
IMEP_std = sqrt(1/(trans+1)*sum(IMEP_error.^2));
COV_IMEP_trans = IMEP_std/(IMEP_HCCI+IMEP_SI)*2;

% Plot IMEP with desired trend
    y1(1:15) = IMEP_SI;
    if trans > 1
        y2 = IMEP_switch';
    else
        y2 = IMEP_HCCI;
    end
    y3(1:14) = IMEP_HCCI;
    desiredIMEP = [y1 y2 y3];

    figure;
    plot(-14:15+trans-1, desiredIMEP, 'k-',...
      -14:15+trans-1, IMEP(switch_point-14:switch_point+trans+14),'ko--');
    hold on;
    axis([-14 15+trans-1 0 6]);
    xlabel('Cycles After Mode Switch');
    ylabel('IMEP (bar)');
    ax(1) = gca;
    set(ax(1),'YMinorTick','on');

% Similar to steady-state operation, consider any COV_IMEP_trans < 0.05, or
% 5%, to be the desired scenario with no penalty being added.  A
% penalty to MSPC for all values above this point will be applied later.
if COV_IMEP_trans < 0.05
    smoothness = 0;
else
    smoothness = COV_IMEP_trans/0.05 - 1;
end

% Check for mis-fires during mode-switch
misfire = find(IMEP(switch_point+1:switch_point+trans) < 0.5*IMEP_switch);
misfire_val = length(misfire);

% Check for knock cycles during mode-switch (ROPR > 10 bar/CAD)
```

```matlab
stabilize = trans-1; % Initialize; number of cycles until propogating
                     % knock has subsided.
ROPR_check = 11;     % Initialize; maximum rate of pressure rise check for
                     % stabilizing period.
while switch_point+stabilize < num-15 && ROPR_check > 10
    stabilize = stabilize + 1;
    ROPR_check = max(ROPR((switch_point+stabilize):...
        (switch_point+stabilize+15)));
end

% Calculate the relative harshness of all knock cycles
knock = find(ROPR(switch_point:switch_point+stabilize)>10);
if isempty(knock) == 0
    knock_val = sum((ROPR(switch_point+knock-1) - 10));
else
    knock_val = 0;
end

a = 0; % Weight factor for misfires
b = 0.5; % Weight factor for knock
c = 1; % Weight factor for duration
d = 0.5*trans; % Weight factor for smoothness

MSPC = a*misfire_val + b*knock_val + c*trans + d*smoothness;

fprintf(['Misfire: %.3g\nKnock: %.3g\nDuration: %.3g\nSmoothness: %.3g',...
    '\nStabilizes from knock in %.3g cycles\n'],...
    a*misfire_val, b*knock_val, c*trans, d*smoothness, stabilize);
fprintf('The MSPC value is %7.4f\n\n',MSPC);

results = [a*misfire_val; b*knock_val; c*trans; d*smoothness;...
    stabilize; MSPC];
end
```

Appendix H

Analysis File Summary

This appendix provides a summary of the programs developed and utilized throughout this study. LabVIEW programs in Table H.1 are implemented for data collection and on-line processing, while MATLAB programs in Table H.2 are used to perform various calibrations, calculations, and plot generation.

Table H.1: LabVIEW programs used for engine operation and calibrations.

Filename	Purpose
Total Control7.vi	Main engine control program with average intake pressure PI control
Total Control7a_Pivc_Control.vi	Main engine control program with P_{IVC} PI control
DataAnalysis_v5.vi	Data analysis component in engine control program
cr5h.vi	Compression ratio component in engine control program
AirMFCal_Bellprover.vi	Calibration program for air mass flow meter using Bell Prover
CNGMFSCALE.vi	Calibration program to measure scale output for CNG mass flow calibration
EmissionsCal_Daqmx.vi	Calibration program for exhaust emissions
InCylPressureCal.vi	Calibration program for cylinder pressure transducer
PressureCal.vi	Calibration program for gauge pressure transducers
thermocoupleviewer.vi	Calibration program for thermocouples

Table H.2: MATLAB programs used to process data and create figures.

Filename	Purpose
MS_plot_7.m	Generate plots for "intake pressure, CNG PW, and IMEP", "CNG injection timing", and "CA50 and ROPR"
MS_plot_indiv_7.m	Generate plots of intake pressure, CNG PW, IMEP, CNG injection timing, CA50, ROPR, and equivalence ratio
SI_HCCI_MSPC_7.m	Analysis file for Mode-Switching Performance Criterion
air_cng_characterization.m	Generate plots for characterizing CNG injector
cal_plot_print.m	Converts MATLAB plots to .eps format
CFR_timing_plot.m	Generate index plots for Figure F.1
intake_pressure_plot.m	Generate plots of intake pressure and air mass flow rate
PivcPlot.m	Generate plots for P_{IVC} samples and pressure measurements upstream/downstream of throttle
throttle_nonlinear_plot.m	Generate plot for non-linear Woodward throttle trend
AirMF_import.m	Import and organize air mass flow calibration data
AirMF_Cal2.m	Calibration processing for air mass flow meter data
AirMFplot.m	Calibration plot for air mass flow meter
cngMFplot.m	Calibration plot for CNG mass flow meter
PressurePlots.m	Calibration plot for gauge pressure transducers
file_name_extract.m	Extract pressures and test number from filename for cylinder pressure transducer calibration tests
pcal2.m	Calibration processing for cylinder pressure transducer
ThermocouplePlot.m	Calibration plot for thermocouples